BEHAVIOUR OF CHANNEL SHEAR CONNECTORS: PUSH-OUT TESTS

A Thesis

Submitted to the Faculty of Graduate Studies and Research

in Partial Fulfillment of the Requirements

for the

Degree of Master of Science

in the

Department of Civil and Geological Engineering

University of Saskatchewan

by

Amit Pashan

Saskatoon, Saskatchewan

Canada

2006

PERMISSION TO USE

ABSTRACT

This thesis summarizes the results of an experimental investigation involving the testing of push-out specimens with channel shear connectors. The test program involved the testing of 78 push-out specimens and was aimed at the development of new equations for channel shear connectors embedded in solid concrete slabs and slabs with wide ribbed metal deck oriented parallel to the beam.

The test specimens were designed to study the effect of a number of parameters on the shear capacity of channel shear connectors. Six series of push-out specimens were tested in two phases. The primary difference between the two phases was the height of the channel connector. Other test parameters included the compressive strength of concrete, the length and the web thickness of the channel.

Three different types of failure mechanisms were observed. In specimens with higher strength concrete, failure was caused by the fracture of the channel near the fillet with the channel web acting like a cantilever beam. Crushing-splitting of concrete was the observed mode of failure in specimens with solid slabs when lower strength concrete was used. In most of the specimens with metal deck slabs, a concrete shear plane type of failure was observed. In the specimens involving this type of failure, the channel connector remained intact and the concrete contained within the flute in front of channel web sheared off along the interface.

The load carrying capacity of a channel connector increased almost linearly with the increase in channel length. On average, the increase was about 39% when the channel length was increased from 50 mm to 100 mm. There was a further increase of 24% when the channel length was increased from 100 mm to 150 mm. The influence of web thickness of channel connector was significant when the failure occurred due to channel web fracture but was minimal for a concrete crushing-splitting type of failure.

The specimens with solid concrete slabs carried higher load compared to those with metal deck slabs. The increase in load capacity was 33% for specimens with 150 mm long channels but only 12% for those with 50 mm long channel connectors.

This investigation resulted in the development of a new equation for predicting the shear strength of channel connectors embedded in solid concrete slabs. The proposed equation provides much better correlation to test results than those obtained using the current CSA equation.

The results of specimens with metal deck slabs were used to develop a new equation for predicting the shear capacity of channel connectors embedded in slabs with metal deck oriented parallel to the beam. The values predicted by the proposed equation were in good agreement with the observed test values.

ACKNOWLEDGMENTS

I would like to extend my most sincere thanks to Professor Mel Hosain, my supervisor, for his valuable guidance and mentorship throughout the preparation of this thesis. I also would like to acknowledge the contributions of Professors Bruce Sparling, Leon Wegner and Gordon Putz, who were the members of my advisory committee. Special thanks are extended to Mr. Dale Pavier for his tremendous help and guidance in conducting the experimental work in the structures laboratory.

I would like to acknowledge the funding agency, the Natural Sciences and Engineering Research Council (NSERC), for providing funds for my research through a discovery grant awarded to Professor Hosain. Thanks are extended to Vic West Steel of Oakville for the donation of the metal decks and to Supreme Steel of Saskatoon for the donation of some of the steel beams.

I am grateful to all my friends and fellow graduate students, Greg Del Frari, Emma Boghossian, Najeeb Muhammad, Niraj Sinha, Jaimin Patel, Janak Kapadia, Manish Baweja, Anna Paturova and Fazlollah Shahidi, for their assistance during the experimental work.

Finally, I would like to thank my grandmother, my parents and my brothers and sisters, who have always been a source of inspiration to me and the foundation stone of my success. I owe a debt of gratitude to my wife Sonu, for her support and encouragement during the times of frustration and stress.

This thesis is dedicated to my Grandfather, the Late Shri Karam Chand.

TABLE OF CONTENTS

LIST OF FIGURES

LIST OF TABLES

CHAPTER ONE

INTRODUCTION

1.1 Preface

Steel-concrete composite beams have been used for a considerable time in bridge and building construction. A composite beam consists of a steel section and a reinforced concrete slab interconnected by shear connectors, as shown in Fig. 1.1. It is common knowledge that concrete is strong in compression but weak when subjected to tension, while steel is strong in tension but slender steel members are susceptible to buckling while under compressive forces. The fact that each material is used to take advantage of its positive attributes makes composite steel-concrete construction very efficient and economical (Hegger and Goralski 2004).

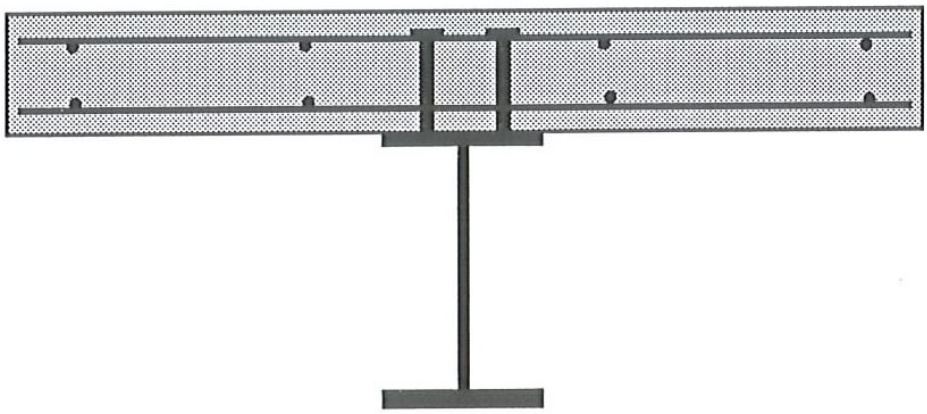

Figure 1.1 Composite beam with solid slab.

Composite beams with solid concrete slabs are frequently used in bridge construction. In recent years, the development of an effective composite flooring deck system has greatly enhanced the competitiveness and effectiveness of steel-framed construction for high-rise buildings (Trumpf

and Sedlacek 2004). In today's building industry, composite beams invariably incorporate a formed metal deck as shown in Fig. 1.2. This type of composite flooring system consists of a cold-formed, profiled steel sheet which acts not only as the permanent formwork for an in-situ cast concrete slab, but also acts as tensile reinforcement for the slab. The metal deck can be oriented parallel to the beam (Fig. 1.2) or perpendicular to the beam (Fig. 1.3).

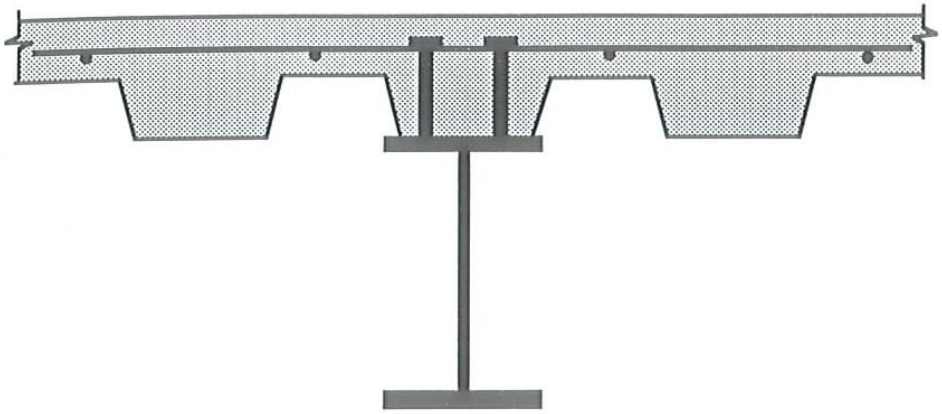

Figure 1.2 Composite beam with ribbed metal deck (oriented parallel to the beam).

Composite beams offer several advantages over non-composite sections. Since the load is carried jointly by the concrete slab and the steel beam, the size of the steel section is smaller than otherwise would be required. This reduces the overall height of the building and the steel tonnage required, thus resulting in a direct cost reduction. A composite beam is also stiffer than a non-composite beam of the same size and thus experiences less deflection and floor vibrations.

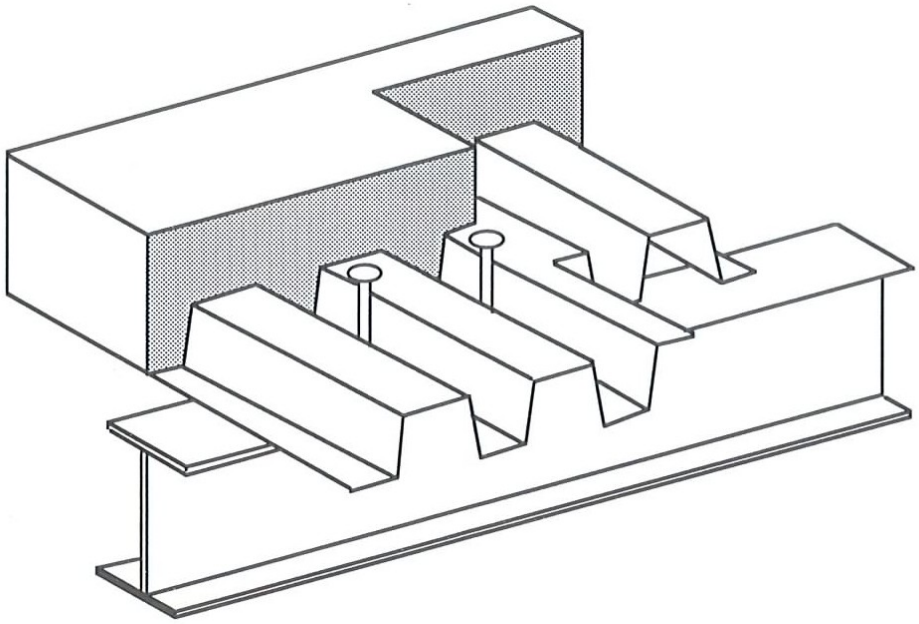

Figure 1.3 Composite beam with ribbed metal deck (oriented perpendicular to the beam).

An essential component of a composite beam is the shear connection between the steel section and the concrete slab. This connection is provided by mechanical shear connectors, which allow the transfer of forces in the concrete to the steel and vice versa and also resist vertical uplift forces at the steel-concrete interface. The shear connectors are installed on the top flange of the steel beam, usually by means of welding, before the slab is cast. These connectors ensure that the two different materials that constitute the composite section act as a single unit.

A variety of shapes and devices have been in use as shear connectors and economic considerations continue to motivate the development of new products. Presently, the headed stud is the most widely used shear connector in composite construction. Its popularity stems from proven performance and the ease of installation using a welding gun, as shown in Fig. 1.4.

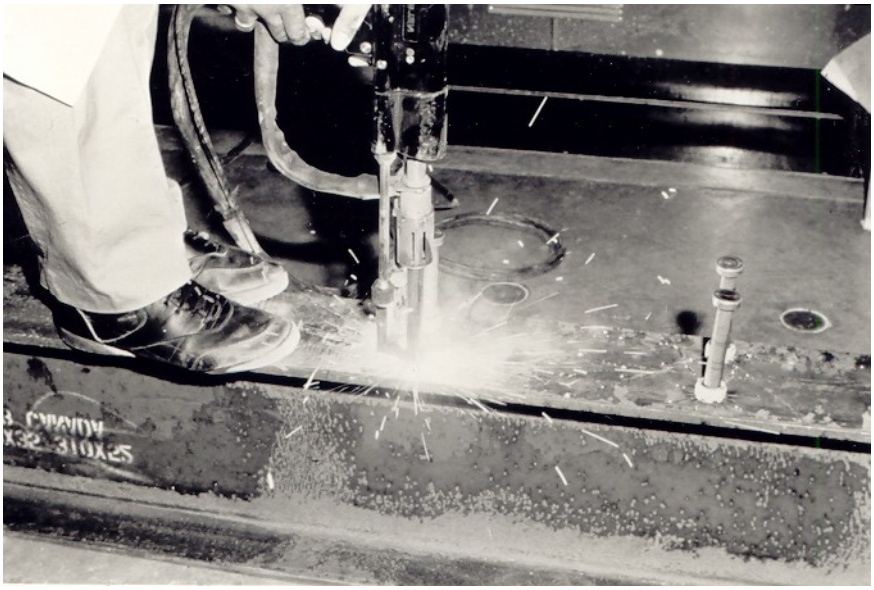

Figure 1.4 Welding of stud shear connector using a welding gun.

However, some concerns have been expressed as to the reliability of the installation technique. Unless special care is taken, the strength of the weld can be adversely affected by poor weather, the surface condition of the metal decking or the coating on steel beams (Chien and Ritchie 1984). In addition, due to the small load carrying capacity of a connector, stud connectors have to be installed in large numbers, as shown in Fig.1.5. This usually produces a cluttering effect and an unsafe working place. Due to these drawbacks, the new perfobond rib connector (Figure 1.6) is being promoted as a viable alternative to headed stud connectors (Zellner 1987, Veldanda and Hosain 1992). Some older generations of shear connectors such as channels and T-sections are also gaining resurgence (Hidehiko and Hosaka 2002).

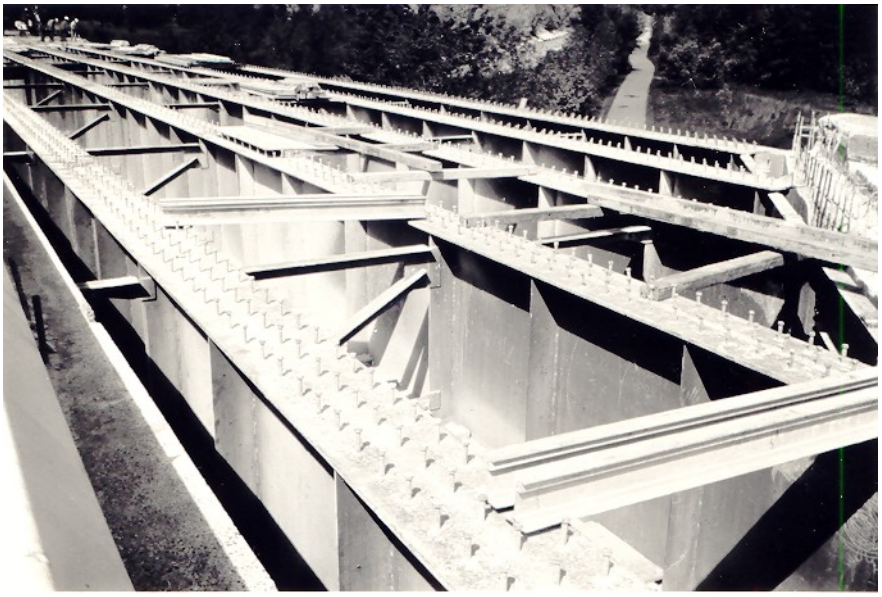

Figure 1.5 Cluttering effect of stud shear connectors.

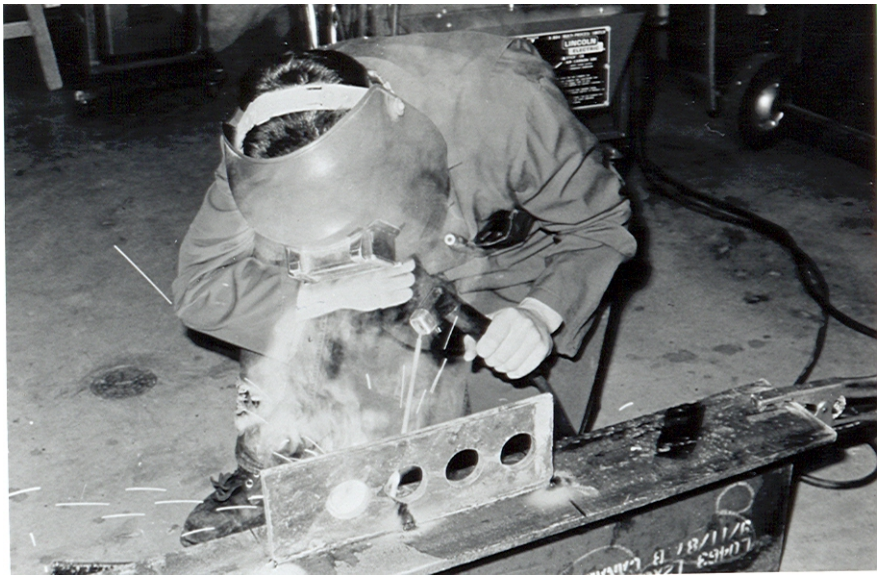

Figure 1.6 Perfobond rib connector welded to beam flange.

Since the conventional welding system used for welding channel connectors is very reliable, inspection procedures such as the bending test for headed studs (Chien and Ritchie 1984) may not be necessary for channel connectors. A channel shear connector has a considerably higher load

carrying capacity than a stud shear connector. As a result, a few channel connectors will replace a large number of headed studs. This would avoid the clutter usually produced by stud connectors. This thesis deals with channel shear connectors.

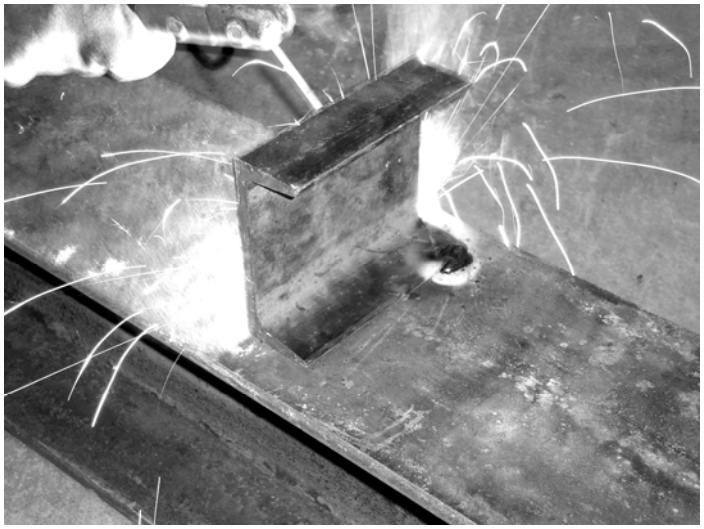

Figure 1.7 Channel shear connector welded to beam flange.

1.2 Design Provisions for Channel Shear Connectors

The current Canadian Standard, CAN/CSA-S16-2001 (Canadian Standard Association 2001) specifies that the factored resistance, q_{rs}, of a channel shear connector embedded in a solid concrete slab be evaluated using Eq. [1.1].

$$q_{rs} = 36.5\phi_{sc}(t + 0.5w)L_c\sqrt{f'_c} \qquad [1.1]$$

where:

ϕ_{sc} = Resistance factor for shear connectors

t = Flange thickness of channel [mm]

w = Web thickness of channel [mm]

L_c = Length of channel shear connector [mm]

f'_c = Compressive cylinder strength of concrete [MPa]

Eq. [1.1] is based on the results of 41 push-out specimens tested at Lehigh University (Slutter and Driscoll 1965). Unfortunately, 34 of these specimens featured 4 inch (102 mm) high channels. Five specimens had 3 inch (76 mm) high channels and only two featured 5 inch (127 mm) high channels. Thus, Equation 1.1 is strictly applicable to 4 inch high channels and does not include channel height as a parameter. Moreover, 35 out of the 41 push-out specimens had 6 inch (152 mm) long channels. Four specimens had 4 inch (102 mm) long channels. Five inch (127 mm) and 8 inch (204 mm) long channels were used in the other two. Although channel length (L_c) is included as a parameter, Eq. [1.1] is only representative of 6 inch long channel connectors.

The current equation included in the American Institute of Steel Construction Specifications and Codes (AISC 1993) for evaluating the nominal strength of a channel connector embedded in a solid concrete slab is also based on the Lehigh test results. Therefore, the limitations indicated earlier in connection with the CSA version of the formula (Eq. 1.1) will also apply to the AISC equation.

No equation is currently available for the design of channel shear connectors embedded in concrete slabs with ribbed metal deck. Wide ribbed metal decks are the most common type of deck profile used in composite construction in Canada. As discussed earlier in this chapter, since composite beams with ribbed metal decks are gaining popularity in the construction of

high rise buildings, there is a definite need to develop new formulations for the design of channel shear connectors in slabs with ribbed metal deck.

1.3 Objectives

This experimental thesis project involved the testing of 78 push-out specimens and had the following as its objectives:

1. To evaluate the reliability of the existing provisions of Canadian Standard (CAN/CSA-S16-01) for the design of channel shear connectors;
2. To develop, if necessary, an equation for the evaluation of the shear resistance of channel shear connectors embedded in solid concrete slabs;
3. To develop new equations which can be used to calculate the shear capacity of channel shear connectors embedded in solid concrete slabs and slabs with wide ribbed metal deck oriented parallel to the beam, and
4. To study the influence of the following parameters on the behaviour, failure modes and shear strength of channel shear connectors:
    (i) Length of the channel shear connector;
    (ii) Web thickness of the channel shear connector;
    (iii) Compressive strength of concrete;
    (iv) Height of the channel connector; and
    (v) Deck geometry.

CHAPTER TWO

SHEAR CONNECTORS IN STEEL-CONCRETE COMPOSITE BEAMS

2.1 Introduction

A great deal of research has been conducted to improve the understanding of the behaviour of steel-concrete composite beams. Reviews of research on composite beams from 1920 to 1958 and 1960 to 1970 were reported by Viest (1960) and Johnson (1970), respectively. An overview of composite construction in the United States was reported by Moore (1987). The flexural behaviour of composite beams is well understood and well documented in many texts (Chien and Ritchie 1984, Kulak et al. 1990). The current research is mainly aimed at the study of shear connectors. Some new provisions have recently been included in the Canadian Standard for the design of composite beams CAN/CSA-S16-01 (CSA 2001). These changes reflect results of recent research in North America while others recognize the need to incorporate requirements similar to those included in European codes. In the Canadian standard, the provisions for the design of composite beams are mainly related to simply supported beams where the concrete is in compression.

2.2 Shear Strength of Headed Stud Connectors

An experimental investigation by Ollgaard et al. (1971), involving the testing of 48 push-out specimens with 16 mm and 19 mm studs embedded in normal and lightweight concrete, revealed that the ultimate strength of the shear connector was influenced by the compressive strength and modulus of elasticity of concrete. The authors arrived at the following empirical equation on the basis of the results obtained from the investigation:

$$Q_u = 1.106\, A_S\, f'^{0.3}_c\, E_c^{0.44} \qquad [2.1]$$

where:

Q_u = Ultimate shear capacity of the stud connector (kips)
A_S = Cross sectional area of the stud connector (in^2)
f'_c = Specified concrete compressive strength (ksi)
E_c = Elastic modulus of concrete (ksi)

For design purposes, the authors proposed a simplified version of Eq. [2.1] which is as follows:

$$Q_u = 0.5\, A_S \sqrt{f'_c}\; E_c \qquad [2.2]$$

Equation [2.2] provides the stud capacity based on the failure of adjacent concrete due to crushing. It has been adopted by the American Institute of Steel Construction (AISC 1986) in their Load and Resistance Factor Design (LRFD) standard for evaluating the nominal strength of a stud connector embedded in a solid concrete slab. Equation [2.2] has also been incorporated in the Canadian Standard CAN/CSA-S16-01 (CSA 2001) in the form provided below.

For end welded studs in solid slabs, headed or hooked with $\frac{h}{d} \geq 4.0$, the shear capacity of a stud is

$$q_{rs} = 0.5\, \phi_{sc}\, A_{sc} \sqrt{f'_c}\; E_c \leq \phi_{sc} A_{sc}\, F_u \qquad [2.3]$$

where:

q_{rs} = Factored resistance of a shear connector in a solid slab [N]
ϕ_{sc} = Resistance factor for shear connectors [0.8]
A_{sc} = Area of stud shear connector [mm^2]
F_u = Tensile strength of stud connector [MPa]
h = Height of stud [mm]

d = Diameter of stud [mm]

The limiting value of $\phi_{sc}A_{sc}F_u$ in Eq. [2.3] represents the factored tensile capacity of the stud connectors. This is to ensure that the computed capacity does not exceed the tensile capacity of the stud as the stud may eventually bend over and fail in tension. The provision $h/d \geq 4.0$ for studs restricts the use of very short studs and is based on the work by Driscoll and Slutter (1961) which showed that the height to diameter ratio must be at least 4 for a stud embedded in normal weight concrete to reach its full capacity. The longitudinal stud spacing was not taken into consideration in the development of Equation [2.3], although subsequent research indicated that this parameter was very important (Johnson 1970; Yam 1981; Mottaram and Johnson 1990).

2.2.1 Deck Ribs Oriented Perpendicular to Steel Beam

For deck ribs oriented perpendicular to the beam, it is recommended in the LRFD (AISC 1993) standard that the nominal shear strength for stud shear connector obtained using Eq. [2.2] be multiplied by the following reduction factor:

$$\frac{0.85}{\sqrt{N_r}}\frac{w_r}{h_r}\left[\frac{H_s}{h_r}-1.0\right]\leq 1.0 \qquad [2.4]$$

where N_r is the number of stud connectors on a beam in one rib. Prior to 1989, Eq. [2.4] was also included in the Canadian Standard (CSA 1984). New provisions have now been incorporated in the current CSA standard based on recent research in Canada (Jayas and Hosain 1988, 1989). Push-out tests, as well as full size beam tests, indicated that failure in this type of

composite beams would likely occur due to concrete pull-out (Fig. 2.1). The reduction factor method (AISC 1986) was found to overestimate the strength of headed studs for concrete pull-out failure. The following expressions were proposed after carrying out regression analyses, which considered the results of push-out tests conducted by Robinson and Wallace (1973), Hawkins and Mitchell (1984), Fisher et al. (1967), Brattland and Kennedy (1986), as well as those tested by Jayas and Hosain (1987):

(i) For 76 mm deck

$$V_c = 0.35 \lambda A_c \sqrt{f'_c} \leq (n/\phi_{sc}) q_{rs} \qquad [2.5]$$

(ii) For 38 mm deck:

$$V_c = 0.61 \lambda A_c \sqrt{f'_c} \leq (n/\phi_{sc}) q_{rs} \qquad [2.6]$$

where:

V_c = Shear capacity due to concrete pull-out failure for one pull-out cone [N]

f'_c = Specified concrete compressive strength [MPa]

λ = 1.0, 0.85 and 0.75 for normal, semi-low and low density concrete, respectively

A_c = The total conical area (mm^2) of a pull-out concrete cone with due consideration of deck profile

n = Number of studs included in a pull-out concrete cone

For the regression analyses, the values of A_c were calculated using expressions provided by Hawkins and Mitchell (1984). In CAN/CSA-S16.1-M89 (CSA 1989), Eqs. [2.5] and [2.6] have been incorporated under Clause 17.7.2.3 using slightly different nomenclature. In estimating the area A_c, the pull-out surface may be assumed to be pyramidal in shape. The centre of the

top surface of the stud may be taken as the apex of the pyramid, with four sides sloping at 45^{o}. For a pair of studs per rib, the straight line joining the centres of the top surfaces of the two studs can be taken as the ridge from where the four sides, sloping at 45^{o}, originate.

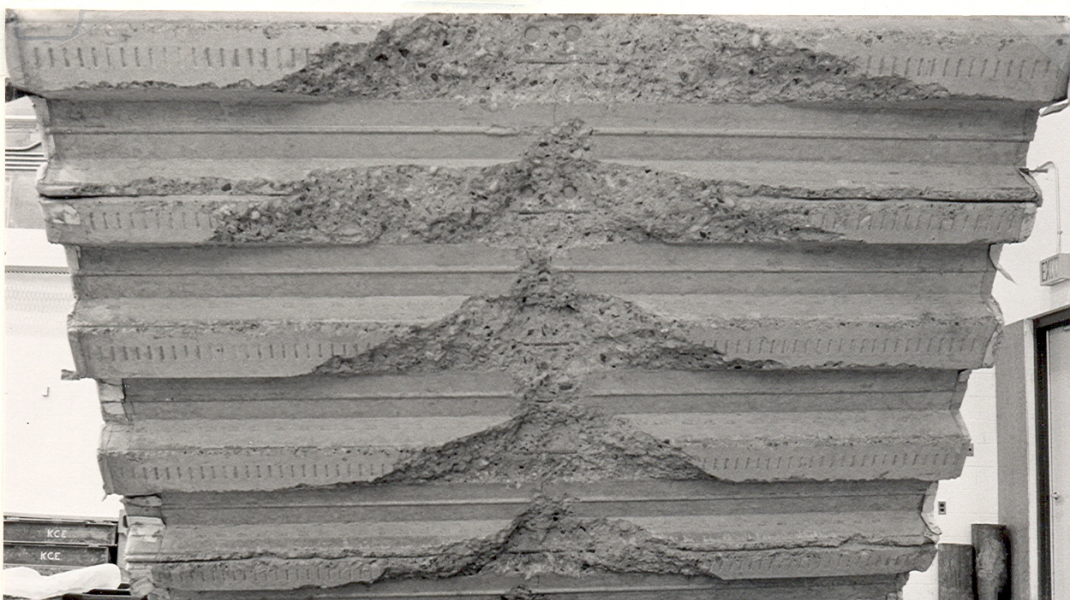

Fig. 2.1 Concrete Pull-out Failure.

Based on the results of the 33 push-out tests considered by Jayas and Hosain (1988), the average ratio of the test to predicted strength given by Eqs. [2.5] and [2.6] was found to be 1.012, with a coefficient of variation of 0.174. On the other hand, the reduction factor approach (AISC 1986) yielded a test to predicted strength ratio of only 0.658, with a large coefficient of variation of 0.38. Equations 2.5 and 2.6 fit the data much better.

2.2.2 Deck Ribs Oriented Parallel to Steel Beam

2.2.2.1 Narrow Ribbed Deck

In the 1990's, North American provisions [CSA (1994) and AISC (1993)] specified that, for parallel narrow ribbed metal deck, the nominal shear strength of a stud connector embedded in a solid slab be multiplied by the following reduction factor suggested by Grant et al. (1977):

$$0.6 \frac{w_d}{h_d}\left[\frac{h}{h_d} - 1.0 \right] \leq 1.0 \qquad [2.7]$$

where h is the height of stud connector after welding, w_d is the average width of the deck rib and h_d is the height of the deck.

Recent studies by Androutsos and Hosain (1993) have raised some doubts concerning the reliability of the reduction factor equation. Although this reduction factor has also been adopted by Eurocode 4 (CEN 1994), predicted values based on this reduction factor differ considerably from test results. A major drawback of the reduction factor approach is that the failure mechanism of a specimen with solid slabs could be different from that of a specimen with metal deck and, thus, the stud capacity cannot be arbitrarily adjusted. Moreover, the deficiency of the parent equation, i.e., the equation for a stud connector embedded in solid slab, is inherited.

In order to resolve this issue, a comprehensive test program was started at the University of Saskatchewan in 1992. The main objective of this project was to develop an equation that could be used to calculate the shear capacity

of headed studs in parallel narrow ribbed metal decks directly without having to use Eqs. [2.2] and [2.7].

The first phase of the experimental program involved the testing of 85 push-out specimens by Androutsos and Hosain (1994). Twenty six of the push-out specimens had a solid slab while the remaining specimens featured a parallel narrow ribbed metal deck. The deck profile, w_d/h_d, varied from 0.78 to 2.0. The headed studs were either 16x76 mm or 19x125 mm, depending upon the overall slab thickness of 102 mm and 150 mm, respectively. The longitudinal stud spacing was the principal experimental parameter. Concrete strength was also varied. For the push-out specimens with metal deck, the studs were welded through the decking. For those with a solid slab, the studs were welded directly onto the beam flange.

A regression analysis of 85 push-out specimens resulted in the following equation for predicting the capacity of headed studs in parallel narrow ribbed metal deck:

$$q_u = 0.92 \frac{w_d}{h_d} d\, h\, (f'_c)^{0.8} + 11.0\, s\, d\, (f'_c)^{0.2} \leq 0.8\, A_{sc}\, F_u \qquad [2.8]$$

$$s \leq 120 \text{ mm and } w_d \leq 6d$$

where s is the longitudinal stud spacing.

Equation [2.8] was found to provide much better correlation to test results than the CSA and Eurocode 4 provisions. The average absolute difference between the observed strengths and those predicted by Eq. [2.8] was found

to be 7.34%, compared to 40.72% and 63.85% for CSA and Eurocode, respectively. The standard deviation of the predicted values was estimated to be 0.0844. The better results provided by Eq. [2.8] were attributed to the fact that, unlike CSA and Eurocode 4 provisions, it takes into account the influence of the stud spacing.

The second phase of this investigation involved the testing of six full size composite beams by Androutsos and Hosain (1994). The first three beams featured a 150 mm thick concrete slab with a 76 mm HB 308 type narrow-ribbed metal deck. Standard 19x125 mm studs were welded onto the beam flange through the metal deck using a TR 2400 stud welder. The other three beams had a 102 mm thick concrete slab with a 38 mm HB 938 type narrow-ribbed metal deck. The headed studs used for these specimens were 16x76 mm.

The experimentally determined ultimate flexural capacity of the first three full size beam specimens agreed extremely well with the predicted values based on the proposed equation. However, for composite beams with 38 mm metal deck, the experimental values were somewhat higher than the predicted ones. This was not considered to reflect on the accuracy of Eq. [2.8] since the same degree of discrepancy was also observed when the actual push-out test results were utilized to predict the moment capacity. Equation [2.8] has recently been incorporated in the latest edition of the Canadian Standard (CSA 2001).

2.2.2.2 Wide Ribbed Deck

Currently, the Canadian Standard CAN/CSA-S16-01 (CSA 2001) specifies that Eq. [2.3], which is based on test results of push-out specimens with solid slabs, can also be applied for calculating the stud capacity in wide ribbed metal decks, i.e., when the width to height ratio (w_d/h_d) of the metal deck exceeds 1.5. AISC and Eurocode 4 also provide the same specification. However, a study by Gnanasambandam and Hosain (1996) has raised some doubts concerning the reliability of this approach. Equation [2.1] does not take into account the effects of stud spacing and transverse reinforcement. Moreover, the current approach ignores the influence of the w_d/h_d ratio.

A parametric study was conducted by Wu and Hosain (1997) to evaluate the effects of the aforementioned factors on the strength of headed studs in wide ribbed metal decks and, ultimately, to suggest an alternate formulation. A total of 44 push-out specimens and 4 full size beam specimens with wide ribbed metal deck were tested. A general form of the proposed equation was first established in terms of 11 different coefficients. A least squares regression analysis of test results yielded a long and complex expression. After a series of regression analyses, the following simplified version was recommended:

$$q_u = \left(0.264\left(\frac{S_\ell}{d}\right) + 0.821\frac{w_d}{h_d} + 3.120 \right) dh\sqrt{f'_c} \qquad [2.9]$$

$$0.30 \le \frac{S_t}{W_d} \le 0.63 \;\; ; \;\; 3 \le \frac{S_\ell}{d} \le 8$$

where:

q_u = Predicted ultimate load per stud (N)

S_ℓ = Longitudinal stud spacing (mm)

S_t = Transverse stud spacing (mm)

The average absolute difference between the observed values and those predicted by Eq. [2.9] was found to be 5.5%. The average arithmetic mean of the test/predicted ratio (μ), the standard deviation (σ) and the coefficient of variation (C.V.) for this equation were 1.024, 0.078 and 7.6%, respectively.

The proposed equation, i.e. Eq. [2.9], was used to predict the ultimate moment values of the four full size beams. The average absolute difference between the observed ultimate moments and those predicted by Eq. [2.9] was found to be 2.36%. The average arithmetic mean of the test/predicted ratio (μ), the standard deviation (σ), and coefficient of variation (C.V) were 1.019, 0.022 and 2.2%, respectively.

No other comprehensive research project on headed stud connectors has been undertaken in North America in recent years. However, some useful research is underway at the University of Western Sydney.

The results of an experimental investigation were used by Patrick and Bridge (2000) to develop a standard reinforcing component that could be used in deck slabs to prevent a rib shear failure. This component consisted of a waveform piece of reinforcing mesh laid directly on the profiled steel sheeting, to locally reinforce the concrete around the welded stud connector.

Another study on the performance of lying stud connectors (studs placed horizontally) is in progress at University of Stuttgart (Kuhlmann and Breuninger 2000). The objective of this research is to investigate the possibility of eliminating the top flange of the beam.

Ernst and Patrick (2004) developed an innovative, steel performance-enhancing device called STUDRING. In this approach, a helix shaped reinforcing element consisting of mild steel wire is placed over the studs, thereby increasing the rated shear strength and stiffness of the headed studs.

2.3 New Shear Connectors

The perfobond rib connector shown earlier in Fig. 1.6 was developed by the German consulting engineering firm, Leonhardt, Andra, and Partners of Stuttgart, during the design of the 3rd Caroni Bridge in Venezuela, as a solution to fatigue problem encountered with headed stud shear connectors (Zellner 1987). In order to investigate the possibility of using perfobond rib connectors in composite floor systems in buildings, an experimental program was conducted at University of Saskatchewan by Veldanda and Hosain (1992). The test results indicated that the perfobond rib shear connector was a viable alternative to headed stud connectors. An appreciable improvement in the shear capacity of the connection was observed when additional reinforcing bars were passed through the perfobond rib holes.

Additional push-out tests (Oguejiofor and Hosain 1994) and full size beam tests (Oguejiofor and Hosain 1995) further confirmed the viability of perfobond rib connectors and resulted in the development of a semi-empirical equation to evaluate the shear strength of perfobond rib

connectors. It was revealed that passing of transverse reinforcing bars through the perfobond rib connector holes increased the ultimate capacity of the connection by over 30%.

Quddusi and Hosain (1993) noted that, although the addition of transverse reinforcing bars through the perfobond rib connector holes increased the ultimate capacity of the connection, passing reinforcing bars through the rib holes in an actual construction site may be cumbersome. Introduction of vertical slits in the perfobond ribs would greatly simplify the task as well as increase the flexibility of the perfobond connector. Two series of tests involving 24 push-out specimens were carried out to investigate the effectiveness of slotted perfobond rib connectors in comparison to normal perfobond rib connectors and headed studs.

The test results indicated that slotted perfobond rib connectors improved the overall ductility of the test specimens. However, the increased concrete dowel area provided by the slots tended to eclipse its flexibility characteristics in the initial stages. The flexibility of a perfobond rib connector can also be enhanced by reducing the thickness of the plate. Besides savings in the cost of material, thinner plates would allow punching of holes rather than drilling. Two additional series of tests involving 24 push-out specimens indicated that the flexibility of the connector was greatly enhanced by reducing the thickness of the plate, without a drastic reduction in shear capacity.

Other innovative applications are being investigated in Australia (Roberts and Heywood 1992). Further research is in progress in Europe (Studnicka et

al. 2002) and Japan (Nishido et al. 2002) for a better understanding of the behaviour of perfobond rib connectors.

The Hilti Corporation, located in Liechtenstein, has developed a mechanical type of shear connector, which can be nailed on to a steel flange using a special fastening device. The fastening device is a powder-actuated tool equipped with a special base plate to hold the shear connector during the fastening operation. The major advantage is that no electricity is needed for the installation. The manufacturer carried out some proprietary investigations to ascertain the strength of these connectors; some push-out tests have also been conducted in Europe (Crisinel 1987). However, the author is not aware of a comprehensive test program conducted in North America. Some concerns have been expressed that, unless extreme caution is taken, the nails may cause injury to persons working on the floor below.

2.4 Channel Shear Connectors

A review of literature indicated that very little research work has been done on channel shear connectors. The test results of full size and push out specimens were reported in a University of Illinois Bulletin by Viest et al. (1952). This preliminary study was focused on understanding the behaviour of channel shear connectors and evaluating the feasibility of using channels as shear connectors. Forty three push-out specimens and four full size T-beams were tested in this experimental program. In most of the specimens, 4 inch (102 mm) high channel connectors were used. Only two specimens had 5 inch (127 mm) channels and three specimens had 3 inch (76 mm) high channel connectors.

The test results revealed that flange thickness, web thickness and length of the channel affected the behaviour of a channel connector. The orientation of the channel connector, i.e. whether the load was applied on the face or back of the channel, had no significant effect on the behaviour of the channel shear connector. Other conclusions drawn from this work were that the flange thickness and the size of the fillet of the channel were considered to be important factors as critical concrete pressure and maximum moments are located near the fillet. As discussed in the report, the data for eight specimens were either unreliable or missing due to various experimental difficulties encountered during the tests. Also, the number of specimens tested for each variable was considered to be inadequate. Thus, a reliable formulation for the design of channel shear connectors could not be made. Although this research provided a good understanding of the contribution of different channel parameters, a detailed research on channel connectors was still required.

The results of tests on small-scale push out specimens with shear connectors were reported by Rao (1970). The experimental work was conducted at University of Sydney and involved the testing of different types of mechanical connectors. The main categories of the shear connectors were bond type connectors (i.e. hook, loop and spiral), rigid shear connectors (i.e., angle, T-bar and rectangular bar) and flexible shear connectors (viz. channel, z-section and stud shear connectors). The bond between the beam and the concrete slab was prevented by coating the flanges of the joist with a thin film of oil. This was done to ensure that the strength and behaviour of the connectors alone was obtained from the test. All of the push-out specimens were cast in a horizontal position. The specimens were then tested in a

hydraulic machine with continuous increments of load applied until the failure of the specimen. After the completion of a series of push-out tests, the most promising connectors were used in full-size beam tests. The test results indicated that the channel shear connectors provided reasonable flexibility and had much greater load carrying capacity than the headed stud type of flexible connectors.

The results of another experimental study on shear connectors carried out at the Lehigh University were reported by Slutter and Driscoll (1965). The overall test program involved testing of push-out and beam specimens with headed stud connectors, spiral connectors and channels. Five beam specimens were tested with channel shear connectors, of which four involved 4 inch (102 mm) high channels and one had three inch (76 mm) high channels. The study also included 41 push-out specimens with channel connectors. As indicated earlier in Chapter 1, 34 of these specimens featured 4 inch (102 mm) high channels, five specimens had 3 inch (76 mm) high channels, and only two featured 5 inch (127 mm) high channels. A total of 35 out of the 41 push-out specimens had six inch (152 mm) long channels. Four specimens had 4 inch (102 mm) long channels, while 5 inch (127 mm) and 8 inch (204 mm) long channels were used in the other two.

The current American Standard (AISC 1993) provides the following equation for calculating the strength of a channel shear connector embedded in a solid concrete slab:

$$Q_n = 0.3\,(t_f + 0.5t_w)Lc\,\sqrt{f'_c}\,E_c \qquad [2.10]$$

where:

Q_n = Nominal strength of one channel shear connector

t_f = Flange thickness of channel shear connector (inches)

t_w = Web thickness of channel shear connector (inches)

Lc = Length of channel shear connector (inches)

f'_c = Specified compressive strength of concrete in ksi

E_c = Modulus of elasticity of concrete in ksi

This equation is a slightly modified form of the formula developed by Slutter and Driscoll (1965). The factor E_c has been introduced into Eq. [2.10] to extend its use to determine the shear strength of channel connectors with different weights of concrete.

Since this equation is also based on the Lehigh test results, the limitations indicated earlier in connection with the CSA version of the formula (Eq. 1.1) will also apply here. Although wide ribbed metal decks are the most common type of deck profile used in composite construction in North America, no equation is currently available for the design of channel shear connectors embedded in concrete slabs with ribbed metal deck.

The European standard on the design of composite steel and concrete structures (Eurocode 4; CEN 2001) provides a formulation for the design of a rigid channel connector. The typical orientation of this connector is as shown in Fig. 2.2. This connector is referred to as a block connector. Because of the orientation of the channel, a steel tie is provided to prevent uplift.

Figure 2.2 Rigid channel shear connector.
[Picture taken from Eurocode 4; CEN 2001]

The design resistance (P_{Rd}) of this type of connector is as follows:

$$P_{Rd} = \eta A_{f1} F_{ck} / \gamma_c \qquad [2.11]$$

where:

A_{f1} = Area of the front surface, as shown in Fig. 2.3

A_{f2} = Area of the front surface enlarged at a slope of 1:5 to the rear surface of the adjacent connector (Fig. 2.3).

η = $\sqrt{Af2/Af1}$, but not greater than 2.5 for normal density concrete or 2 for lightweight aggregate concrete.

γ_c = Partial safety factor for concrete.

These block shear type of connectors are very rigid, and the need to provide an additional tie makes it unpopular in North America.

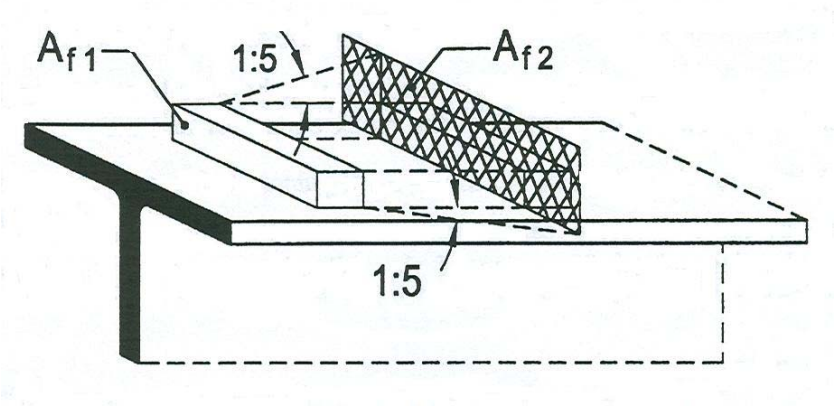

Figure 2.3 Parameters of rigid shear connectors.
[Picture taken from Eurocode 4; CEN 2001]

In the European standard, the strength (P_{Rd}) of an angle shear connector in a solid slab (as shown in Fig. 2.4) is given as:

$$P_{Rd} = 10bh^{3/4} f_{ck}^{2/3} / \gamma_v \qquad [2.12]$$

where:

P_{Rd} is in Newtons

b = Length of the angle (mm)

h = Width of the upstanding leg of the angle (mm)

f_{ck} = Characteristic strength of concrete in N/mm^2

γ_v = Partial safety factor, taken as 1.25 for the ultimate limit state

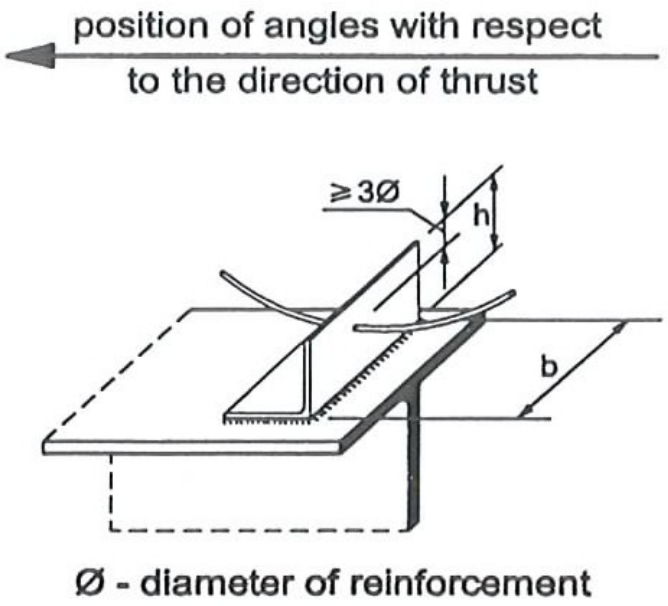

Figure 2.4 Angle shear connector as used in Europe.
[Picture taken from Eurocode 4; CEN 2001]

As shown in the figure, the hoop reinforcement is provided to prevent uplift. A channel connector in a vertical orientation (i.e. resting on one flange and the other flange embedded into the concrete), would be a better alternative as the top flange of the connector would provide resistance to uplift, eliminating the need to provide a hoop, as well as provide a more flexible shear connector.

Results of an experimental study carried out in Japan on the flexible shear connectors in composite girder bridges were reported by Hidehiko and Hosaka (2002). The conclusions drawn from this study indicated that the flexible shear connectors were very useful in reducing the tensile stresses generated in the negative moment regions at the intermediate supports of a continuous span bridge. This type of connector also behaved very well in resisting fatigue loading, especially in bridges.

Because of the advantages discussed earlier, further research on channel shear connectors is warranted. Re-evaluation of the current North American provisions for evaluating the shear capacity of channel connectors embedded in solid concrete slabs is essential. Moreover, since composite beams with ribbed metal decks are gaining popularity in the construction of high rise buildings, there is a definite need to develop new formulations for the design of channel shear connectors in slabs with ribbed metal deck. This thesis attempts to address these objectives.

CHAPTER THREE

EXPERIMENTAL PROGRAM

3.1 Preamble

The experimental program involved the testing of 78 push-out specimens with channel shear connectors. The testing was done in two different phases. Phase 1 consisted of three series, each with twelve push-out specimens. Six specimens in each series had solid concrete slabs, while the other six had concrete slabs with wide ribbed metal deck. All the specimens of this phase featured 127 mm high channels. In Phase 2, 36 push-out specimens were tested in three series, but with 102 mm high channels.

The test specimens were designed to study the effects of a number of parameters on the shear capacity of the channel shear connectors. The test parameters included the compressive strength of concrete, as well as the length, height and web thickness of the channel connector.

3.2 Test Program

As shown in Fig. 3.1, a push-out specimen consisted of two identical reinforced concrete slabs attached to the flanges of a short steel wide flange section (W200x59) by means of shear connectors. The assembly was subjected to a vertical load which produced shear load along the interface between the concrete slab and the steel beam flange on both sides. The shear load was transferred to the concrete slabs through shear connectors. As shown in the figure, a recess of 100 mm was provided between the bottom

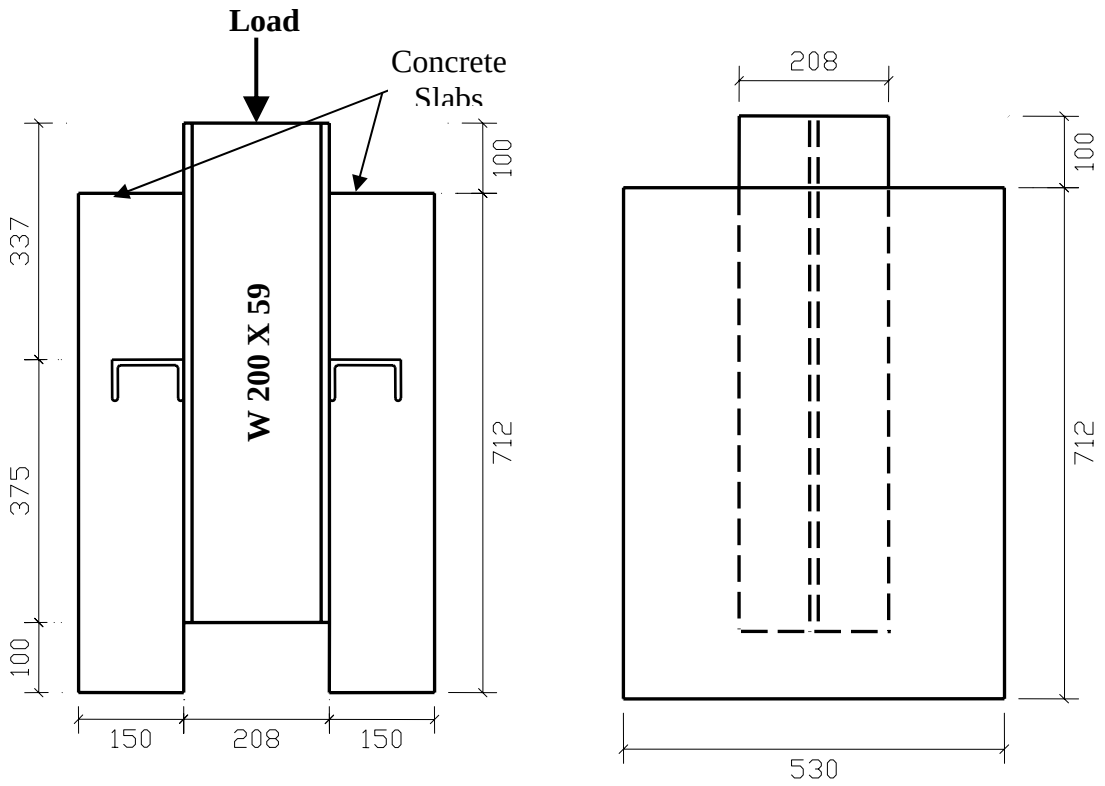

(a) Side view (b) Front view

Figure 3.1 Push-out specimen with solid concrete slab (dimensions in mm).

of the slab and the lower end of the steel beam to allow for the slip at the steel-concrete interface during testing. The overall thickness of the slabs in all of the specimens was 150 mm. The height and width of the slabs were 712 mm and 530 mm, respectively, in all of the specimens. These dimensions were similar to those used in earlier tests at the University of Saskatchewan (Wu and Hosain 1999, Androutsos 1994).

For all push-out specimens in this test program, the distance between the web of the channel connector and the bottom of the slab was kept constant at 475 mm, as shown in Fig. 3.2. The channel connector was welded directly to the beam flange. In all cases, 6 mm (E49XX electrodes) fillet welds were used. In the specimens featuring metal deck slabs, a rectangular opening was

made in the metal deck at the location of the channel connector and the metal deck was then lowered onto the beam flange. Parallel wide ribbed metal deck of type HB 30V, 75 mm in height, was used (VicWest 2002). The metal deck profiles and material properties provided by the manufacturer are presented in Appendix A.

As shown in Fig. 3.2, longitudinal reinforcement in all the specimens, consisted of four No.10 bars (diameter = 11.3 mm). These reinforcing bars were placed at a centre to centre spacing of 160 mm. For transverse reinforcement, four No.10 bars were again used. These bars were placed 25 mm from the bottom of the slab in the case of the solid slab; in the case of specimens with metal deck slabs, these bars were placed 25 mm above the metal deck. The longitudinal reinforcing bars were placed on the top of these bars. A single layer of 152 x 152 x MW 25.8 welded wire mesh, placed at a distance of 25 mm from the top surface of the slab, was used in the slabs of all specimens. Construction details of the test specimens are summarized in Appendix B.

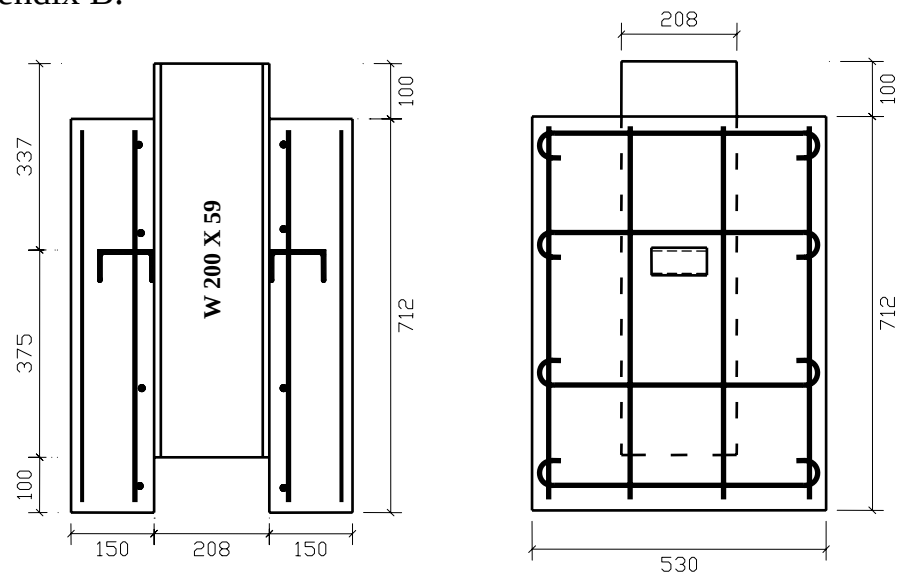

Figure 3.2 Rebar details: push-out specimen.

The slabs of all the push-out specimens were cast horizontally, to simulate the actual casting condition in a composite beam. In Phase 1, the specimens were fabricated using the University of Illinois technique. This technique involved casting the two slabs of a push-out specimen at different times. Five days were allowed for the concrete of the first slab to gain sufficient strength. The specimens were then flipped upside down and the other slab was cast exactly a week after the first slab. A slightly higher strength concrete was ordered for the second slab to compensate for the one week time lag. During the casting of the concrete specimens, twenty-four 6 inch (152 mm) diameter x 12 inch (304 mm) long concrete cylinders were prepared for each pour. The concrete strength was monitored for both the slabs at regular intervals with the intension that the specimens could be tested when both slabs attained approximately the same concrete strength. Since the concrete was supplied by a ready-mixed concrete supplier, the concrete strengths could not be precisely controlled, which resulted in the necessity of testing when the two slabs had unequal strengths.

To be able to pour concrete in both the slabs of a push-out specimen at the same time, the German method of fabrication was adopted in Phase 2. This technique was more complicated than that used in Phase 1, but yielded greater reliability and better results. In this technique, the steel I-beam section was cut along the middle of the web into two identical T-sections. After the concrete slabs had been cast on both the flanges separately, the companion T-sections were welded back together.

3.3 Description of Specimen Characteristics

3.3.1 Description of Specimens of Phase 1

As indicated earlier, six specimens in each series had solid concrete slabs and another six specimens had slabs with parallel wide ribbed metal deck. The push-out specimens in Series A, B and C of Phase 1 were fabricated using 127 mm high channels of type C130x13 and C130x10. As shown in Fig. 3.3, each push-out specimen in this test program was designated by one capital letter indicating the name of the series followed by the serial number of the specimen and either S or D, indicating a solid slab or metal deck slab, respectively. The test parameters included the compressive strength of concrete, as well as the length, height and web thickness of the channel connector. Individual characteristics of each series are described in detail below.

3.3.1.1 Test Series A

All twelve specimens of this series had 150 mm thick solid concrete slabs. Initially, it was decided to test the specimens in duplicate; hence, the specimens in this series were designated in a different way than other series. For the push-out specimens in this series, the first capital letter in the designation indicated the name of the series followed by the serial number of the specimen. The lowercase letters “a” and “b” identified the companion specimens.

Referring to Fig. 3.3 and Table 3.1, the lengths of channels in specimens A1a, A2a and A3a was 50.8 mm, 101.6 mm and 152.4 mm, respectively. In these three specimens, C130x13 channels with a web thickness of 8.3 mm

were used. The test parameters in specimens A4a, A5a and A6a were identical, except that in these three specimens, C130x10 channels with a web

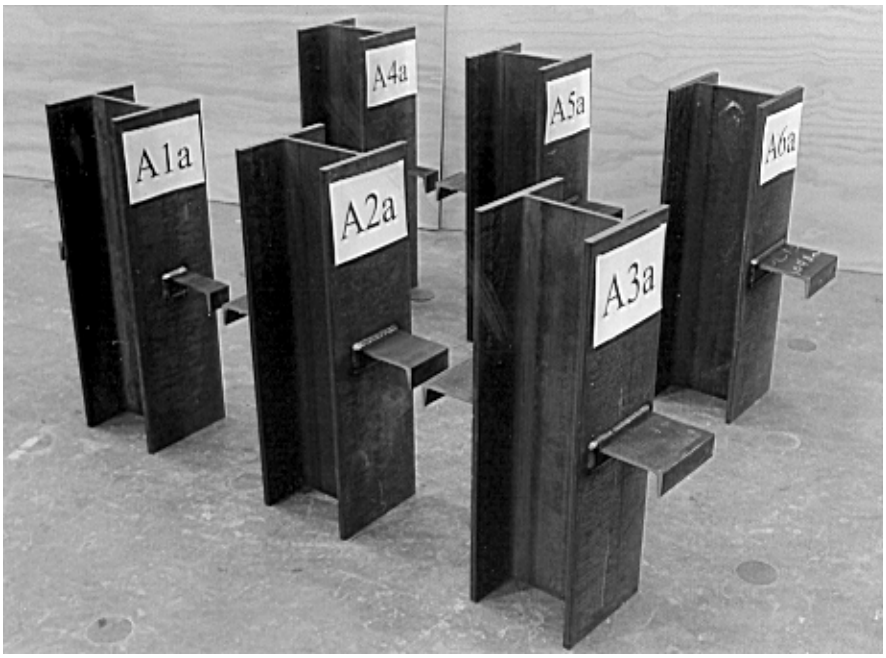

(a) Specimens with solid slabs.

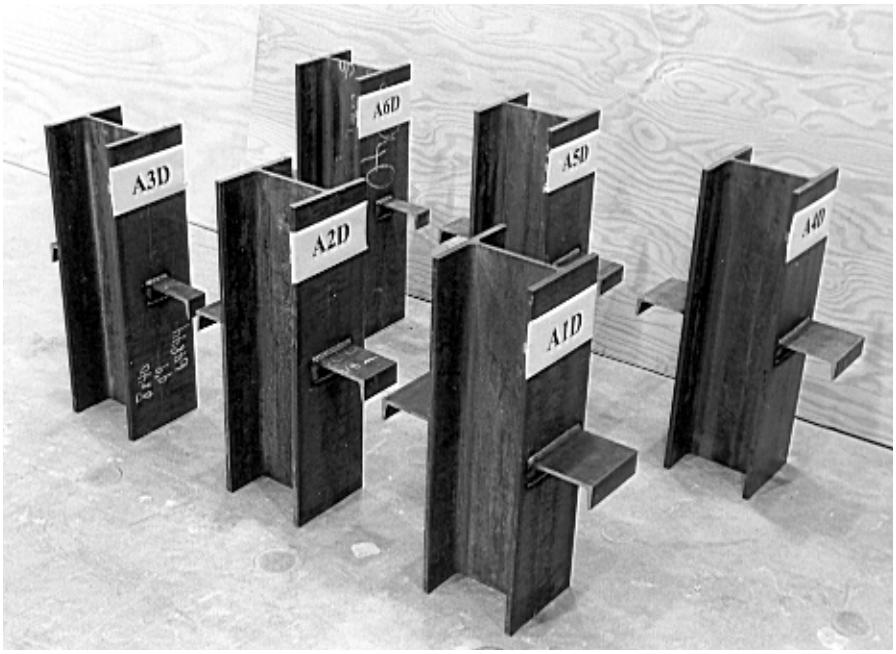

(b) Specimens with metal deck slabs.

Figure 3.3 Push-out specimens: Series A.

Table 3.1 Specimen Characteristics of Series A, B and C

Series	Specimen	f'c (MPa) Slab 1	f'c (MPa) Slab 2	Channel Details Type	L (mm)	d (mm)	w (mm)	Slab Type
A (12 Specimens)	A1a	f'c = 30.49 n = 24 σ = 0.34 COV= 1.1%	f'c = 33.87 n = 24 σ = 0.39 COV= 1.1%	C130 x 13	152.4	127	8.3	Solid
	A1b			C130 x 13	152.4	127	8.3	Solid
	A2a			C130 x 13	101.6	127	8.3	Solid
	A2b			C130 x 13	101.6	127	8.3	Solid
	A3a			C130 x 13	50.8	127	8.3	Solid
	A3b			C130 x 13	50.8	127	8.3	Solid
	A4a			C130 x10	152.4	127	4.8	Solid
	A4b			C130 x10	152.4	127	4.8	Solid
	A5a			C130 x10	101.6	127	4.8	Solid
	A5b			C130 x10	101.6	127	4.8	Solid
	A6a			C130 x10	50.8	127	4.8	Solid
	A6b			C130 x10	50.8	127	4.8	Solid
B (12 Specimens)	B1S	f'c = 18.65 n = 24 σ = 0.35 COV= 1.9%	f'c = 24.24 n = 24 σ = 0.2 COV= 0.8%	C130 x 13	150	127	8.3	Solid
	B2S			C130 x 13	100	127	8.3	Solid
	B3S			C130 x 13	50	127	8.3	Solid
	B4S			C130 x 10	150	127	4.8	Solid
	B5S			C130 x 10	100	127	4.8	Solid
	B6S			C130 x 10	50	127	4.8	Solid
	B1D			C130 x 13	150	127	8.3	Deck
	B2D			C130 x 13	100	127	8.3	Deck
	B3D			C130 x 13	50	127	8.3	Deck
	B4D			C130 x 10	150	127	4.8	Deck
	B5D			C130 x 10	100	127	4.8	Deck
	B6D			C130 x 10	50	127	4.8	Deck
C (12 Specimens)	C1S	f'c = 37.0 n = 24 σ = 0.34 COV= 0.9%	f'c = 44.9 n = 24 σ = 0.57 COV= 1.3%	C130 x 13	150	127	8.3	Solid
	C2S			C130 x 13	100	127	8.3	Solid
	C3S			C130 x 13	50	127	8.3	Solid
	C4S			C130 x 10	150	127	4.8	Solid
	C5S			C130 x 10	100	127	4.8	Solid
	C6S			C130 x 10	50	127	4.8	Solid
	C1D			C130 x 13	150	127	8.3	Deck
	C2D			C130 x 13	100	127	8.3	Deck
	C3D			C130 x 13	50	127	8.3	Deck
	C4D			C130 x 10	150	127	4.8	Deck
	C5D			C130 x 10	100	127	4.8	Deck
	C6D			C130 x 10	50	127	4.8	Deck

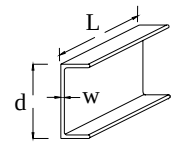

Channel Connector

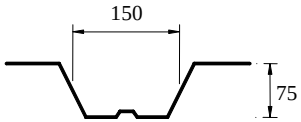

Metal Deck Profile

f'c = Comp. Strength of Concrete
n = Number of Cylinders Tested
σ = Standard Deviation
COV = Coefficient of Variation

Table 3.1 (cont'd) Specimen Characteristics of Series A*

Series	**Specimen**	**f'c** (MPa) Slab 1	Slab 2	**Channel Details** Type	L (mm)	d (mm)	w (mm)	**Slab Type**
A* (6 Specimens)	A1D	f'c = 27.14 n = 24 σ = 0.32 COV= 1.2%	f'c = 33.42 n = 24 σ = 0.38 COV= 1.8%	C130 x 13	152.4	127	8.3	Deck
	A2D			C130 x 13	101.6	127	8.3	Deck
	A3D			C130 x 13	50.8	127	8.3	Deck
	A4D			C130 x 10	152.4	127	4.8	Deck
	A5D			C130 x 10	101.6	127	4.8	Deck
	A6D			C130 x 10	50.8	127	4.8	Deck

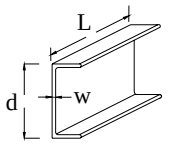

Channel Connector

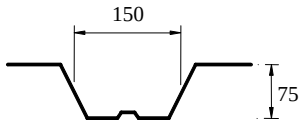

Metal Deck Profile

f'c = Comp. Strength of Concrete
n = Number of Cylinders Tested
σ = Standard Deviation
COV = Coefficient of Variation

thickness of 4.8 mm were used. As indicated earlier, all specimens in Phase 1 featured 127 mm high channel shear connectors. As shown in Table 3.1, the average compressive strength of concrete in slab 1 and slab 2 was 30.49 and 33.87 MPa, respectively. Twenty four concrete cylinders were tested to determine the average compressive strength of each slab. The standard deviation and the coefficient of variation of the concrete strengths of this series, as well as those for the other two series, are listed in Table 3.1.

After the observation of the test results of this series, the behaviour and performance of the two companion specimens was found to be almost the same (Table 4.2). Hence, for further testing, only one specimen was tested for each type of variable.

Six additional specimens, A1D – A6D (in Table 3.1), which were identical to the above mentioned six pairs of specimens except that they incorporated metal decks, were tested as part of Series A.

3.3.1.2 Test Series B

In this series, 12 push-out specimens with an over-all slab thickness of 150 mm were tested. However, six specimens were made with solid concrete slabs; in the other six, concrete slabs with parallel wide ribbed metal deck were used. These specimens were designated by a capital letter, indicating the name of the series, followed by the serial number of the specimen, and either S or D, identifying solid or deck slab, respectively.

Referring to Table 3.1, Specimens B1S, B2S and B3S were made with C130x13 channels whereas B4S, B5S and B6S were made with C130x10

channels. These specimens had solid concrete slabs. Specimens in group B1D to B3D and in group B4D to B6D also featured similar channel connector variables, but these specimens had concrete slabs with metal deck. Of the three different strengths of concrete used in Phase 1, this series had the lowest strength. The average compressive strengths of concrete in slabs 1 and 2 were 18.65 and 24.24 MPa, respectively.

3.3.1.3 Test Series C

Series C involved exactly the same variables as were used in Series B, except that a different concrete strength was used in the specimens of this series. As described in Table 3.1, the average compressive cylinder strengths of concrete used turned out to be 37.0 and 44.9 MPa in slab 1 and slab 2, respectively.

3.3.2 Description of Specimens of Phase 2

In this phase, 36 specimens were tested in three series, series D, E and F, each involving 12 specimens. Six specimens in each of these series had solid concrete slabs and the other six had slabs with parallel wide ribbed metal deck. Two types of channels, C100 x 11 and C100 x 8, with an overall channel height of 102 mm were used in all the specimens of Phase 2. As shown in Fig. 3.4, each push-out specimen in this phase was also designated by one capital letter, indicating the name of the series, followed by the serial number of the specimen, and a final letter (S or D), indicating solid slab or metal deck slab.

A different method of fabrication was adopted in series D, E and F of Phase 2, as compared to series A, B and C of Phase 1. The wide flange I-section was cut in the middle of the web to make two identical T-sections, as shown in Fig. 3.4. The concrete was poured on both flanges of the companion T-sections at the same time. The overall slab thickness was kept constant at 150 mm. The size and number of reinforcing bars as longitudinal and transverse reinforcement was kept the same as those used in Phase 1. A single layer of 152 x 152 x MW 25.8 welded wire mesh was also provided in all the slabs. Individual characteristics of all the series in Phase 2 are described in detail below.

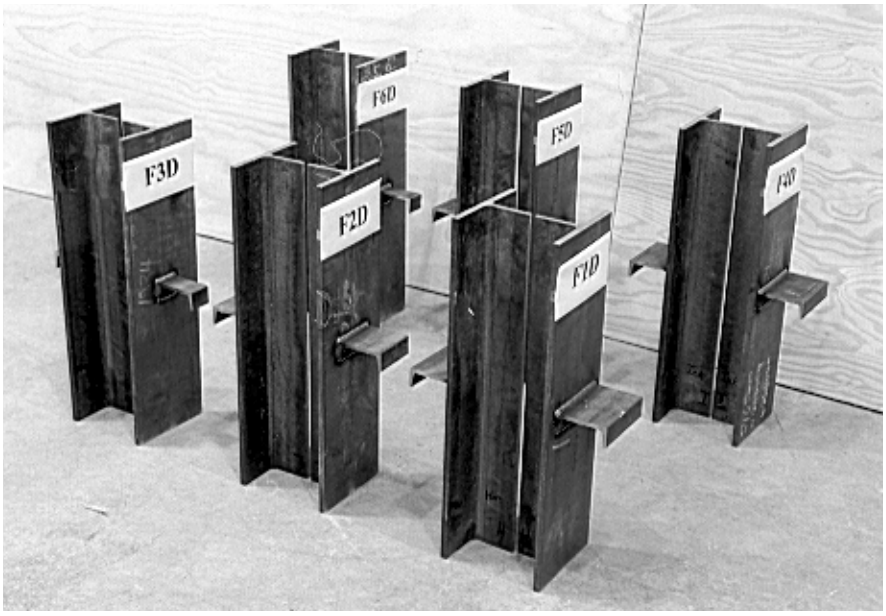

Figure 3.4 Push-out specimens: Series F.

3.3.2.1 Test Series D

The 12 specimens in this series were designated as D1S to D6S and D1D to D6D, following the same pattern described earlier in Section 3.3. Referring to Table 3.2, the lengths of the channel connectors in specimens D1S, D2S and D3S were 150 mm, 100 mm and 50 mm, respectively. For these specimens, C100 x 11 channels were used. Specimens D4S, D5S and D6S featured C100 x 8 channels and the variations in the channel length were again 150 mm, 100 mm and 50 mm, respectively. All these specimens had solid slabs. The companion set of specimens D1D, D2D, D3D and D4D, D5D and D6D had exactly the same connector details, but the concrete slabs in these specimens featured ribbed metal deck. The average compressive strength of concrete used in this series was 21.18 MPa. Once again, 24 concrete cylinders were tested. The standard deviation and the coefficient of variation of the concrete strengths of this series, as well as those for the other two series, are listed in Table 3.2.

3.3.2.2 Test Series E

The 12 specimens in this series were also fabricated using C100 x 11 and C100 x 8 channels. The variations in the parameters of channel connectors were exactly the same as those in the specimens of series D, but a different strength of concrete was used in the specimens of this series. The compressive strength of concrete was 34.8 MPa.

3.3.2.3 Test Series F

As listed in Table 3.2, Series F involved similar connector variables as those in Series D and E. However, the compressive strength of concrete used was 28.57 MPa.

Table 3.2 Specimen Characteristics of Series D, E and F

Series	Specimen	f'c (MPa) Both Slabs	Channel Details Type	L (mm)	d (mm)	w (mm)	Slab Type
D (12 Specimens)	D1S	f'c = 21.18 n = 24 σ = 0.34 COV= 1.62%	C100 x 11	150	102	8.2	Solid
	D2S		C100 x 11	100	102	8.2	Solid
	D3S		C100 x 11	50	102	8.2	Solid
	D4S		C100 x 8	150	102	4.7	Solid
	D5S		C100 x 8	100	102	4.7	Solid
	D6S		C100 x 8	50	102	4.7	Solid
	D1D		C100 x11	150	102	8.2	Deck
	D2D		C100 x11	100	102	8.2	Deck
	D3D		C100 x11	50	102	8.2	Deck
	D4D		C100 x 8	150	102	4.7	Deck
	D5D		C100 x 8	100	102	4.7	Deck
	D6D		C100 x 8	50	102	4.7	Deck
E (12 Specimens)	E1S	f'c = 34.8 n = 24 σ = 0.83 COV= 2.5%	C100 x 11	150	102	8.2	Solid
	E2S		C100 x 11	100	102	8.2	Solid
	E3S		C100 x 11	50	102	8.2	Solid
	E4S		C100 x 8	150	102	4.7	Solid
	E5S		C100 x 8	100	102	4.7	Solid
	E6S		C100 x 8	50	102	4.7	Solid
	E1D		C100 x11	150	102	8.2	Deck
	E2D		C100 x11	100	102	8.2	Deck
	E3D		C100 x11	50	102	8.2	Deck
	E4D		C100 x 8	150	102	4.7	Deck
	E5D		C100 x 8	100	102	4.7	Deck
	E6D		C100 x 8	50	102	4.7	Deck
F (12 Specimens)	F1S	f'c = 28.57 n = 24 σ = 0.44 COV= 1.53%	C100 x 11	150	102	8.2	Solid
	F2S		C100 x 11	100	102	8.2	Solid
	F3S		C100 x 11	50	102	8.2	Solid
	F4S		C100 x 8	150	102	4.7	Solid
	F5S		C100 x 8	100	102	4.7	Solid
	F6S		C100 x 8	50	102	4.7	Solid
	F1D		C100 x11	150	102	8.2	Deck
	F2D		C100 x11	100	102	8.2	Deck
	F3D		C100 x11	50	102	8.2	Deck
	F4D		C100 x 8	150	102	4.7	Deck
	F5D		C100 x 8	100	102	4.7	Deck
	F6D		C100 x 8	50	102	4.7	Deck

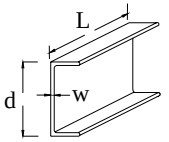

Channel Connector

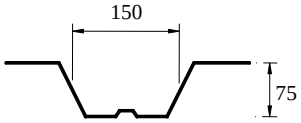

Metal Deck Profile

f'c = Comp. Strength of Concrete
n = Number of Cylinders Tested
σ = Standard Deviation
COV = Coefficient of Variation

3.4 Fabrication of Specimens

As shown in Fig. 3.5, the push-out specimens were fabricated using 712 mm long pieces of a W200 x 59 steel section. The channel connectors were cut to the appropriate lengths using a steel band saw in the College of Engineering Central Shop. The channels were then welded to the steel flanges of the steel sections by a certified welder. As indicated earlier, for all push-out specimens, the distance between the web of the channel connector and the bottom end of the concrete slab, i.e. the end distance, was kept constant at 475 mm. Welding was applied along all four sides of the channel connector to assure that the connector would not fail due to weld fracture.

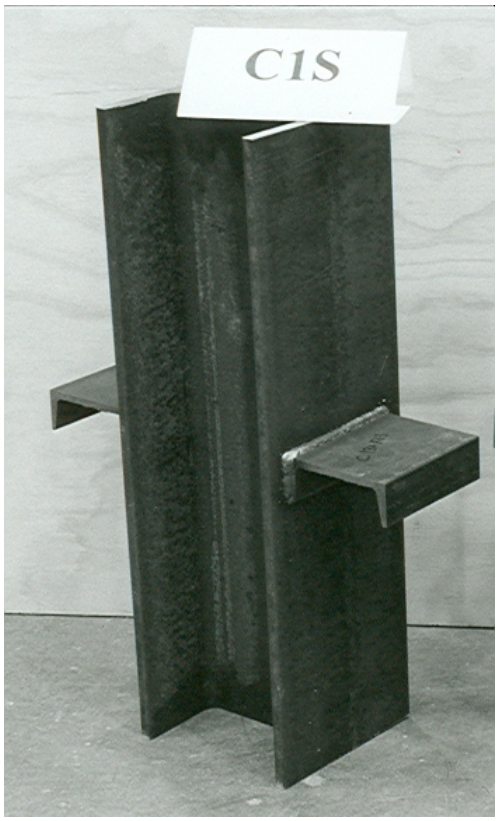

Figure 3.5 Push-out specimen: before concrete pouring.

After the welding of the channels, the W200 x 59 steel sections were supported on wooden planks and, as shown in Fig. 3.6, plywood forms were erected around the flange for casting concrete. These forms were constructed to ensure a 100 mm recess between the bottom end of the steel section and the end of the concrete slabs.

In the specimens with metal deck, a rectangular opening slightly larger than the channel connector was made at the location of the channel connector and the deck was then lowered onto the beam flange. The free edges of metal deck were supported by deck screws placed at 200 mm intervals along the side boards of the wooden forms.

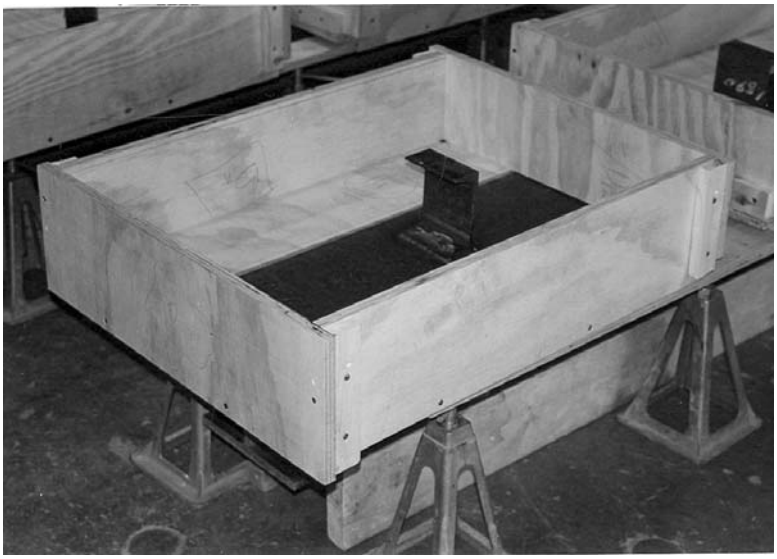

Figure 3.6 Typical formwork for push-out specimen.

In all specimens, the transverse reinforcement was placed first, followed by the longitudinal reinforcement. As indicated earlier, a concrete cover of 25 mm was provided for the transverse reinforcement. In order to achieve proper development length, standard 180^{o} hooks were provided for the

transverse reinforcement bars. A layer of 152 x 152 x MW 25.8 welded wire mesh was placed 25 mm from the top surface of slabs of all specimens.

The slabs of all the push-out specimens were cast horizontally, to simulate the actual casting conditions in a composite beam. Normal weight concrete was supplied by a local ready mixed plant. The concrete was delivered in the supply truck, as shown in Fig. 3.7. As shown in Fig. 3.8, the concrete was poured directly into the forms with the help of steel chutes attached to the truck. After pouring, the concrete was properly consolidated using a needle vibrator (Fig. 3.9).

Figure 3.7 Ready mix concrete truck.

In Phase 1, as described earlier in Section 3.2, the two slabs of a push-out specimen were cast at different times. After the pouring of the first slab, the concrete was allowed to gain sufficient strength. As shown in Fig. 3.10, the

specimens were then flipped upside down and the other slab was cast exactly a week after the first slab. As stated earlier, a slightly higher strength concrete was ordered for the second slab to compensate for the one week time lag. As shown in Fig. 3.11, a large number of concrete cylinders (6 inch diameter x 12 inch length) were prepared during each pouring. The concrete strength for both slabs was monitored regularly. It was intended that the specimens could be tested when both slabs attain approximately the same concrete strength. Since the concrete was supplied by a ready-mixed concrete supplier, the concrete strengths could not be precisely controlled and resulted in slabs with unequal strengths.

Figure 3.8 Concrete pouring in progress.

Figure 3.9 Vibrating and finishing.

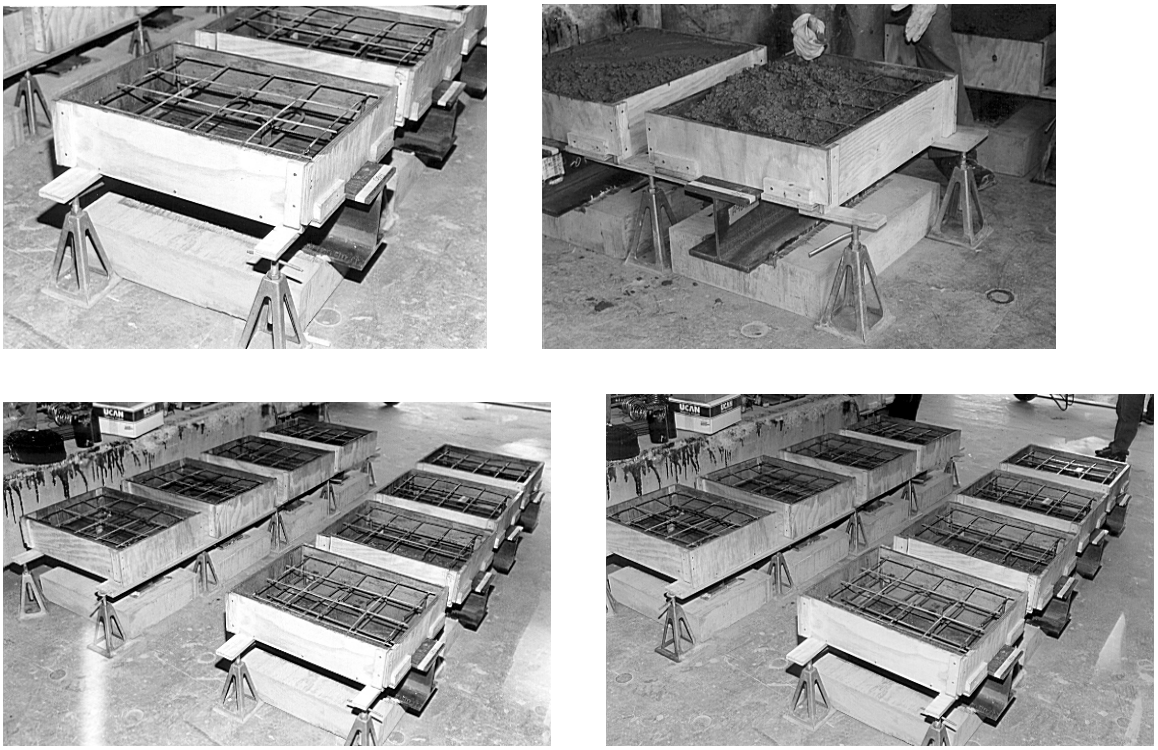

Figure 3.10 Pouring the second slab: Phase 1 specimens.

Figure 3.11 Preparation of concrete cylinders.

To eliminate the problem of unequal concrete strengths in the two slabs of the same specimen, it was decided to use a different fabrication technique for the push-out specimens of Phase 2. To be able to pour concrete in both the slabs of a push-out specimen at the same time, it was necessary to cut the steel I-beam section along the middle of the web into two identical T-sections. As shown in Fig. 3.12, a Hydro-jet Precision cutting machine was utilized to ensure enhanced accuracy of cutting with minimum loss of material. A jet of water containing abrasive material at pressure as high as 55,000 psi (379,212 kPa) was used to cut the steel. This technique avoided undue temperature stresses during the cutting process. The chances of warping and the development of additional stresses during the cutting of metal were therefore minimal with this cutting system.

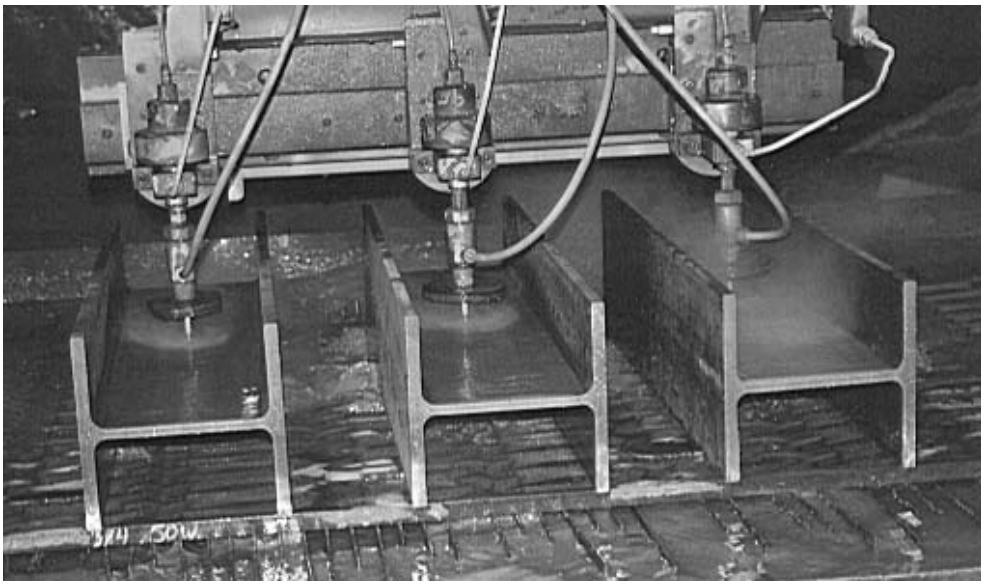

Figure 3.12 Hydro-jet precision cutting of I-beams.

As shown in Fig. 3.13, concrete was poured on the flanges of the two companion T-sections at the same time. After pouring of concrete, the forms were covered completely by a plastic sheet and the concrete was left to cure for two weeks. The plywood forms were then dismantled to be used again.

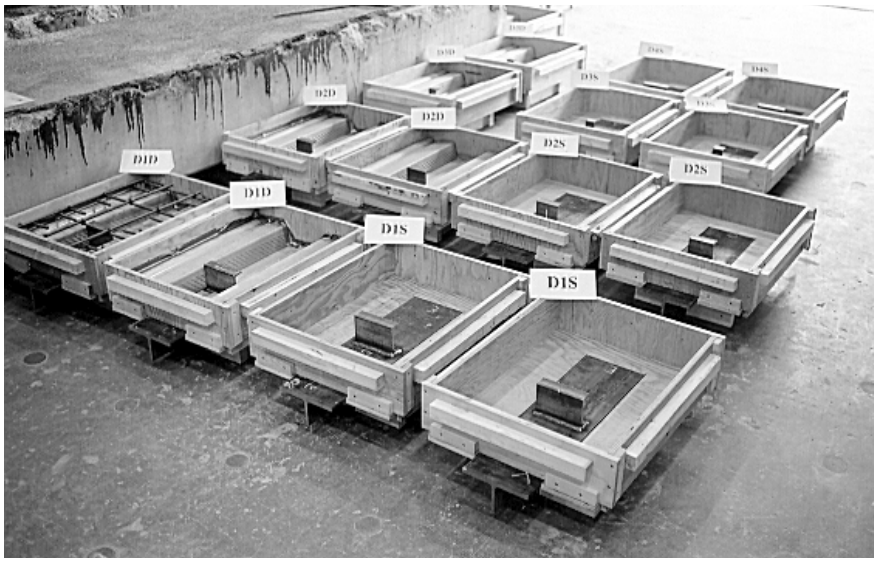

Figure 3.13 Pouring of concrete slabs: Phase 2 specimens.

As indicated earlier, the companion T-sections were welded back together after the casting of slabs to form the push-out specimens. Figure 3.14 shows a push-out specimen before the welding was applied. In order to ensure proper alignment, two 5/8 inch (16 mm) thick steel plates were placed on each side of the webs of these sections. These plates were clamped at both ends as well as in the middle. Referring to Fig. 3.15, welding was first applied along the four pre-cut openings in the steel plates. The steel plates were then removed and the welding was completed.

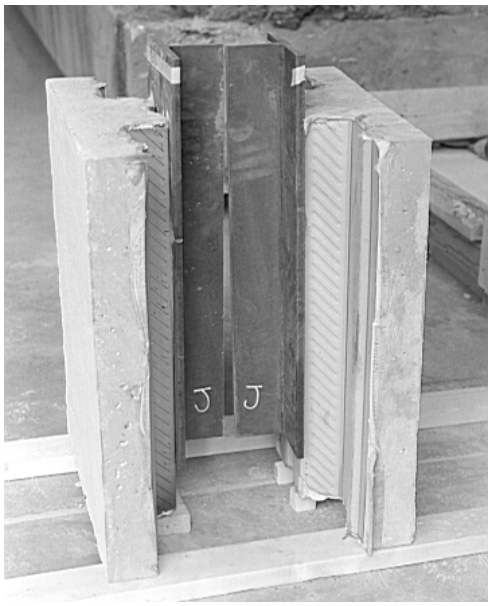

Figure 3.14 Companion T-sections of a push-out specimen.

Figure 3.15 Welding of T-sections of a push-out specimen.

3.5 Testing of Specimens

3.5.1 Test Setup and Instrumentation

The specimens were tested in an Amsler Hydraulic Testing Machine of 2000 kN loading capacity. A 50 mm thick steel plate, which served as a platform for the push-out specimens, was placed on the testing machine. Two pieces of 10 mm thick tentest press boards were placed at the point of contact of the push-out specimens with the steel plate to help distribute the load uniformly to the concrete slabs. The specimens were loaded onto the machine using a 10 ton crane. The position of a specimen was then adjusted until it was symmetrically placed on the base plate. At the top end of the specimens, a 25 mm thick steel plate was placed on the steel section. A distributing

spherical block was placed between this plate and the loading head of the testing machine, as shown in Fig. 3.16.

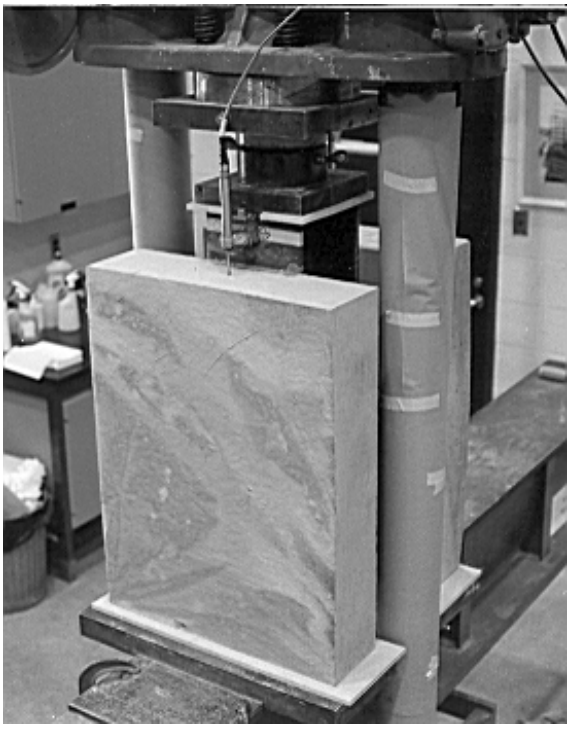

Figure 3.16 Typical test setup and instrumentation.

Two LVDT displacement transducers were installed on either side of the specimen to measure the slip at the interface of the concrete slab and the steel beam flange. The base of the LVDT was set against the top surface of the I-beam and the stem was set bearing against the centre of the top surface of the concrete slab. The displacement readings were recorded through a data acquisition system connected to the displacement transducers.

3.5.2 Test Procedure

All the specimens were tested under monotonic loading. Initially, the load was applied in increments of 50 kN; when the load-slip curve started to

deviate from a straight line, the load increment was reduced to 20 kN. At the non-linear stage, the applied load was recorded at 0.005 inch (0.127 mm) increments of slip. This was done to define the load-slip curve more accurately and record the deformation at the ultimate load. However, it was not possible to record any readings after the ultimate load for many specimens with channel rupture failure, because of the sudden failure of the shear connector. In specimens involving concrete related failures, the loading was continued until collapse occurred or a significant amount of load release had occurred beyond the ultimate load.

3.6 Material Properties

The properties of the materials used in this test program relating to channel connectors and beam sections for each series of tests were determined by tension tests. The properties of the reinforcing and wire mesh bars were also determined. The yield stress, ultimate stress and the percentage elongation properties of these materials are listed in Tables C-1 to C-4 of Appendix C. The determination of yield stress was based on the 0.2% offset rule.

CHAPTER FOUR

EXPERIMENTAL RESULTS

4.1 Failure Mechanisms and Load-Slip Behaviour

In this section, the experimental results related to the Push-out specimens are presented, along with a description of observed failure mechanisms. The main test results are shown in the form of load-slip curves. In all the load-slip graphs shown in this section, the abscissa represents the average slip in mm at the interface of the steel section and the concrete slab. The ordinate represents the load per connector in kN, i.e. the total load carried by the specimen is twice this value.

The failure modes observed in all the push-out specimens can be broadly classified into three types, as presented in Table 4.1.

Table 4.1 Failure Mechanisms

Failure Type	Description
(1)	Fracture of the Channel Connector
(2)	Concrete Crushing-Splitting
(3)	Concrete Shear Plane Failure

Photographs illustrating the three modes of failure are presented in the following sub-sections. The load-slip curves associated with the failure mechanisms are also included.

4.1.1 Failure Mode 1: Fracture of Channel Connector

(a) Phase 1 (solid slabs)

The characteristic feature of this failure mechanism was the fracture of the channel web near the fillet, with the channel acting like a cantilever beam. As shown in Fig. 4.1, one of the flanges remained attached to the steel section and the rest of the channel remained buried in the concrete slab, which appeared to be virtually intact. It is clear from Fig. 4.2 that the failure was caused by channel web fracture and not by shearing of the weld.

A close view of the failure surface of the channel web is shown in Fig. 4.3. The rectangular gap parallel to the sheared surface indicates the amount of deformation at the interface prior to failure. This specimen had a 150 mm thick solid concrete slab and featured a 100 mm long channel connector. The web thickness of the channel connector was 4.8 mm. As shown in Fig. 4.4, the maximum interfacial slip of this specimen was 9 mm. This figure illustrates the typical load-slip behaviour associated with this type of failure. The load-slip curve, although indicating quite ductile behaviour, ends abruptly, indicating a total loss of interaction between the concrete slab and the steel section at failure, a condition which occurred at or very soon after the ultimate load was reached. In Fig. 4.4, and in all subsequent load-slip curves related to Phase 1 specimens, the compressive strength of the concrete is that of the slab where failure occurred.

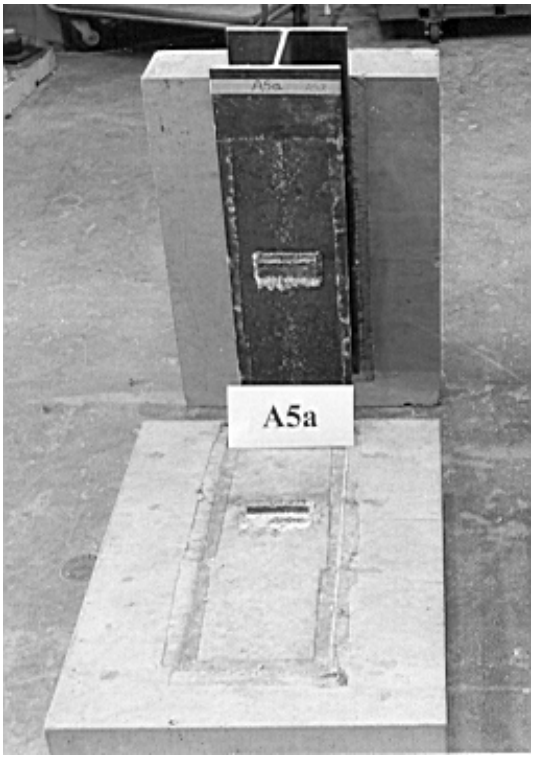

Figure 4.1 Channel fracture failure: Specimen A5a.

Figure 4.2 Channel fracture surface: part attached to the I-section.

Figure 4.3 Channel fracture surface: part embedded into the slab.

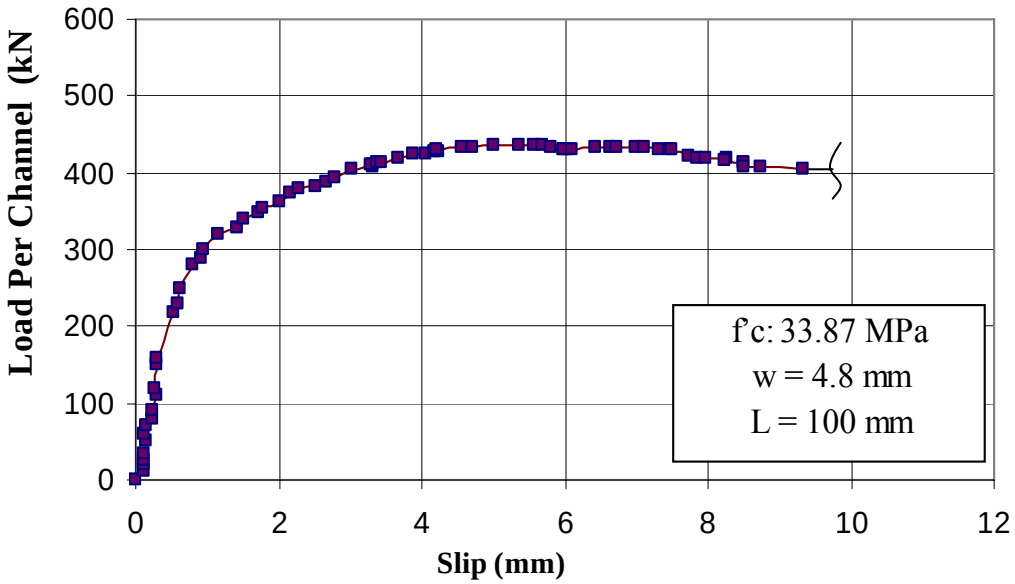

Figure 4.4 Load-Slip curve for specimen A5a.

As shown in Table 4.2, fracture of channel web was the most common type of failure in the push-out specimens with solid concrete slabs, especially in those with higher strength concrete. It was observed that channels with smaller length and/or smaller web thickness were more susceptible to channel fracture because of the smaller load carrying capacity of the connector.

(b) Phase 1 (metal deck slabs)

Channel fracture type of failure was not observed in most of the specimens with metal deck slabs in Phase 1. Fig. 4.5 shows specimen C3D after failure. The length of the channel connector for this specimen was the least (50 mm) and the compressive strength of the concrete was very high (44.9 MPa). Although the web thickness was 8.3 mm, this specimen failed due to web fracture. Once again, as shown in Fig. 4.6, the interfacial deformation produced a rectangular gap above the sheared web surface. The load-slip curve of this specimen also ends abruptly (Fig. 4.7).

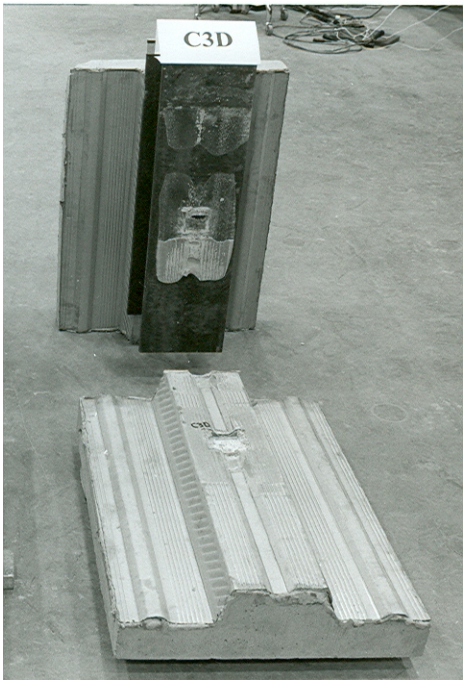

Figure 4.5 Channel fracture failure: specimen C3D.

Figure 4.6 Channel fracture surface: part embedded into the slab.

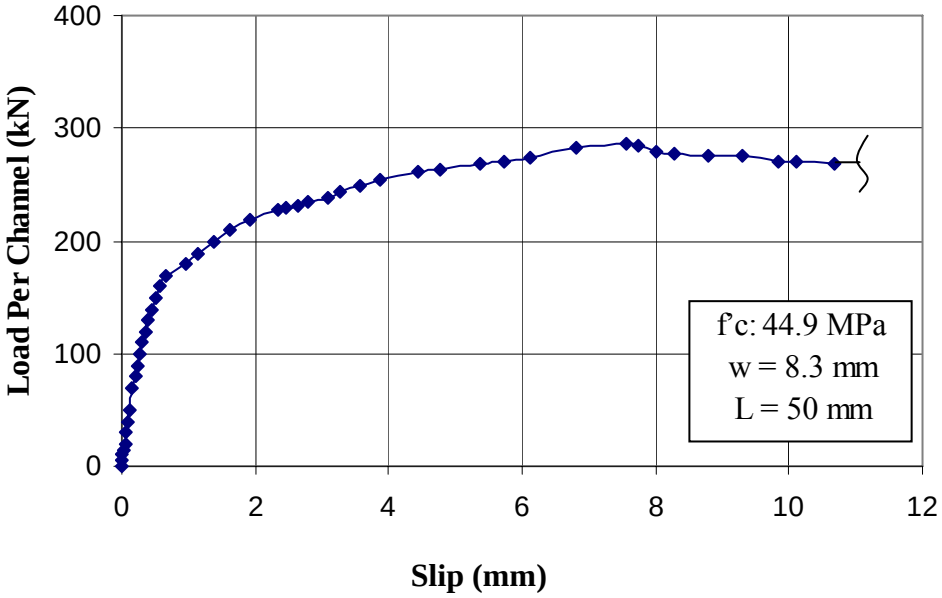

Figure 4.7 Load-Slip curve for specimen C3D.

(c) Phase 2 (solid slabs)

In Phase 2, with 102 mm high channels, web fracture failure was observed mainly in specimens with channel connectors of 50 mm length and 4.7 mm web thickness when lower or moderate strength concrete was involved. When higher strength concrete was used, specimens with even 150 mm long connectors failed due to web fracture. The web failure surface for specimen E4S is shown in Fig. 4.8. The length of the channel connector for this specimen was 150 mm and the web thickness was 4.7 mm. The compressive strength of the concrete was 34.8 MPa.

Figure 4.8 Channel fracture surface: part attached to the I-section.

(d) Phase 2 (deck slabs)

Channel fracture type of failure was not very common in the specimens of Phase 2 with metal deck slabs. Most of the specimens with metal deck slabs experienced concrete related failures because of the smaller concrete area of the flute surrounding the channel connector. Only two specimens, both involving 50 mm long channel connectors and 4.7 mm web thickness, failed due to channel web fracture. These specimens were made with moderate and high strength concrete of 28.57 and 34.8 MPa, respectively. The characteristics of the failure were very similar to those in the specimens described earlier in this section.

4.1.2 Failure Mode 2: Crushing-Splitting of Concrete

(a) Phase 1 (solid slabs)

In a few specimens with solid slabs made using low and moderate strength concrete, failure was initiated by concrete crushing followed by splitting of the concrete slab. This type of failure is illustrated in Figs. 4.9 and 4.10, showing the front and side views, respectively, of specimen A1a after failure. This specimen had a 150 mm long channel connector with an 8.3 mm web thickness. It had solid concrete slabs and the compressive strength of the concrete in the weaker slab was 30.49 MPa.

After the removal of the damaged concrete, it was observed that the channel connectors had undergone considerable deformations but remained attached to the steel section (Fig. 4.11). Fig. 4.12 shows the load-slip curve of the same specimen. It behaved linearly up to a load of 450 kN and developed a crack in the slab with lower concrete strength at the level of the channel connector at approximately 485 kN. As the applied load was increased,

splitting cracks were observed in both slabs. When the load reached 602 kN, the specimen started to unload. However, the specimen continued to support a significant amount of load, as reflected by the load-slip curve. It appears that even after the crushing of concrete, the friction between the cracked concrete surfaces continued to provide shear resistance. The concrete crushing-splitting type of failure provides considerable warning as the load carrying capacity decreases slowly.

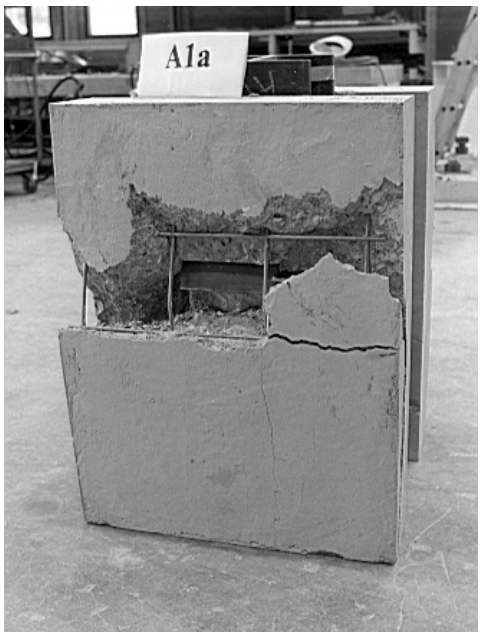

Figure 4.9 Concrete crushing-splitting failure: specimen A1a.

Of the 24 specimens with solid concrete slabs in Phase 1, the concrete crushing-splitting type of failure was observed in only four specimens, as indicated in Table 4.2.

Figure 4.10 Splitting of concrete: specimen A1a.

Figure 4.11 Channel deformation after failure: specimen A1a.

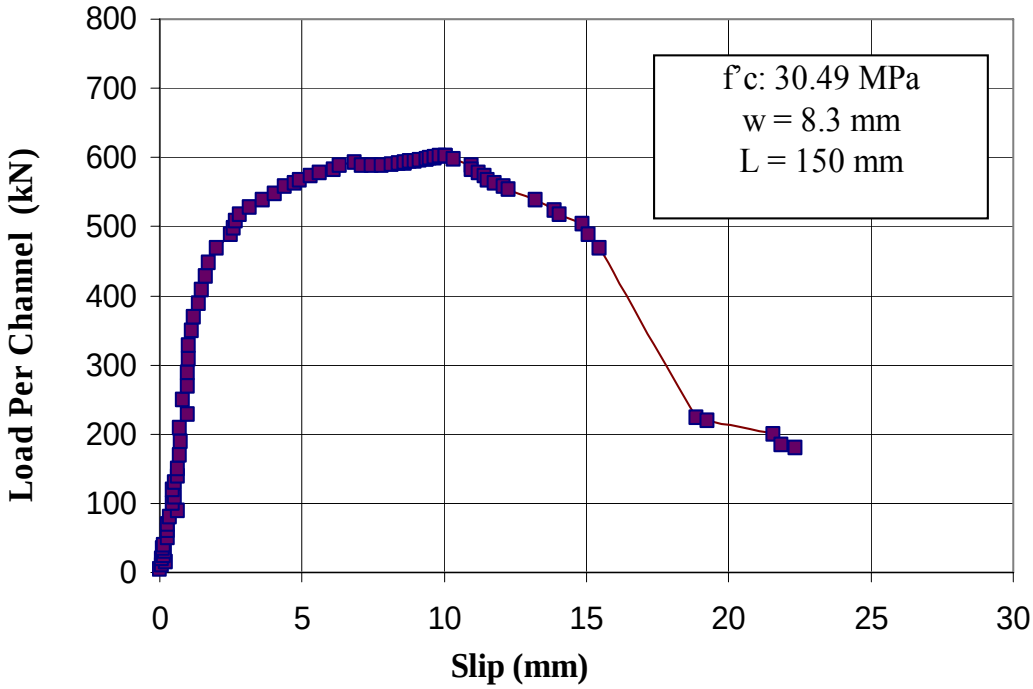

Figure 4.12 Load-Slip curve for specimen A1a.

(b) Phase 1 (deck slabs)

Of the 18 specimens with metal deck slabs in Phase 1, concrete related failures were observed in twelve specimens, as indicated in Table 4.2. Specimens with metal deck slabs are more susceptible to concrete related failures because of a very high concentration of stresses within a smaller area of concrete. In these specimens, failure was caused by the crushing of the concrete contained in the flute below the channel connector, as shown in Fig. 4.13, which shows specimen A2D after failure. This specimen (A2D) had 100 mm long channel connectors with an 8.3 mm web thickness. The overall thickness of the slab was 150 mm, including the 76 mm high metal deck. There was no sign of concrete splitting, as was observed in specimens with solid concrete slabs, as described above. Because of the small amount of concrete within the flute, crushing of concrete occurred before a significant amount of deformation took place in the channel connector.

Table 4.2. Specimen Failure Characteristics of Series A, B and C.

Series	Specimen	f'c (MPa) Slab 1	f'c (MPa) Slab 2	Channel Type	Failure Type	Failure Side	Failure Load per Channel (kN)
A	A1a	30.49	33.87	C130 x 13	Concrete crushing-splitting	Slab1	602.60
(12 specimens)	A1b	30.49	33.87	C130 x 13	Concrete crushing-splitting	Slab1	603.60
	A2a	30.49	33.87	C130 x 13	Channel Fracture	Slab1	472.10
	A2b	30.49	33.87	C130 x 13	Channel Fracture	Side2	474.10
	A3a	30.49	33.87	C130 x 13	Channel Fracture	Both	288.85
	A3b	30.49	33.87	C130 x 13	Channel Fracture	Slab2	295.80
	A4a	30.49	33.87	C130 x10	Channel Fracture	Slab1	563.75
	A4b	30.49	33.87	C130 x10	Channel Fracture	Slab2	576.70
	A5a	30.49	33.87	C130 x10	Channel Fracture	Slab2	436.25
	A5b	30.49	33.87	C130 x10	Channel Fracture	Slab2	464.15
	A6a	30.49	33.87	C130 x10	Channel Fracture	Slab2	250.50
	A6b	30.49	33.87	C130 x10	Channel Fracture	Slab2	256.95
B	B1S	18.65	24.24	C130 x 13	Concrete crushing-splitting	Slab1	368.50
(12 specimens)	B2S	18.65	24.24	C130 x 13	Concrete crushing-splitting	Slab1	330.15
	B3S	18.65	24.24	C130 x 13	Channel Fracture	Slab2	236.55
	B4S	18.65	24.24	C130 x 10	Concrete crushing-splitting	Slab1	408.85
	B5S	18.65	24.24	C130 x 10	Channel Fracture	Slab2	336.65
	B6S	18.65	24.24	C130 x 10	Channel Fracture	Slab2	224.85
	B1D	18.65	24.24	C130 x 13	Concrete Crushing	Slab1	278.40
	B2D	18.65	24.24	C130 x 13	Concrete Crushing	Slab1	292.80
	B3D	18.65	24.24	C130 x 13	Concrete Crushing	Slab2	190.75
	B4D	18.65	24.24	C130 x 10	Concrete Crushing	Slab1	277.90
	B5D	18.65	24.24	C130 x 10	Concrete Crushing	Slab1	234.05
	B6D	18.65	24.24	C130 x 10	Channel Fracture	Slab2	180.30
C	C1S	37.0	44.9	C130 x 13	Channel Fracture	Slab 2	694.70
(12 specimens)	C2S	37.0	44.9	C130 x 13	Channel Fracture	Slab 2	516.45
	C3S	37.0	44.9	C130 x 13	Channel Fracture	Slab 1	313.75
	C4S	37.0	44.9	C130 x 10	Channel Fracture	Slab 1	677.30
	C5S	37.0	44.9	C130 x 10	Channel Fracture	Slab 2	486.05
	C6S	37.0	44.9	C130 x 10	Channel Fracture	Slab 2	262.95
	C1D	37.0	44.9	C130 x 13	Concrete Crushing	Slab 1	498.00
	C2D	37.0	44.9	C130 x 13	Concrete Crushing	Both	463.15
	C3D	37.0	44.9	C130 x 13	Channel Fracture	Slab 1	285.85
	C4D	37.0	44.9	C130 x 10	Concrete Crushing	Slab 1	476.10
	C5D	37.0	44.9	C130 x 10	Channel Fracture	Slab 2	406.35
	C6D	37.0	44.9	C130 x 10	Channel Fracture	Slab 2	231.00

Table 4.2 (cont'd) Specimen Failure Characteristics of Series A*.

Series	**Specimen**	**f'c** (MPa) Slab 1	Slab 2	**Channel Type**	**Failure Type**	**Failure Side**	**Failure Load per Channel** (kN)
A*	A1D	27.14	33.42	C130 x 13	Concrete Crushing	Slab1	388.45
(6 Specimens)	A2D	27.14	33.42	C130 x 13	Concrete Crushing	Slab1	344.60
	A3D	27.14	33.42	C130 x 13	Channel Fracture	Slab2	254.00
	A4D	27.14	33.42	C130 x 10	Concrete Crushing	Slab1	390.45
	A5D	27.14	33.42	C130 x 10	Concrete Crushing	Both	339.65
	A6D	27.14	33.42	C130 x 10	Channel Fracture	Slab2	212.15

It is also evident from the load-slip curve of this specimen (Fig. 4.14), that the amount of slip at the ultimate load was much smaller than that observed in Fig. 4.12 for specimen A1a [10 mm vs. 4 mm]. Referring to Fig. 4.14, the specimen continued to retain a large portion of the ultimate load in the unloading stage, well after the maximum load was reached.

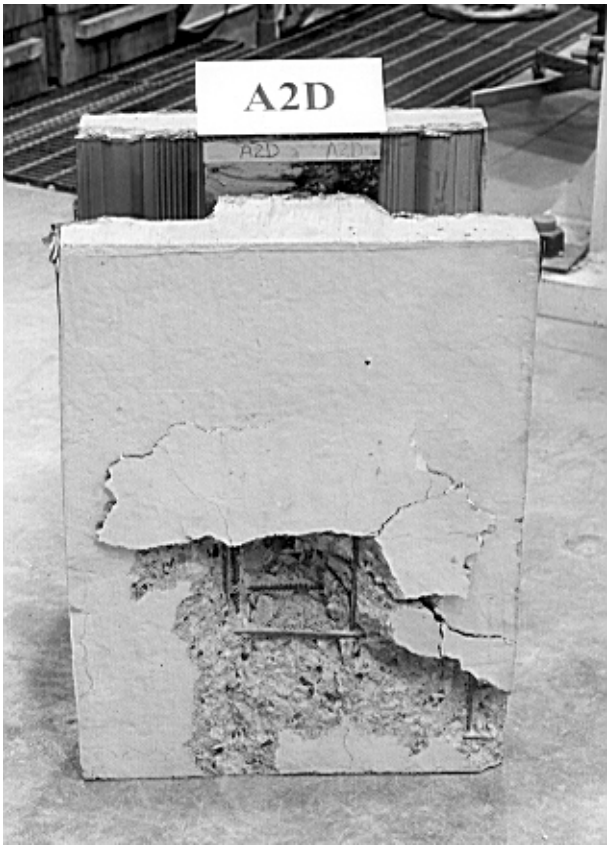

Figure 4.13 Concrete crushing of deck slab: specimen A2D.

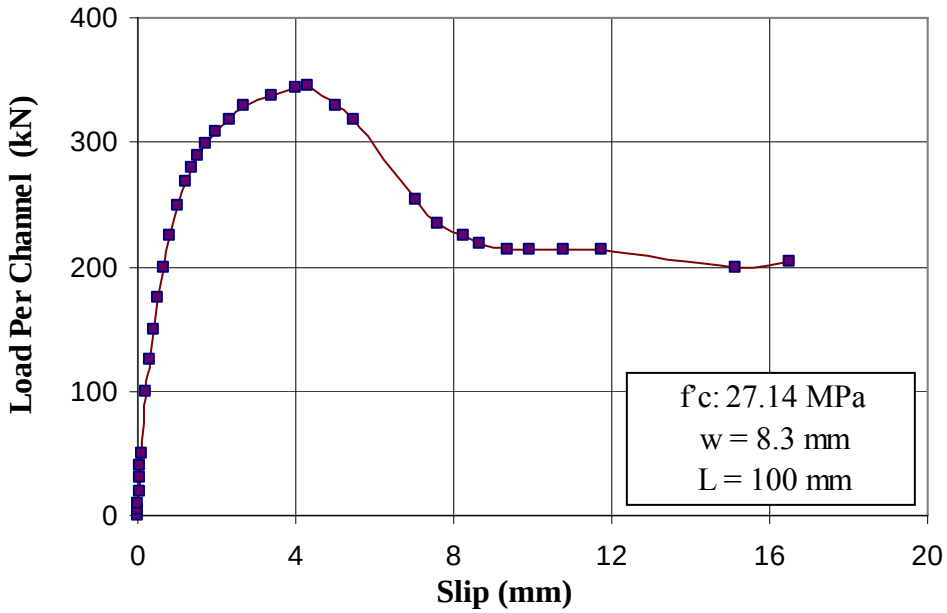

Figure 4.14 Load-Slip curve for specimen A2D.

(c) Phase 2 (solid slabs)

Of the 18 specimens with solid concrete slabs in Phase 2, the concrete crushing-splitting type of failure was observed in nine specimens, as indicated in Table 4.3. Fig. 4.15 shows the load-slip behaviour of specimen D1S. This specimen had 150 mm long channel connectors with an 8.2 mm web thickness. It had solid concrete slabs with a compressive strength of 21.18 MPa. The height of the channel used in this specimen was 102 mm. As shown in the figure, the pattern of the failure mechanism was very similar to that observed in specimens with solid slabs in Phase 1. It was noticed that due to the smaller height of the channel (102 mm) in the specimens of Phase 2, as compared to those of Phase 1 (channel height 127 mm), there was a higher concentration of stresses on the surface of the concrete in contact with the channel web. As a result, concrete crushing-splitting type of failure was more predominant in specimens of this Phase.

Table 4.3. Specimen Failure Characteristics of Series D, E and F.

Series	Specimen	f'c (MPa) Both Slabs	Channel Type	Failure Type	Failure Side	Failure Load per Channel (kN)
D (12 specimens)	D1S	21.18	C100x11	Concrete crushing-splitting	Both	403.40
	D2S	21.18	C100x11	Concrete crushing-splitting	Both	326.70
	D3S	21.18	C100x11	Channel Fracture	Slab1	239.05
	D4S	21.18	C100x8	Concrete crushing-splitting	Both	396.40
	D5S	21.18	C100x8	Concrete crushing-splitting	Both	301.80
	D6S	21.18	C100x8	Channel Fracture	Slab1	201.20
	D1D	21.18	C100x11	Concrete Shear Plane	Both	318.70
	D2D	21.18	C100x11	Concrete Shear Plane	Slab1	278.90
	D3D	21.18	C100x11	Concrete Shear Plane	Both	179.30
	D4D	21.18	C100x8	Concrete Shear Plane	Slab1	283.85
	D5D	21.18	C100x8	Concrete Shear Plane	Both	244.00
	D6D	21.18	C100x8	Concrete Shear Plane	Slab1	159.35
E (12 specimens)	E1S	34.8	C100x11	Concrete crushing-splitting	Slab1	583.65
	E2S	34.8	C100x11	Concrete crushing-splitting	Slab1	488.05
	E3S	34.8	C100x11	Channel Fracture	Slab2	345.60
	E4S	34.8	C100x8	Channel Fracture	Slab1	542.80
	E5S	34.8	C100x8	Channel Fracture	Slab2	433.25
	E6S	34.8	C100x8	Channel Fracture	Slab2	244.00
	E1D	34.8	C100x11	Concrete Shear Plane	Slab2	443.20
	E2D	34.8	C100x11	Concrete Shear Plane	Slab1	381.45
	E3D	34.8	C100x11	Concrete Shear Plane	Both	260.95
	E4D	34.8	C100x8	Concrete Shear Plane	Slab1	407.35
	E5D	34.8	C100x8	Concrete Shear Plane	Slab2	353.60
	E6D	34.8	C100x8	Channel Fracture	Slab2	218.10
F (12 specimens)	F1S	28.57	C100x11	Concrete crushing-splitting	Both	485.05
	F2S	28.57	C100x11	Concrete crushing-splitting	Both	375.50
	F3S	28.57	C100x11	Channel Fracture	Slab2	268.90
	F4S	28.57	C100x8	Concrete crushing-splitting	Both	450.20
	F5S	28.57	C100x8	Channel Fracture	Slab1	358.55
	F6S	28.57	C100x8	Channel Fracture	Slab2	222.10
	F1D	28.57	C100x11	Concrete Shear Plane	Slab1	347.60
	F2D	28.57	C100x11	Concrete Shear Plane	Slab1	288.85
	F3D	28.57	C100x11	Concrete Shear Plane	Both	208.15
	F4D	28.57	C100x8	Concrete Shear Plane	Slab1	336.65
	F5D	28.57	C100x8	Concrete Shear Plane	Slab2	273.90
	F6D	28.57	C100x8	Channel Fracture	Slab2	182.25

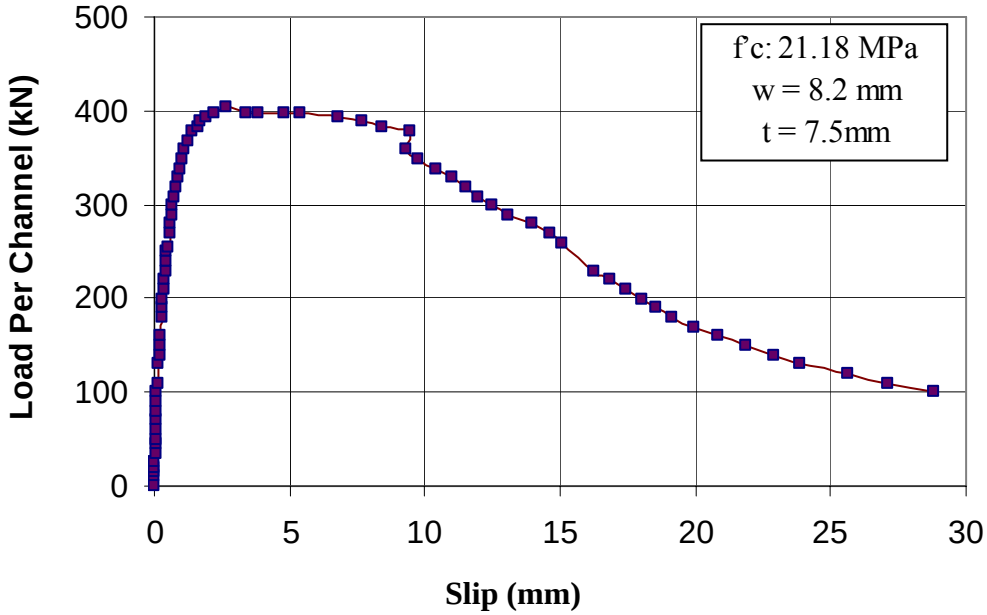

Figure 4.15 Load-Slip curve for specimen D1S.

(d) Phase 2 (Deck slabs)

In the specimens of Phase 2 with metal deck slabs, the concrete crushing-splitting type of failure was not observed. In these specimens, a concrete shear plane type of failure was observed which is illustrated in the following subsection.

4.1.3 Failure Mode 3: Concrete Shear Plane Failure

A concrete shear plane type of the failure was observed in almost all of the specimens with deck slabs and 102 mm high channels. Specimens with deck slabs were more susceptible to concrete related failures because of a very high concentration of stresses within a smaller area. Fig. 4.16 shows the typical shear plane type of failure observed in the specimens with metal deck slabs. The channel connector remained intact and the concrete contained within the flute in front of the channel web sheared off along the interface.

Fig. 4.17 shows that a considerable amount of deformation occurred before the concrete failed in shear.

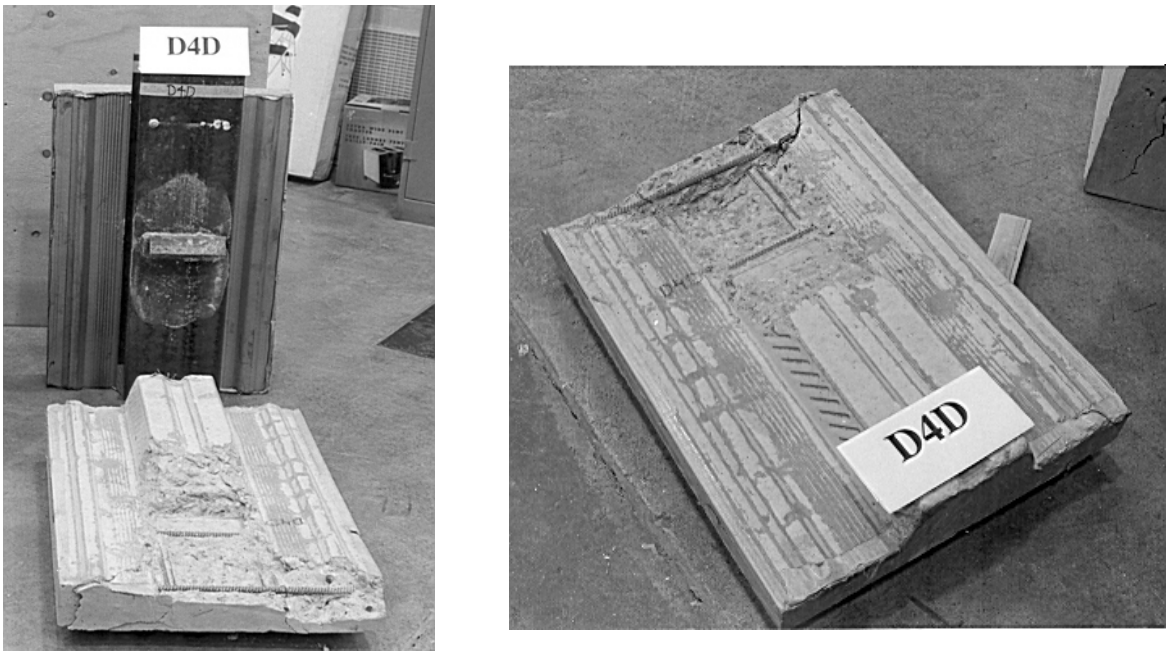

Figure 4.16 Concrete shear plane failure: specimen D4D.

Figure 4.17 Channel deformation after failure: specimen D4D.

The load-slip curve for specimen D4D is presented in Fig. 4.18. It appears that there was a significant decrease in the load carrying capacity once the shear failure plane was well formed. However, the specimen continued to support a portion (30-50%) of the ultimate load in the unloading stage due to friction between the sheared surfaces.

The shear plane failure surfaces observed in specimens D1D and D2D are shown in Figs. 4.19 and 4.20, respectively.

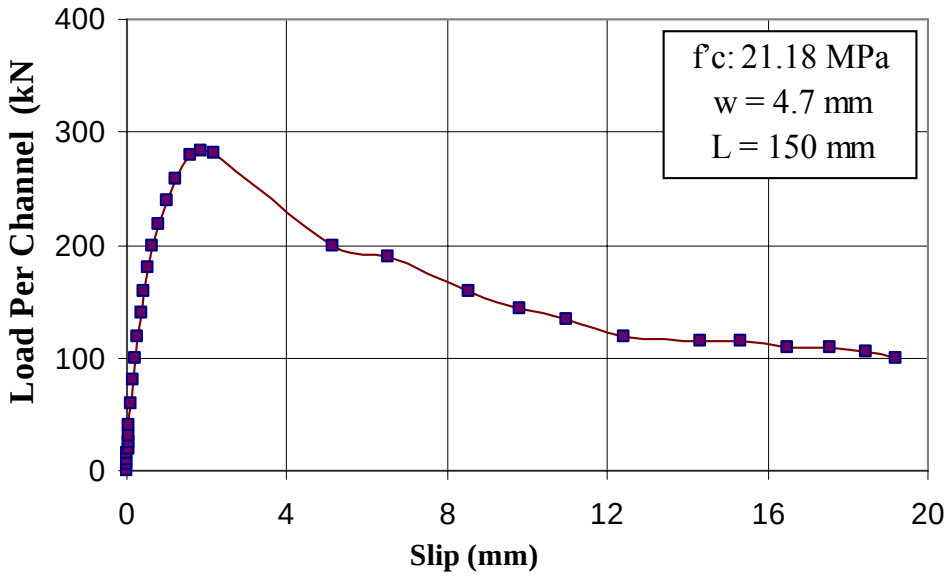

Figure 4.18 Load-Slip curve for specimen D4D.

Figure 4.19 Concrete shear plane failure: specimen D1D.

Figure 4.20 Concrete shear plane failure: specimen D2D.

As indicated in Table 4.3, concrete shear plane type of failure was observed in 16 specimens with metal deck slabs and 102 mm high channel connectors. In only two specimens, channel web fracture was observed because of the smaller load carrying capacity of the channel resulting from smaller web thickness (4.7 mm) and smaller length (50 mm) of the channel.

4.2 Parametric Study

4.2.1 Effect of Concrete Strength

The concrete strength was the principal variable between the three series of each phase. Fig. 4.21 represents the load-slip curves for three companion

specimens (D4S, E4S and F4S) from series D, E and F with the same type of channel connector. It appears that, for a given length of channel, the concrete strength governed the mode of failure. Channel web fracture type of failure, with the signature abrupt termination of the load-slip curve, was observed in the specimens with the highest strength concrete while, in the specimens with lower and moderate strength concrete, failure was concrete related. All these specimens had solid concrete slabs and 150 mm long channel connectors with a web thickness of 4.7 mm. The compressive strength of concrete used in the three series was 21.18, 34.80 and 28.57 MPa, respectively. Once again, the load-slip curve for channel web fracture type of failure comes to an abrupt end, whereas those related to concrete failure exhibit a gradual drop in load carrying capacity.

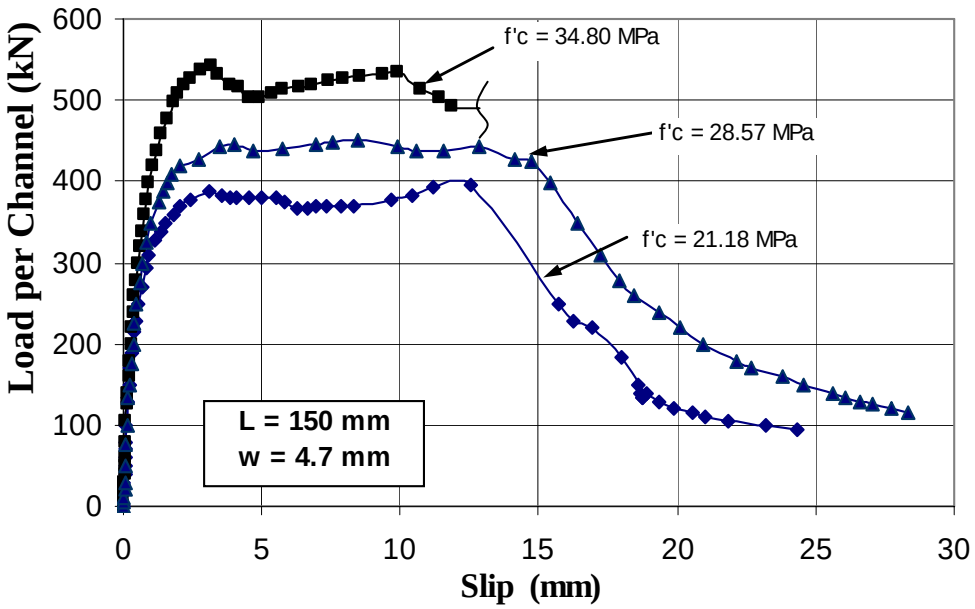

Figure 4.21 Load-Slip curves for specimen D4S, E4S and F4S.

Fig. 4.22 presents the ultimate load vs. $\sqrt{f'c}$ curves for nine specimens, again from series D, E and F. The lengths of the channel connectors used in these specimens were 50 mm, 100 mm and 150 mm. All these specimens were made with solid concrete slabs and the channels had a web thickness of 8.2 mm. Six out of nine specimens that involved 100 mm and 150 mm long channel connectors, experienced concrete-related failures. According to Viest (1956), Davies (1967), Slutter and Driscoll (1962), Ollgaard et al. (1971) and Androutsos and Hosain (1994), for concrete related failures, the ultimate capacity of the shear connector is proportional to $\sqrt{f'c}$.

The increase in load with the square root of compressive strength of concrete for three curves in Fig. 4.22 is seen to be approximately linear.

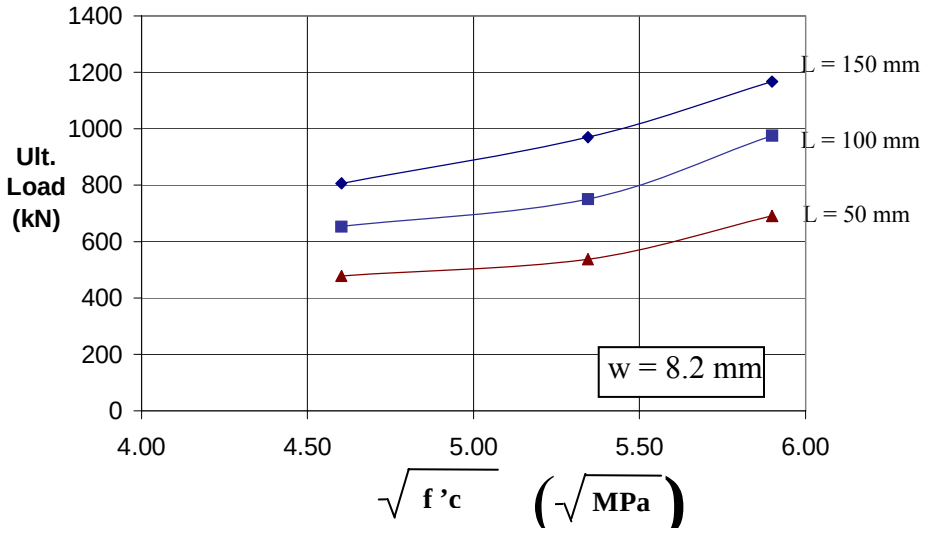

Figure 4.22 Load per channel vs. $\sqrt{f'c}$: Solid slab specimens of series D, E and F.

Fig. 4.23 presents the load vs. $\sqrt{f'c}$ curves for another nine specimens, again from series D, E and F, but with metal deck slabs. The channel connectors used in these specimens had 4.7 mm web thickness and the length of channel connectors ranged from 50 mm to 150 mm. It appears that the load carrying capacity of the channel shear connector, in case of metal deck slabs, also increased approximately in proportion to the increase in $\sqrt{f'c}$.

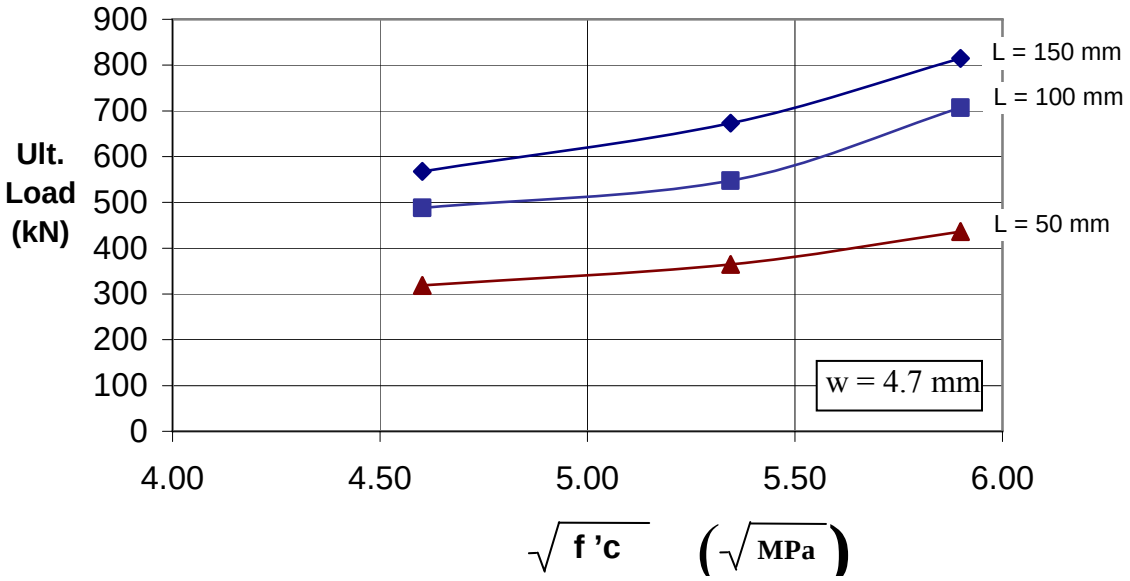

Figure 4.23 Load per channel vs. $\sqrt{f'c}$: Deck slab specimens of series D, E and F.

4.2.2 Effect of Variation in Channel Length

Fig. 4.24 represents the load-slip curves for specimens E4S, E5S and E6S. These specimens were similar in every respect except that the length of the channel connector was 150 mm, 100 mm and 50 mm, respectively. All these specimens were made with solid concrete slabs with the compressive strength of concrete being 34.8 MPa. The web thickness of the channel connectors was 4.7 mm. As can be seen from the characteristics of the load-

slip curves, all three specimens failed due to channel web fracture. As expected, the load carrying capacity of the channel connector increased with the increase in the length of connector. The ultimate loads of the three specimens were 1085 kN, 866 kN and 488 kN, respectively. A general discussion concerning the relationship between the load capacity and the variation in channel lengths follows.

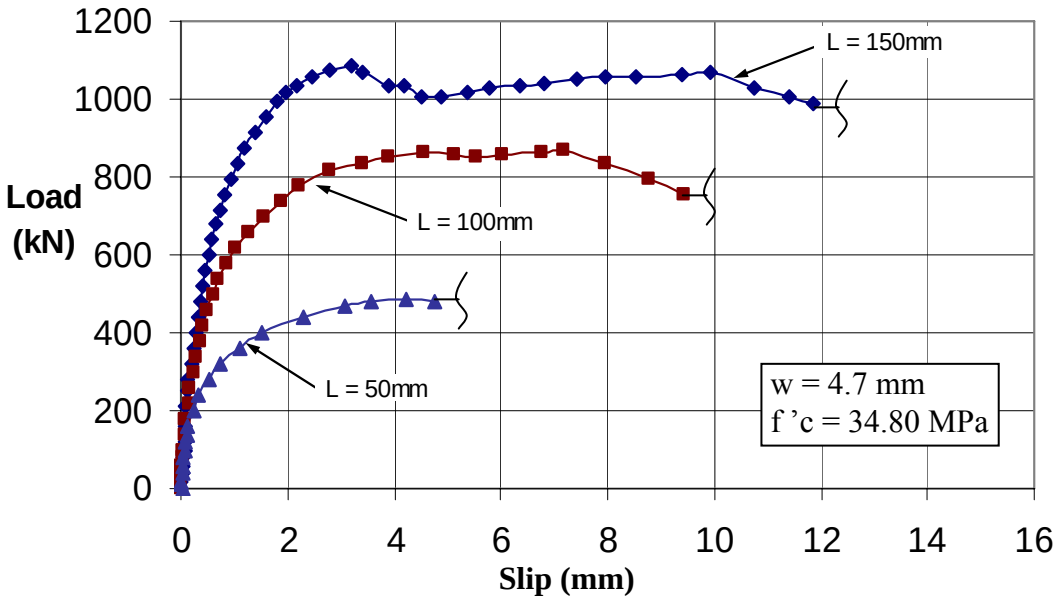

Figure 4.24 Load-Slip curves for specimen E4S, E5S and E6S.

Fig. 4.25 shows the effect of variation in the channel length for nine specimens in series D, E and F. All these specimens had channels with a web thickness of 8.2 mm and length ranging from 50 mm to 150 mm, as shown in the figure. It appears that the load carrying capacity increased almost linearly with the increase in channel length. On average, the load carrying capacity increased by about 39% when the channel length was increased from 50 mm to 100 mm. There was a further increase of 24% when the channel length was increased from 100 mm to 150 mm. The rate of

increase appears to be approximately the same regardless of the compressive strength of concrete. One discrepancy that must be pointed out is that the load vs. channel length curves do not pass through the origin, i.e., load capacity does not become zero when the channel length is assumed to be zero.

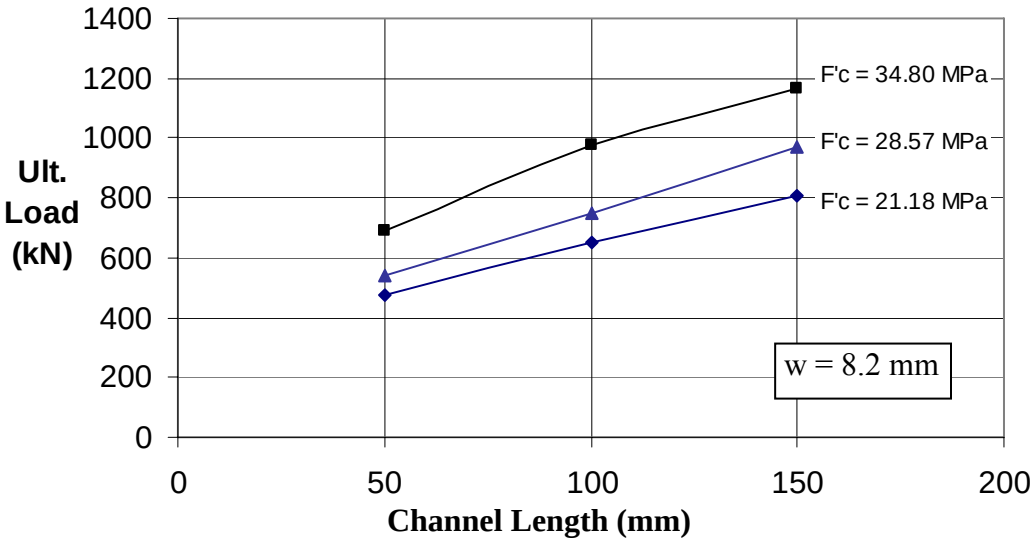

Figure 4.25 Load per channel vs. channel length:
Solid slab specimens of series D, E and F.

Fig. 4.26 presents similar results for another set of nine specimens but with channel connectors of 4.7 mm web thickness. The results are similar to those presented in Fig. 4.25 for 100 mm and 150 mm long channels. On average, the load carrying capacity increased by about 27% compared to 24% for specimens with 4.7 mm thick web. With the exception of one specimen (channel length = 50 mm and f'c = 34.80 MPa), the results for 50 mm channels are also similar to those presented in Fig. 4.25.

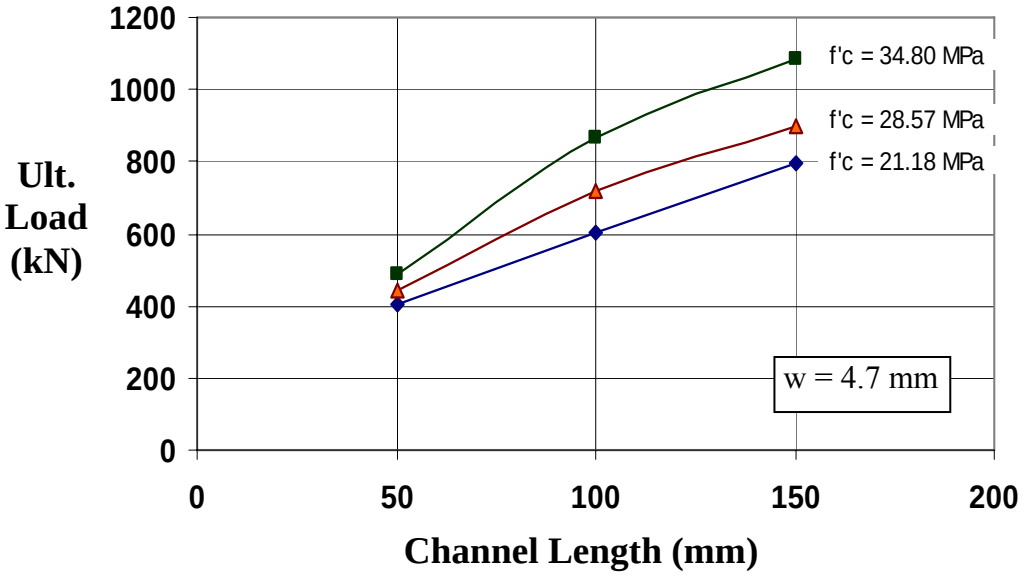

Figure 4.26 Load per channel vs. channel length:
Specimens with solid slabs [series D, E and F].

Fig. 4.27 presents the load-slip curves for three specimens of series E. These specimens had metal deck slabs and channel connectors with a web thickness of 8.2 mm. The compressive strength of concrete used was 34.80 MPa. All these specimens failed due to concrete shear plane type of failure. As indicated earlier in Section 4.1.3, there was a rapid loss of load carrying capacity once the shear failure plane was well formed, but the specimen continued to support a small portion of the ultimate load in the unloading stage due to friction between the sheared surfaces.

Fig. 4.28 shows the effect of variation in the channel length for nine specimens with metal deck slabs. The length of the channel connector in these specimens ranged from 50 mm to 150 mm, as shown in the figure. It can be seen that in the case of specimens with metal deck slabs, the load

capacity vs. channel length curves are not as linear as those for specimens with solid slabs.

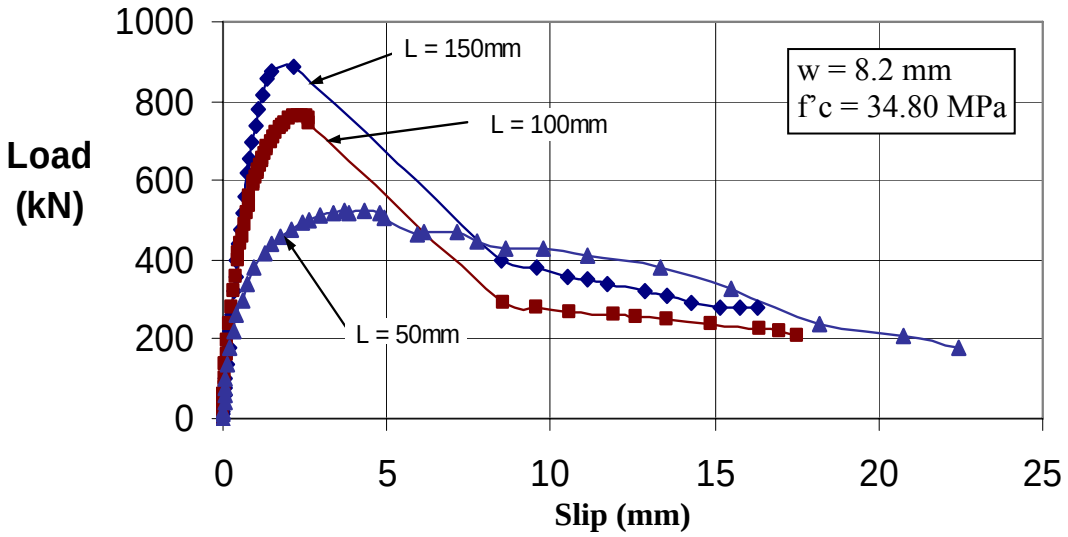

Figure 4.27 Load-Slip curves for specimen E1D, E2D and E3D.

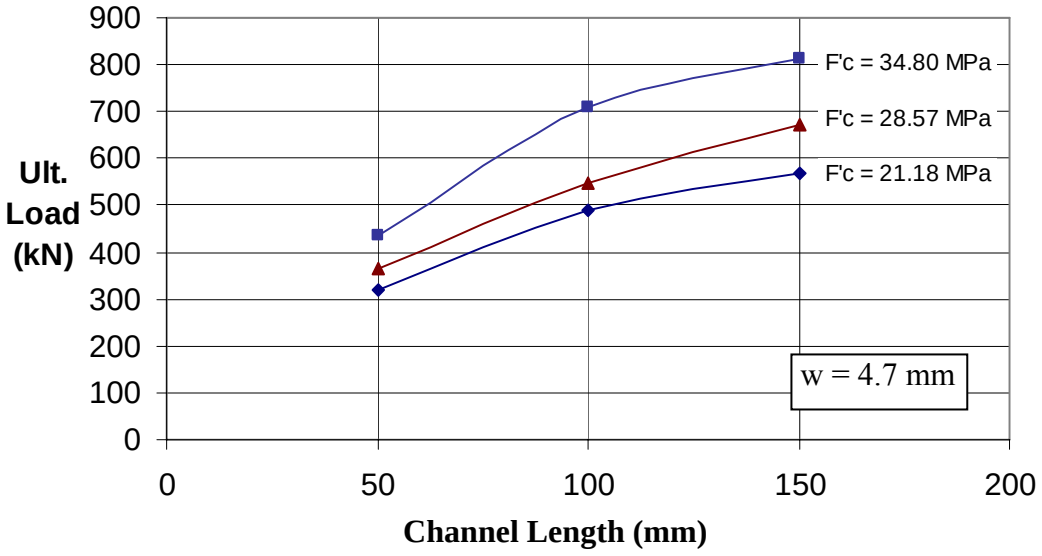

Figure 4.28 Load per channel vs. channel length:
Deck slab specimens of series D, E and F.

4.2.3 Solid Slab Versus Metal Deck Slab

Figures 4.29 and 4.30 illustrate the effects of slab geometry on the load carrying capacity of the channel connectors. The load-slip curves for specimens F1S and F1D are shown in Fig. 4.29. Both of these specimens had 150 mm long channel connectors with an 8.2 mm web thickness. The only difference between the two was that specimen F1S was made with solid concrete slabs whereas F1D had metal deck type of slabs. The compressive strength of concrete was 28.57 MPa. The specimen with solid concrete slabs carried over 39% more load than that carried by the specimen with metal deck slabs. Both specimens experienced concrete related failures.

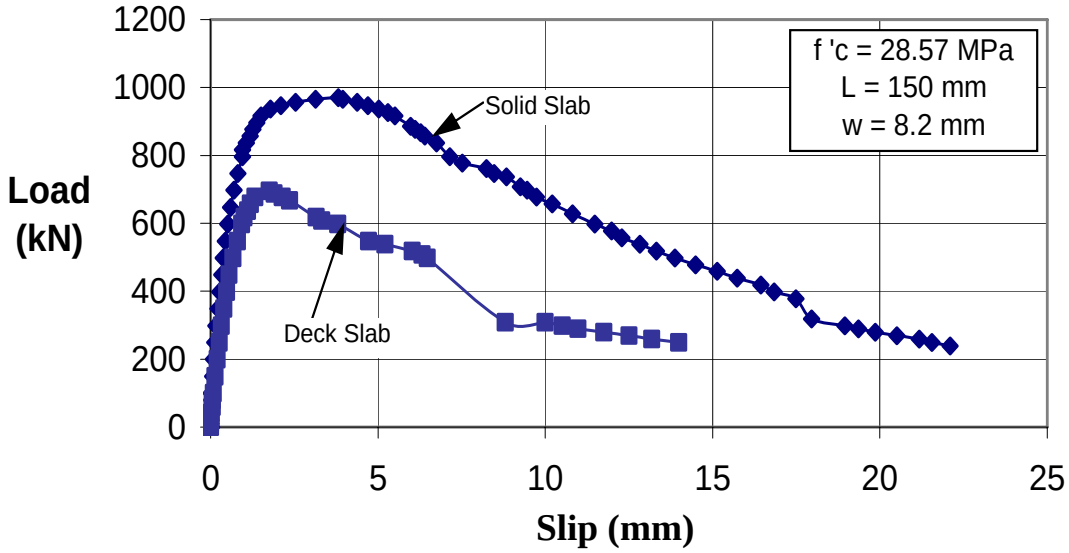

Figure 4.29 Load-Slip curves for specimen F1S and F1D.

The relationship between load and channel length for specimens E4S, E5S and E6S, all with solid concrete slabs, is shown in Fig. 4.30. The same curve for the companion specimens with metal deck slabs (specimens E4D, E5D and E6D) is also shown for comparison. All these specimens had C100x8

type of channel connectors with a web thickness of 4.7 mm. The length of the channel connector varied between 50 mm and 150 mm, as indicated in the figure. The compressive strength of the concrete used in the slabs of these specimens was 34.80 MPa. The overall increase in load capacity for the specimens with solid slabs was 22.5% as compared to those with deck slabs. However, the increase in the load capacity of the specimens with solid concrete slabs varied from 12% (for 50 mm long channel connectors) to more than 33% (for 150 mm long channel connectors). This was expected, since a channel with a shorter length will be surrounded by relatively more concrete, i.e., it would behave as if it is embedded in a solid concrete slab. The two specimens with the smallest channel lengths (50 mm) failed due to channel fracture; therefore, the deck geometry did not have a significant effect. On the other hand, the specimens with 100 mm and 150 mm channel lengths had different failure mechanisms. The two specimens with solid slabs failed by channel fracture; concrete shear type failure was observed in the other two specimens. Hence, the specimens with solid slabs carried significantly higher loads.

4.2.4 Effect of Channel Web Thickness

The load versus slip curves for specimens F1S and F4S, both with solid concrete slabs, are shown in Fig. 4.31. The two specimens were similar in every respect except that the web thickness of the channel connector was 8.2 mm and 4.7 mm, respectively. As the load-slip curves indicate, both the specimens failed due to concrete crushing and splitting. Specimen F1S, with the thicker channel web carried only 8% more load than that of specimen F4S with the thinner channel web. This was expected, since the web thickness of the channel does not have a major influence when failure is

concrete related. However, the specimen with a thinner web showed a slightly more ductile behaviour. In general, the specimens with thicker channel webs carried only 6.44% higher load when failure was concrete related.

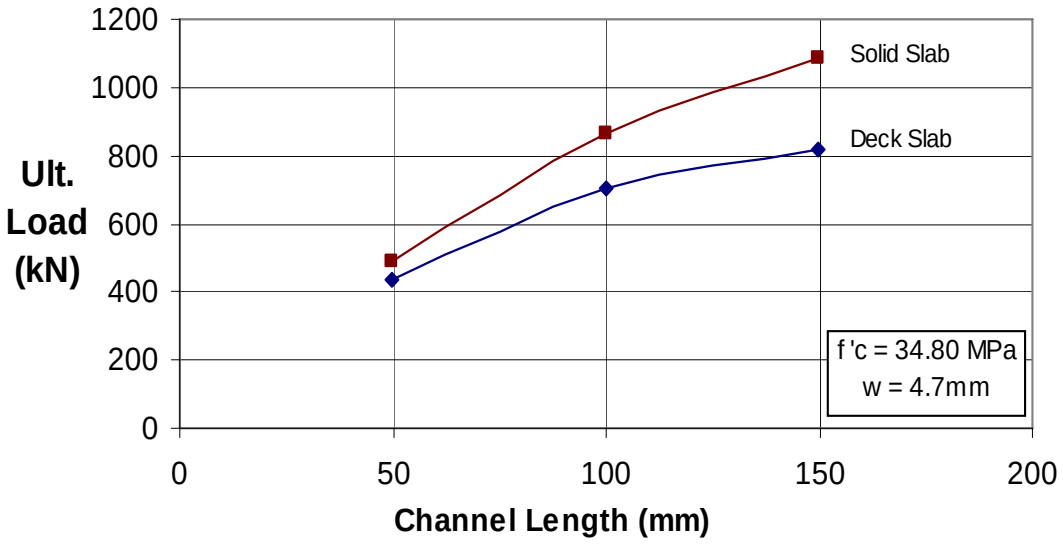

Figure 4.30 Load per channel vs. channel length:
Solid slab and deck slab specimens of series E.

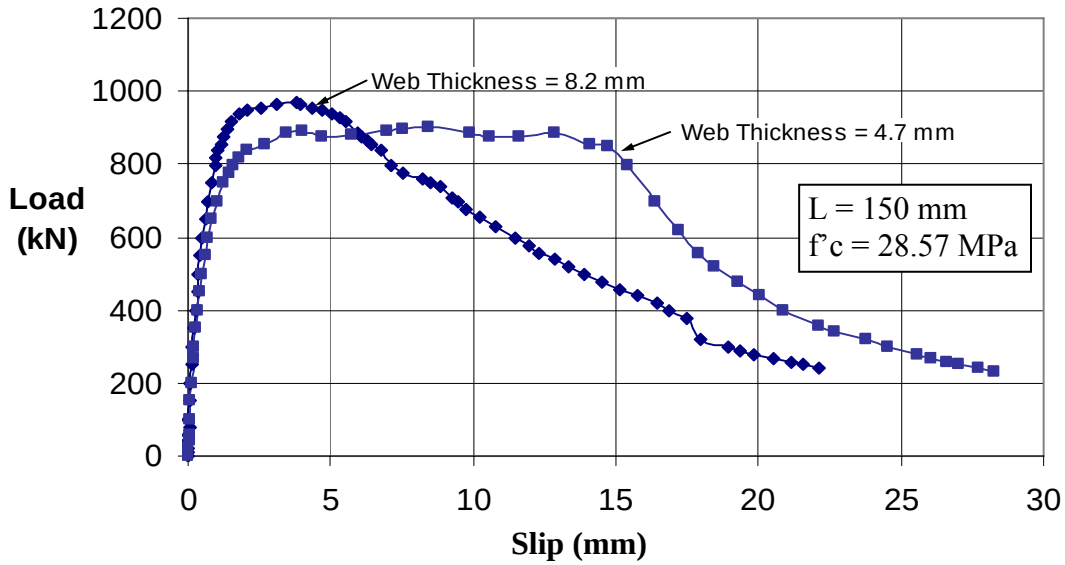

Figure 4.31 Load-Slip curves for specimen F1S and F4S.

The load versus slip curves for specimens F3S and F6S, both with solid concrete slabs, are shown in Fig. 4.32. Once again, the two specimens were similar in every respect except that the web thickness of the channel connector was 8.2 mm and 4.7 mm, respectively. As the load-slip curves indicate, both specimens failed due to channel web fracture. Specimen F3S with the thicker channel web carried 21% higher load than specimen F6S. This shows that in channel web fracture type of failures, the web thickness plays an important role as it increases the area and the moment of inertia of the web section, which in turn increases the shear and flexural capacity of the channel, respectively. However, for the specimens with higher strength concrete, the increase in the load carrying capacity was even higher. Fig. 4.33 shows the load-slip curves for specimens E3S and E6S, both from series E. The web thicknesses of the channel used in these specimens were 8.2 mm and 4.7 mm, respectively. The compressive strength of the concrete was 34.8 MPa. In this case, the load capacity was 41% higher in the channel with the thicker web. This is due to the lower flexural deformation in the channel web in the specimens with higher strength concrete.

Fig. 4.34 shows the load-slip curves for the specimens A2D and A5D, both with metal deck type of slabs. Once again, both of these specimens were similar in every respect except that the web thicknesses of the channel were 8.3 mm and 4.8 mm, respectively. Both of these specimens experienced concrete related failure. As expected, the difference in the load carrying capacity of the two specimens was not very high. The specimen with 8.3 mm channel web thickness carried only 1.5% higher load than that with a web thickness of 4.8 mm. Fig. 4.35 shows the similar curves for specimens A3D

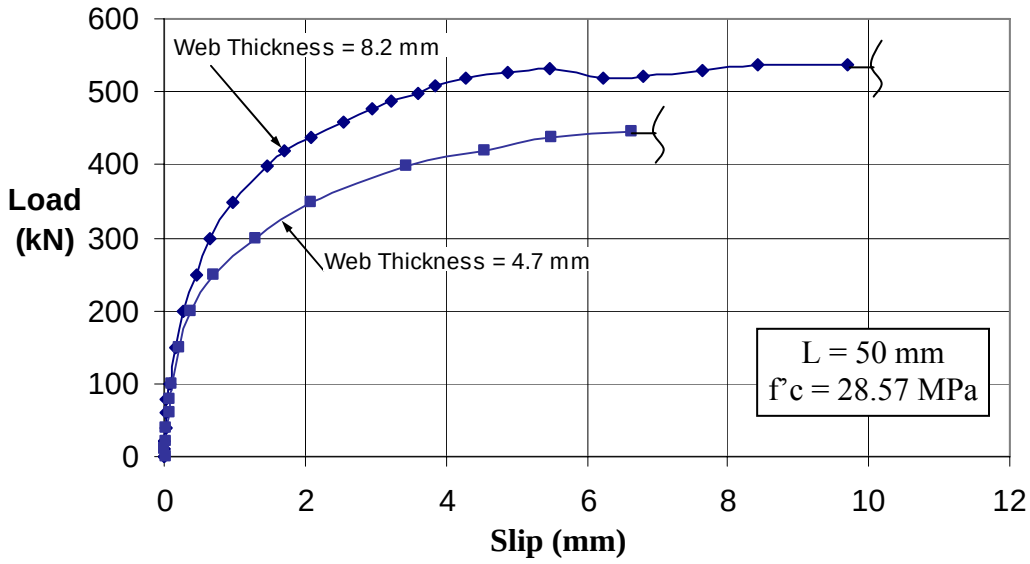

Figure 4.32 Load-Slip curves for specimen F3S and F6S.

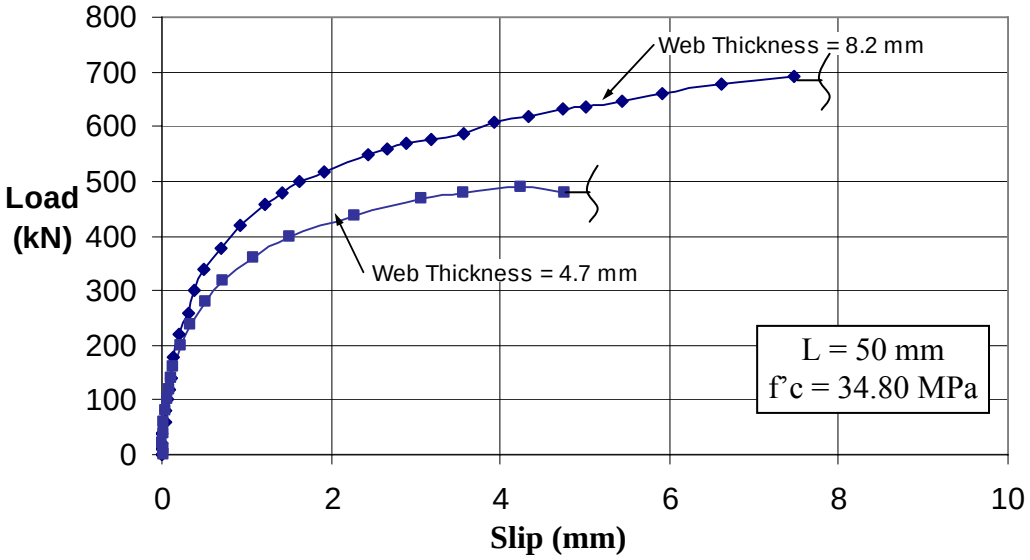

Figure 4.33 Load-Slip curves for specimen E3S and E6S.

and A6D with metal deck slabs. Again, the only difference between these specimens was the web thickness of the channel. Since the curves indicate that the specimens failed due to channel web fracture type of failure, a

similar trend as that observed for specimens with solid concrete slabs is noticed in these specimens. The specimen with an 8.3 mm thick channel web carried approximately 24% higher load than the other. In general, the influence of web thickness of the channel connector was significant when failure occurred due to channel web fracture but was minimal for concrete crushing type of failure.

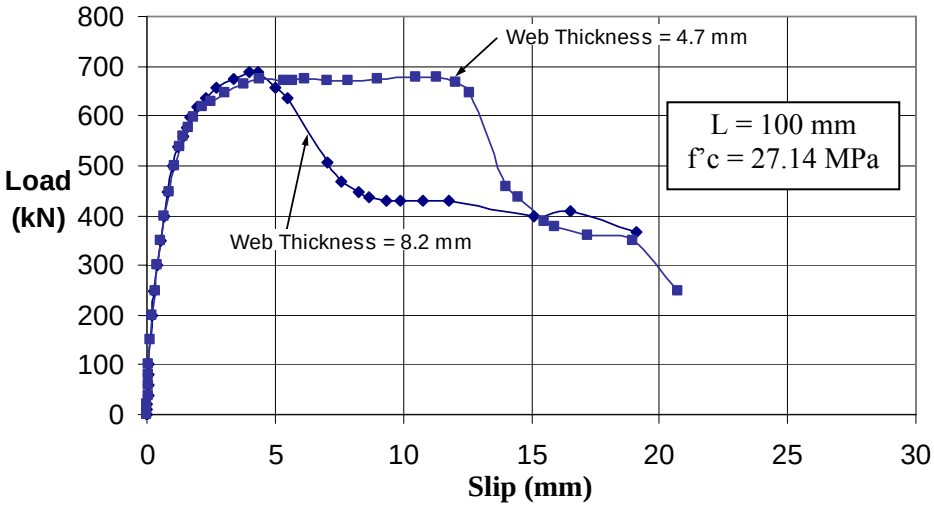

Figure 4.34 Load-Slip curves for specimen A2D and A5D.

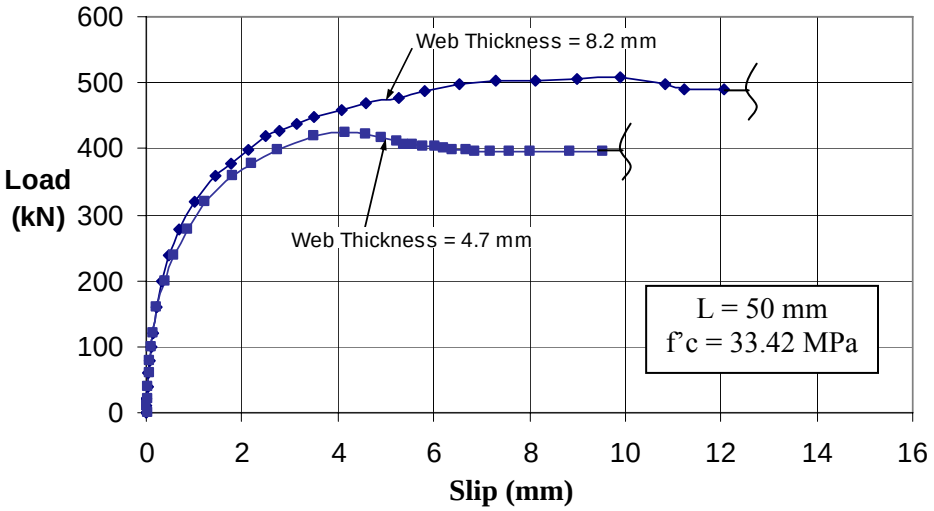

Figure 4.35 Load-Slip curves for specimen A3D and A6D.

4.2.5 Effect of Channel Height

Fig. 4.36 presents the load vs. slip curves for the specimens A1a and E1S from series A and E, respectively. Both of these specimens were made with solid concrete slabs. Specimen A1a had 127 mm high channel connectors with an 8.3 mm web thickness and specimen E1S had 102 mm high channels with a web thickness of 8.2 mm. The concrete compressive strengths were 30.49 and 34.8 MPa, respectively. Both of these specimens experienced concrete related failures.

In spite of the lower strength of concrete used, specimen A1a, with the 127 mm high channel connectors, carried a slightly higher load (1186 kN) compared to 1155 kN recorded for the other. However, if the effect of the difference in concrete strength is taken into account, the normalized* ultimate load values amount to 1227 kN and 1130 kN, respectively. This translates to an increase of 9% in the ultimate load capacity of the specimen with higher channel connectors. Other beneficial effects are discussed below.

The load-slip curves indicate that the specimen with 127 mm high channel connectors was more ductile compared to that with 102 mm high channels. In the initial stage, the specimen with shorter channels exhibits a very inflexible behaviour. The amount of slip at the ultimate load level was less than 2 mm compared to more than 10 mm for the other.

---

*Normalization was carried out by multiplying the load values by the factor $k = \sqrt{f'm/f'c}$, where $f'm$ is the mean concrete strength of two specimens (Androutsos 1994).

A similar comparison of the behaviour of specimens A1a and F1S is shown in Fig. 4.37. Specimen A1a had 127 mm high channel connectors with 8.3 mm web thickness and specimen F1S had 102 mm high channels with a web thickness of 8.2 mm. Both specimens had solid concrete slabs, with compressive strengths of 30.49 MPa and 28.57 MPa, respectively.

Once again, both specimens experienced concrete related failures and specimen A1a, with 127 mm channel connectors, carried a higher load (1186 kN) compared to 970 kN for specimen F1S. The normalized values worked out to be 1167 kN and 986 kN, respectively. The percentage increase in load capacity for this case was 18%. This may be due to the fact that channel connectors with shorter height tend to concentrate the applied load into a smaller area and this effect is more damaging to a specimen with lower strength concrete. Similar to the case discussed earlier, these curves also illustrate that the specimen with 127 mm high channels is more flexible compared to the one with 102 mm high channels.

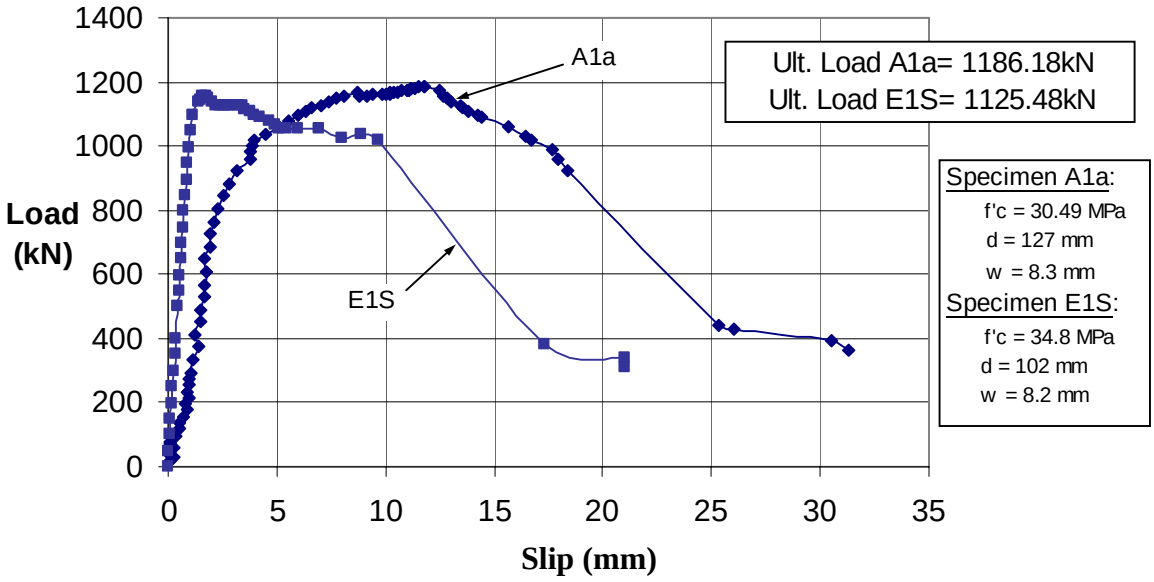

Figure 4.36 Load-Slip curves for specimen A1a and E1S (L =150 mm).

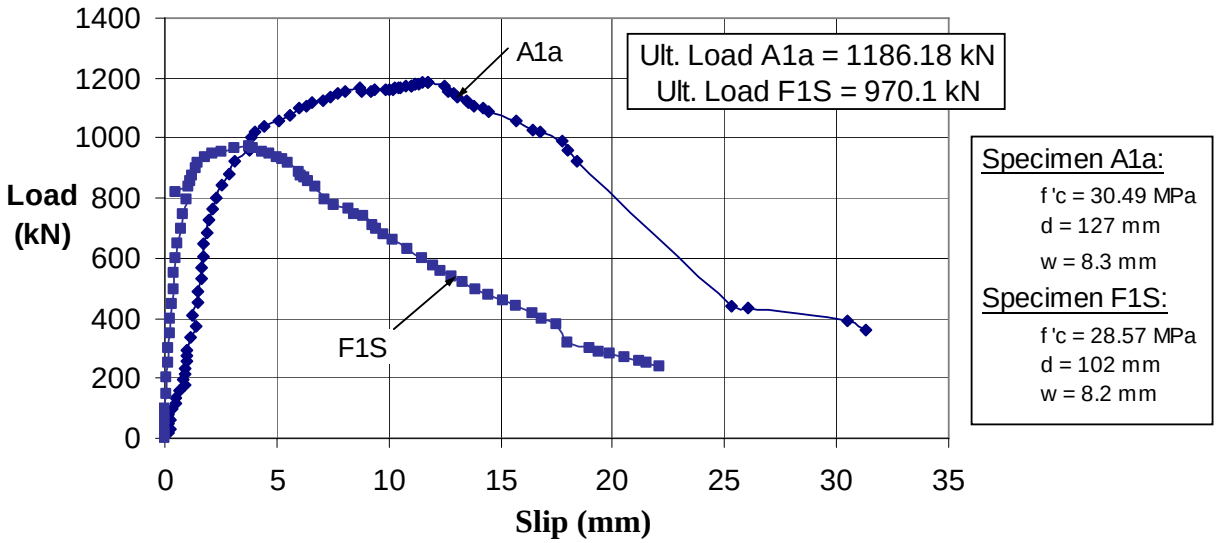

Figure 4.37 Load-Slip curves for specimen A1a and F1S (L = 150 mm).

Fig. 4.38 presents the load vs. slip curves for specimens A3a and E3S. Both of these specimens were made with solid concrete slabs. The compressive strengths of concrete used in these slabs were almost the same (33.87 MPa vs. 34.8 MPa). Specimen A3a had 127 mm high channel connectors with an 8.3 mm web thickness and specimen E3S had 102 mm high channels with a web thickness of 8.2 mm. As shown in Fig. 4.38, both of these specimens failed due to channel web fracture. Unlike the previous cases, specimen E3S, with the 102 mm high channel connectors, carried more than 21% higher load (691 kN) compared to 568 kN recorded for the other.

After the loads were normalized to a mean value of concrete strength (f'm = 34.33 MPa), it was observed that the specimen with a smaller height of channel (102 mm) carried approximately 20% higher load than the specimen with bigger channel height (127 mm). It appears that the height of the channel that behaves like a cantilever arm in the push-out specimens plays a significant role in the development of flexural stresses near the fillet and

becomes a predominant factor when the failure is caused due to channel web fracture. Because of this fact, the specimens with 127 mm high channels experienced much higher flexural stresses near the fillet, resulting from the longer cantilever span, as compared to specimens with 102 mm high channel connectors.

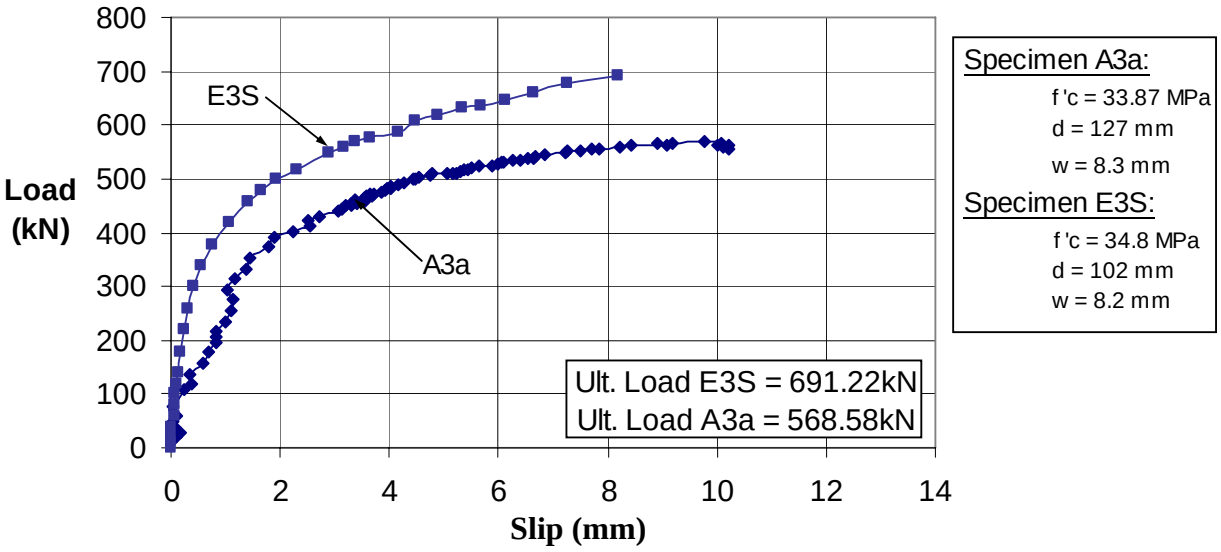

Figure 4.38 Load-Slip curves for specimen A3a and E3S (L = 50 mm).

CHAPTER FIVE

FORMULATION OF DESIGN EQUATIONS

5.1 Preamble

As discussed in Chapter One of this thesis, the current Canadian Standard, CAN/CSA-S16-01 (Canadian Standards Association 2001) specifies that the factored shear resistance, q_{rs}, of a channel shear connector embedded in a solid concrete slab be evaluated using Eq. [5.1].

$$q_{rs} = 36.5\phi_{sc}(t + 0.5w)L_c\sqrt{f'_c} \qquad [5.1]$$

where:

ϕ_{sc} = Resistance factor for shear connectors

t = Flange thickness of channel connector [mm]

w = Web thickness of channel connector [mm]

L_c = Length of channel connector [mm]

f'_c = Specified compressive strength of concrete [MPa]

As described earlier in Chapter 1, Eq. [5.1] is based on the work at Lehigh University by Slutter and Driscoll (1965). The overall test program involved the testing of beam and push-out specimens with headed stud connectors, spiral connectors and channels. Most of the 41 push-out specimens with channel connectors featured six inch (152 mm) long and four inch (102 mm) high channels. Five specimens had 3 inch (76 mm) high channels and only two featured 5 inch (127 mm) high channels. The length of these five channels was also six inches (152 mm). It appears that Eq. [5.1] is strictly

applicable to 6 inch long and 4 inch high channels, although channel length (L) is included as a parameter.

No formulation is currently available for determining the shear capacity of channel connectors in ribbed metal deck slabs.

The main objective of this thesis was to evaluate the reliability of Eq. [5.1] in predicting the shear capacity of channel connectors in solid concrete slabs, and, if necessary, to formulate a new equation that would provide better correlation with the test results. It was also intended to develop an equation to predict the shear capacity of channel connectors in wide ribbed metal deck slabs. An evaluation of Eq. [5.1] is carried out in the following section.

5.2 Evaluation of Current Formulation

A comparison between the ultimate load per channel values obtained from tests carried out in Phase 2 and those predicted by Eq. [5.1] is presented in Table 5.1. Only the results of the 18 specimens from Phase 2 involving solid concrete slabs are included. The predicted values were calculated using Eq. [5.1], without the resistance factor (ϕ_{sc}) so that a comparison could be made with the ultimate load values obtained from the tests. It appears that the CSA formula gives very conservative values of ultimate load per channel connector. The ratio of test over predicted load values ranges from 1.38 to as high as 2.77.

Figs. 5.1 and 5.2 were prepared to present a clearer view of the accuracy of Eq. [5.1]. Fig. 5.1 presents a comparison of test values of ultimate load and

the predicted values by Eq. [5.1] for nine specimens from Phase 2. All these specimens involved solid concrete slabs and a channel web thickness of 8.2 mm. Another set of nine specimens from Phase 2 is considered in Fig. 5.2. These specimens also had solid concrete slabs but the web thickness of the channels in these specimens was 4.7 mm.

Table 5.1 Observed and Predicted Results for Push-out specimens with Solid Concrete Slabs: Phase 2.

Specimen	f'c	Channel Length	Web Thickness	Ultimate Shear Strength per Channel (kN)		Ratio of Test/ Predicted
	(MPa)	(mm)	(mm)	Test	CSA Eq.	
D1S	21.18	150	8.2	403.4	292.28	1.38
D2S	21.18	100	8.2	326.7	194.86	1.68
D3S	21.18	50	8.2	239.05	97.43	2.45
D4S	21.18	150	4.7	396.4	248.19	1.60
D5S	21.18	100	4.7	301.8	165.46	1.82
D6S	21.18	50	4.7	201.2	82.73	2.43
E1S	34.8	150	8.2	583.65	374.66	1.56
E2S	34.8	100	8.2	488.05	249.77	1.95
E3S	34.8	50	8.2	345.6	124.89	2.77
E4S	34.8	150	4.7	542.8	318.13	1.71
E5S	34.8	100	4.7	433.25	212.09	2.04
E6S	34.8	50	4.7	244	106.04	2.30
F1S	28.57	150	8.2	485.05	339.47	1.43
F2S	28.57	100	8.2	375.5	226.31	1.66
F3S	28.57	50	8.2	268.9	113.16	2.38
F4S	28.57	150	4.7	450.2	288.25	1.56
F5S	28.57	100	4.7	358.55	192.17	1.87
F6S	28.57	50	4.7	222.1	96.08	2.31

Once again, it appears that the CSA formula gives very conservative values of ultimate load per channel connector. As mentioned earlier in this chapter, the current CSA equation is based on the work at Lehigh University by Slutter and Driscoll (1965). Most of the 41 push-out specimens tested at Lehigh University had 6 inch (152 mm) long and 4 inch (102 mm) high channel connectors. Therefore, the discrepancy between the observed and predicted values was the least, but still nearly 50%, for similar specimens tested in this project. The predicted values become even more conservative for the specimens with smaller channel lengths.

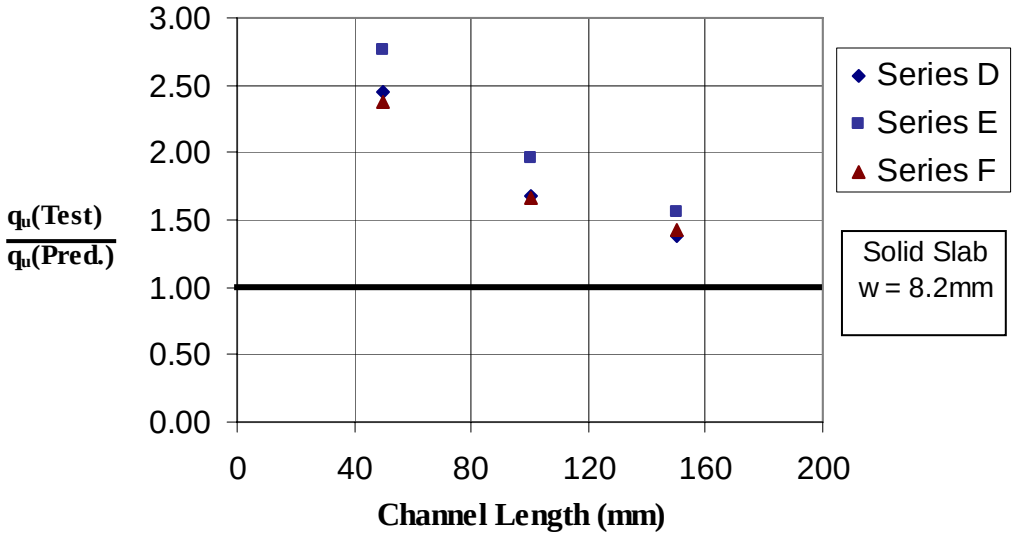

Figure 5.1 Comparison between tested and predicted values of shear resistance for specimens with an 8.2 mm web thickness: CSA S16-01.

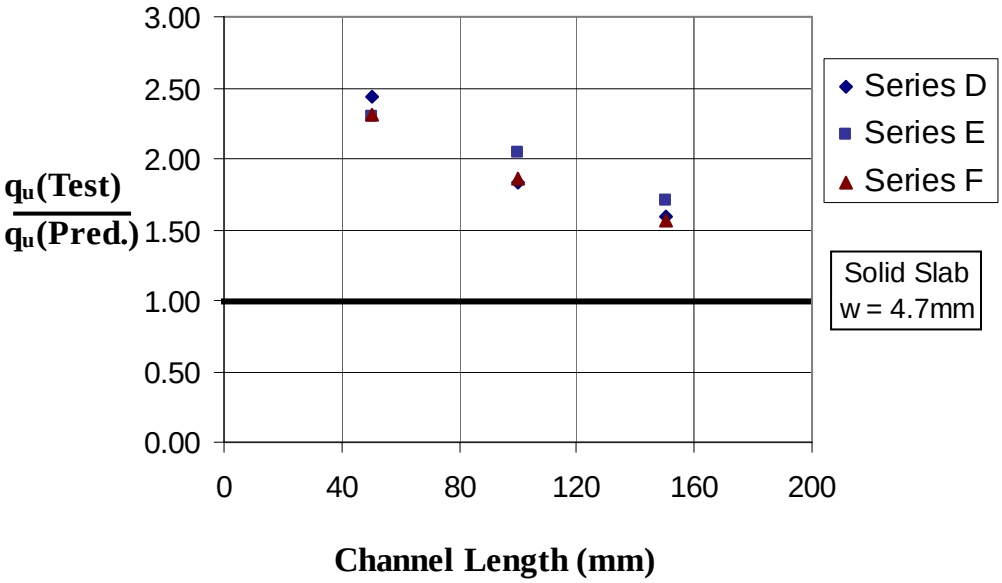

Figure 5.2 Comparison between tested and predicted values of shear resistance for specimens with a 4.7 mm web thickness: CSA S16-01.

The results of a statistical analysis of the push-out test data listed in Table 5.1 revealed that the arithmetic mean (μ) of test values of actual load/ predicted load values by Eq. [5.1] was 1.94. The standard deviation (σ) of these values was 0.398 and the coefficient of variation (ν) was 20.6%. Owing to this significant disagreement between test and predicted values, it was clear that there was a definite need to develop a new equation which would take into account all the important variables involved, in order to provide better accuracy. The rest of this chapter is devoted to fulfilling this objective.

5.3 Channel Shear Connectors Embedded in Solid Concrete Slabs: Development of a New Equation

5.3.1 General Form

Fig. 5.3 shows the load vs. channel length curves of 9 specimens from Phase 2. All these specimens involved solid concrete slabs and the length of

the channel varied from 50 mm to 150 mm. As shown in the figure, the compressive strength of concrete varied from 21.16 MPa to 34.8 MPa. Assuming that the relationship between load and channel length is approximately linear, the following equation is obtained:

$$q_u = A + B(L) \qquad [5.2]$$

where:

q_u = Predicted ultimate load per channel connector [N]

L = Length of channel connector [mm]

A and B are the constants to be determined.

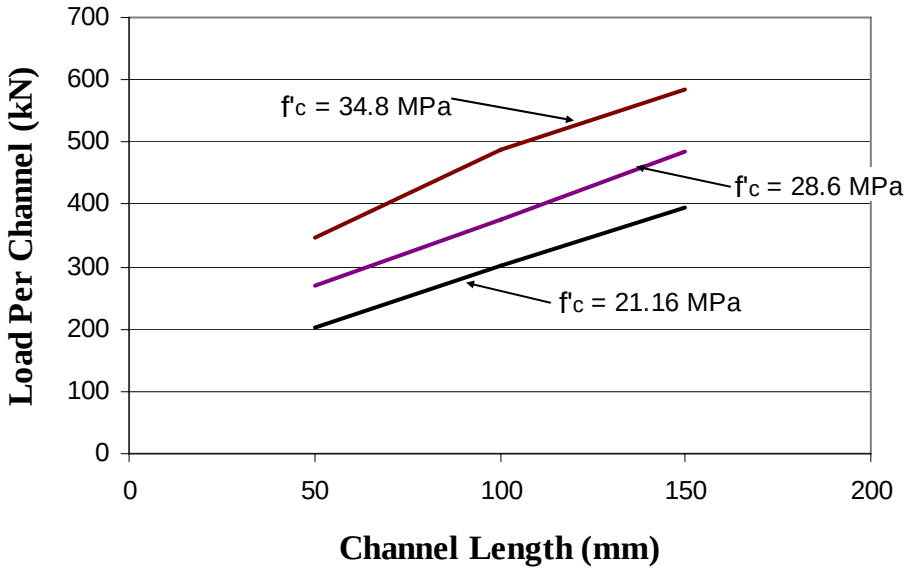

Figure 5.3 Load per channel vs. channel length: Solid slab specimens: Phase 2.

The next factor to be considered is the web thickness of the channel. As discussed earlier in Section 3.2.4, the relationship between ultimate load per channel and the web thickness of channel, was found to be non linear. To include the effect of channel web thickness, the non linear variation can be represented in the following form (Wu 1998):

$$q_u = A + B(L) + C(w) + D(w^2) \qquad [5.3]$$

where:

L = Length of channel connector [mm]

w = Web thickness of channel [mm]

A, B, C and D are constants to be determined

It is obvious from the earlier discussion in Section 3.2.1 that the shear resistance of the channel shear connector is approximately proportional to the square root of the compressive strength of concrete ($\sqrt{f'_c}$). Since previous research (Androutsos 1994 and Wu 1998) showed that the compressive strength of concrete affects the behaviour of all the parameters of a shear connector, Eq. [5.3] can be represented in the following form:

$$q_u = A\sqrt{f'_c} + B(L)\sqrt{f'_c} + C(w)\sqrt{f'_c} + D(w^2)\sqrt{f'_c} \qquad [5.4]$$

The surface area (L x H) of the channel in contact with the concrete is also an important factor. Most of the specimens from Phase 2 (9 out of 18) failed due to crushing-splitting of concrete. Hence, it is logical to include this parameter by multiplying the second term of Eq. [5.4] with H. Making this modification, Eq. [5.4] changes to:

$$q_u = A\sqrt{f'_c} + B(L)(H)\sqrt{f'_c} + C(w)\sqrt{f'_c} + D(w^2)\sqrt{f'_c} \qquad [5.5]$$

However, to ensure dimensional equilibrium, the first and the third terms of the equation must be multiplied by an area and a length parameter, respectively. Since the cross sectional area of the channel web is an important parameter, the third term of Eq. [5.5] is multiplied by the length of channel connector (L). Also, the first term of Eq. [5.5] is multiplied by web thickness (w) and the flange thickness (t). Thus, the following form of the equation is obtained:

$$q_u = A(w)(t)\sqrt{f'_c} + B(L)(H)\sqrt{f'_c} + C(w)(L)\sqrt{f'_c} + D(w^2)\sqrt{f'_c} \qquad [5.6]$$

As described earlier in Chapter 3, two slabs of a push-out specimen in Phase 1 were cast at different times. As a result, the concrete strengths of the 2 slabs of a specimen were different. Hence these specimens were not included in this analysis. Only the specimens from Phase 2 were used.

5.3.2 Regression Analysis

The built-in solver which is available in Microsoft Excel 2002 (Microsoft Office 2002), was applied for the regression analysis using the least squares method. This solver makes use of Newton's method and the central difference approach for solving the equation.

The test results of the 18 push-out specimens with solid concrete slabs which were tested in Phase 2 were used for the regression analysis (Table 5.1).

The least squares regression analysis carried out for Eq. [5.6] yielded:

A = 597.058

B = 5.378

C = -19.066

D = -23.672

By substituting these values in the above equation, Eq. [5.7] was obtained.

$$q_u = [597.058(w)(t) + 5.378(L)(H) - 19.066(w)(L) - 23.672(w^2)]\sqrt{f'_c} \qquad [5.7]$$

The observed ultimate shear strength values per channel and those predicted by Eq. [5.7] for the 18 specimens included in the above analysis are listed in Table 5.2. The average absolute difference between the observed strengths and those predicted by Eq. [5.7] was found to be 5.11%. If the coefficients A, B, C and D in Eq. [5.7] are rounded to 597, 5.4, -19 and -23.7 respectively, the average difference between the observed and predicted values remains approximately the same (5.2%). The final form of the proposed equation is:

$$q_u = [597(w)(t) + 5.4(L)(H) - 19(w)(L) - 23.7(w^2)]\sqrt{f'_c} \qquad [5.8]$$

where:

q_u = Predicted ultimate load per channel connector [N]

t = Flange thickness of channel connector [mm]

w = Web thickness of channel connector [mm]

L = Length of channel connector [mm]

H = Height of channel connector [mm]

f'_c = Specified compressive strength of concrete [MPa]

The observed ultimate shear strength values per channel and those predicted by Eq. [5.8] are listed in Table 5.3. The values predicted by CSA provisions are also included in this table. The average absolute difference between the observed values and those predicted by Eq. [5.8] was found to be 5.2% as

compared to 46.2% for the current CSA equation. The average arithmetic mean of the test/predicted ratio (μ), was found to be 0.9884. The standard deviation (σ) was 0.057 and the coefficient of variation (C.V.) was 1.11%. Corresponding values for the CSA provisions are given in Table 5.4.

Table 5.2 Observed and Predicted Results for Push-out Specimens included in the Regression Analysis.

Specimen	f'c	Channel Length	Web Thickness	Ultimate Shear Strength per Channel (kN)		Ratio of Test/ Predicted
	(MPa)	(mm)	(mm)	Test	Eq.5.7	
D1S	21.18	150	8.2	403.4	432.40	0.93
D2S	21.18	100	8.2	326.7	342.16	0.95
D3S	21.18	50	8.2	239.05	251.91	0.95
D4S	21.18	150	4.7	396.4	411.26	0.96
D5S	21.18	100	4.7	301.8	305.66	0.99
D6S	21.18	50	4.7	201.2	200.05	1.01
E1S	34.8	150	8.2	583.65	554.26	1.05
E2S	34.8	100	8.2	488.05	438.58	1.11
E3S	34.8	50	8.2	345.6	322.90	1.07
E4S	34.8	150	4.7	542.8	527.16	1.03
E5S	34.8	100	4.7	433.25	391.80	1.11
E6S	34.8	50	4.7	244	256.43	0.95
F1S	28.57	150	8.2	485.05	502.20	0.97
F2S	28.57	100	8.2	375.5	397.39	0.94
F3S	28.57	50	8.2	268.9	292.57	0.92
F4S	28.57	150	4.7	450.2	477.65	0.94
F5S	28.57	100	4.7	358.55	355.00	1.01
F6S	28.57	50	4.7	222.1	232.35	0.96

Table 5.3 Observed and Predicted Results for Push-out Specimens by the CSA Equation and Equation 5.8.

Specimen	f'c	Channel Length	Web Thickness	Ultimate Shear Strength per Channel (kN)		
	(MPa)	(mm)	(mm)	Test	CSA Eq.	Eq.5.8
D1S	21.18	150	8.2	403.4	292.28	434.32
D2S	21.18	100	8.2	326.7	194.86	343.42
D3S	21.18	50	8.2	239.05	97.43	252.53
D4S	21.18	150	4.7	396.4	248.19	413.03
D5S	21.18	100	4.7	301.8	165.46	306.83
D6S	21.18	50	4.7	201.2	82.73	200.64
E1S	34.8	150	8.2	583.65	374.66	556.71
E2S	34.8	100	8.2	488.05	249.77	440.21
E3S	34.8	50	8.2	345.6	124.89	323.70
E4S	34.8	150	4.7	542.8	318.13	529.42
E5S	34.8	100	4.7	433.25	212.09	393.30
E6S	34.8	50	4.7	244	106.04	257.18
F1S	28.57	150	8.2	485.05	339.47	504.43
F2S	28.57	100	8.2	375.5	226.31	398.86
F3S	28.57	50	8.2	268.9	113.16	293.30
F4S	28.57	150	4.7	450.2	288.25	479.70
F5S	28.57	100	4.7	358.55	192.17	356.36
F6S	28.57	50	4.7	222.1	96.08	233.02

Table 5.4 Statistical Analysis of Predicted Values by the CSA Equation and Equation 5.8.

Statistics	CSA	Eq. 5.8
μ	1.94	0.988
σ	0.398	0.057
C.V.	20.57%	1.11%

Figures 5.4 and 5.5 depict the ratios of observed over predicted values by Eq. [5.8] for push-out specimens of Phase 2 involving solid concrete slabs. Similar plots of predicted values by CSA provisions were presented earlier in Figs. 5.1 and 5.2. It is obvious that Eq. [5.8] provides much better predictions. The test over predicted values for Eq. [5.8] are concentrated within 0.9-1.11, while the corresponding values for CSA are in the range of 1.3-2.7.

A simplified version of Eq. [5.8] is included in Appendix G.

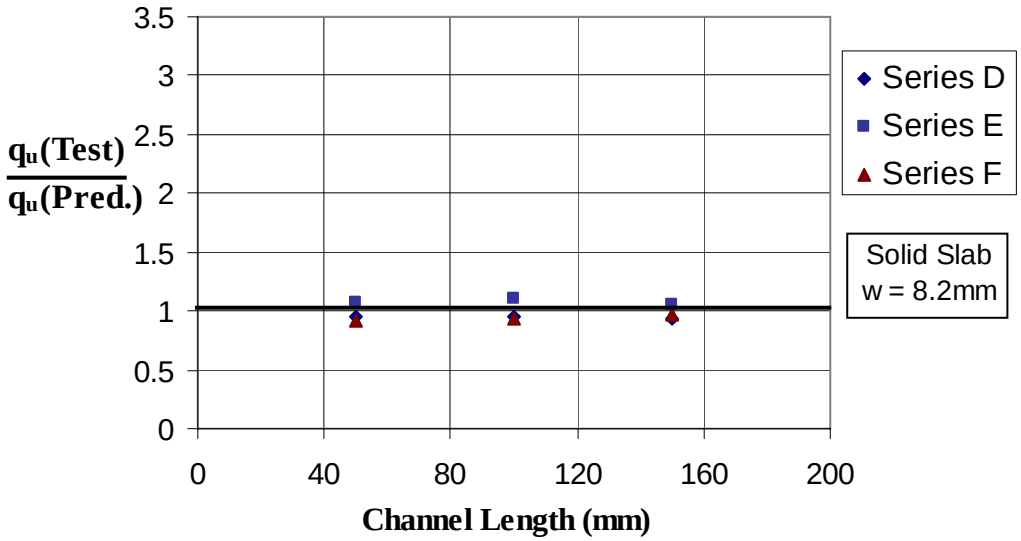

Figure 5.4 Comparison between test values and those predicted by Equation 5.8.

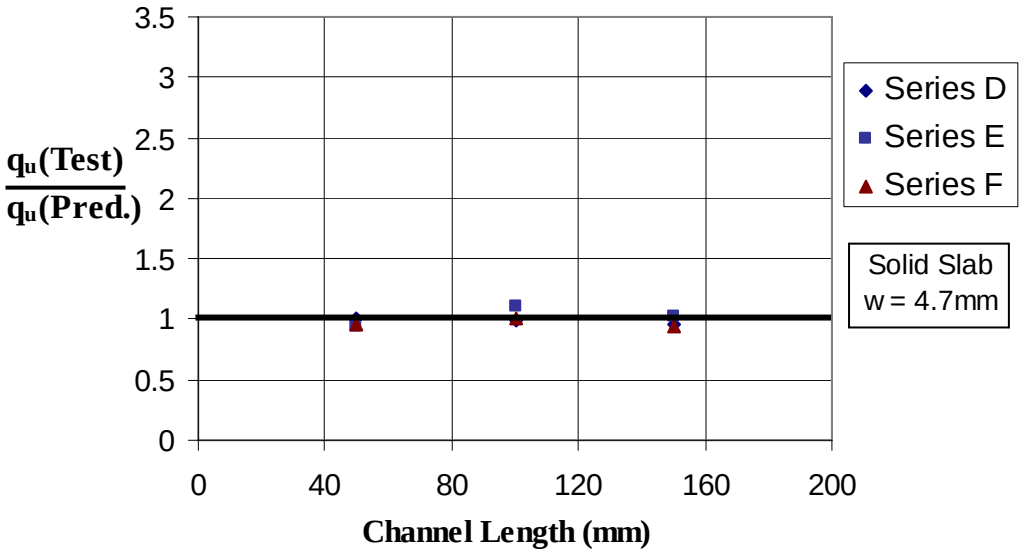

Figure 5.5 Comparison between test values and those predicted by Equation 5.8.

5.4 Channel Shear Connectors Embedded in Slabs with Wide Ribbed Metal Deck: Development of New Equation

5.4.1 General Form

A total of 18 specimens from Phase 2 involving slabs with wide ribbed metal deck were used in this analysis. All these specimens featured metal deck slabs with w_d/h_d ratio of 2.33. The compressive strength of concrete varied from 21.16 MPa (Series D) to 34.8 MPa (Series E). As discussed earlier in Section 3.2.4, a non-linear relationship between the channel web thickness and the ultimate load per channel was observed, which can be represented in the following form:

$$q_u = A + B(w) + C(w^2) \qquad [5.9]$$

where:

q_u = Predicted ultimate load per channel connector [N]

w = Web thickness of channel [mm]

A, B and C are the constants to be determined

The next factor to be considered is the length of the channel connector, L. The observations of the test results in Section 3.2.2 have shown that the load capacity of the channel connector increases linearly with the increase in the length of the channel. Therefore, it is appropriate to include this variable in the first part of Eq. [5.9] as follows:

$$q_u = A(L) + B(w) + C(w^2) \qquad [5.10]$$

Once again, it is clear from the discussion earlier in Section 3.2.1 that the increase of ultimate load per channel is proportional to the square root of the compressive strength of concrete, f'_c. Thus, if the concrete strength is also taken into account, Eq. [5.10] would assume the following form:

$$q_u = A(L)\sqrt{f'_c} + B(w)\sqrt{f'_c} + C(w^2)\sqrt{f'_c} \qquad [5.11]$$

The ratio of the width to depth of the flute of metal deck (w_d/h_d) is also an important factor. In all the specimens involved in this analysis, wide ribbed metal deck with $w_d/h_d = 2.33$ were used. The assumption that the effect of metal deck is linear, seems to be logical and appropriate. Thus, it may be assumed that the w_d/h_d term would affect only the first term of Eq. [5.11]. Making this modification, Eq. [5.11] changes to:

$$q_u = A(L)\frac{w_d}{h_d}\sqrt{f'_c} + B(w)\sqrt{f'_c} + C(w^2)\sqrt{f'_c} \qquad [5.12]$$

As discussed earlier, the surface area (L x H) of the channel connector in contact with the concrete is also an important factor. Concrete related failure was the predominant type of failure in the specimens with ribbed metal deck slabs. In 16 out of 18 specimens from Phase 2, concrete related failures were observed. Hence, this parameter is included in the first term of Eq. [5.12] as follows:

$$q_u = A(L)(H)\frac{w_d}{h_d}\sqrt{f'_c} + B(w)\sqrt{f'_c} + C(w^2)\sqrt{f'_c} \qquad [5.13]$$

To maintain dimensional equilibrium, the second term of the equation must be multiplied by a length term. Since the cross sectional area of the channel web is an important parameter, the second part of Eq. [5.13] is multiplied by the length of the channel connector (L). This modification would lead to Eq. [5.14]:

$$q_u = A(L)(H)\frac{w_d}{h_d}\sqrt{f'_c} + B(w)(L)\sqrt{f'_c} + C(w^2)\sqrt{f'_c} \qquad [5.14]$$

5.4.2 Regression Analysis

The regression analysis was again performed by the built-in solver in Microsoft Excel 2002. As discussed earlier in Section 5.3.1, the test results of the 18 specimens with metal deck slabs of Phase 2 were only used for the regression analysis (Table 5.5).

Table 5.5 Observed Test Results for Push-out Specimens with Metal Deck Slabs.

Specimen	f'c (MPa)	Channel Length (mm)	Web Thickness (mm)	Ratio W_d/h_d	Ultimate Shear Strength per Channel (kN) Test
D1D	21.18	150	8.2	2.33	318.7
D2D	21.18	100	8.2	2.33	278.9
D3D	21.18	50	8.2	2.33	179.3
D4D	21.18	150	4.7	2.33	283.85
D5D	21.18	100	4.7	2.33	244
D6D	21.18	50	4.7	2.33	159.35
E1D	34.8	150	8.2	2.33	443.2
E2D	34.8	100	8.2	2.33	381.45
E3D	34.8	50	8.2	2.33	260.95
E4D	34.8	150	4.7	2.33	407.35
E5D	34.8	100	4.7	2.33	353.6
E6D	34.8	50	4.7	2.33	218.1
F1D	28.57	150	8.2	2.33	347.6
F2D	28.57	100	8.2	2.33	288.85
F3D	28.57	50	8.2	2.33	208.15
F4D	28.57	150	4.7	2.33	336.65
F5D	28.57	100	4.7	2.33	273.9
F6D	28.57	50	4.7	2.33	182.25

The least squares regression analysis carried out for Eq. [5.14] yielded:

A = -39.94

B = 474.06

C = 2.46

Substituting these values in Eq. [5.14], the following form is obtained:

$$q_u = [-39.94(L)(H)\frac{w_d}{h_d} + 474.06(w)(L) + 2.46(w^2)]\sqrt{f'_c} \qquad [5.15]$$

The observed ultimate shear strength values per channel and those predicted by Eq. [5.15] for the 18 specimens included in the above analysis are listed in Table 5.6. The average absolute difference between the observed values and those predicted by Eq. [5.15] was found to be approximately 8.95%. If the coefficients A, B and C given above are rounded to -40, 474 and 2.5, respectively, the average absolute difference between the observed and predicted values remains almost the same (9.03%). The final form of the proposed equation is presented below:

$$q_u = [-40(L)(H)\frac{w_d}{h_d} + 474(w)(L) + 2.5(w^2)]\sqrt{f'_c} \qquad [5.16]$$

where:

q_u = Predicted ultimate load per channel connector [N]

L = Length of channel connector [mm]

H = Height of channel connector [mm]

f'_c = Specified compressive strength of concrete [MPa]

$\frac{w_d}{h_d}$ = Ratio of width to depth of flute of metal deck

w = Web thickness of channel connector [mm]

The average absolute difference between the observed values and those predicted by Eq. [5.16] was found to be 9%. The average arithmetic mean of

Table 5.6 Observed and Predicted Results for Push-out Specimens by Equation 5.15.

Specimen	f'c	Channel Length	Web Thickness	Ultimate Shear Strength per Channel (kN)		Ratio of Test/ Predicted
	(MPa)	(mm)	(mm)	Test	Eq.5.15	
D1D	21.18	150	8.2	318.7	324.92	0.98
D2D	21.18	100	8.2	278.9	265.51	1.05
D3D	21.18	50	8.2	179.3	206.11	0.87
D4D	21.18	150	4.7	283.85	322.92	0.88
D5D	21.18	100	4.7	244	231.35	1.05
D6D	21.18	50	4.7	159.35	139.77	1.14
E1D	34.8	150	8.2	443.2	416.48	1.06
E2D	34.8	100	8.2	381.45	340.34	1.12
E3D	34.8	50	8.2	260.95	264.19	0.99
E4D	34.8	150	4.7	407.35	413.93	0.98
E5D	34.8	100	4.7	353.6	296.54	1.19
E6D	34.8	50	4.7	218.1	179.16	1.22
F1D	28.57	150	8.2	347.6	377.37	0.92
F2D	28.57	100	8.2	288.85	308.37	0.94
F3D	28.57	50	8.2	208.15	239.38	0.87
F4D	28.57	150	4.7	336.65	375.05	0.90
F5D	28.57	100	4.7	273.9	268.69	1.02
F6D	28.57	50	4.7	182.25	162.33	1.12

the test/predicted ratio (μ), was found to be 1.002. The standard deviation (σ) was estimated to be 0.106. The coefficient of variation (C.V.) was 1.17%.

Figs. 5.6 and 5.7 were prepared to provide a clearer observation of the performance of Eq. [5.16]. These figures plot the ratio of observed over predicted values by Eq. [5.16] for push-out specimens of Phase 2 involving

metal deck slabs. The observed over predicted values for Eq. [5.16] are concentrated within 0.86-1.2. It is obvious that Eq. [5.16] is reasonably in agreement with the observed test values.

The ultimate shear strength values predicted by Eq. [5.16] and those observed from Push-out tests are listed in Table F.1 in Appendix F.

A simplified version of Eq. [5.16] is included in Appendix G.

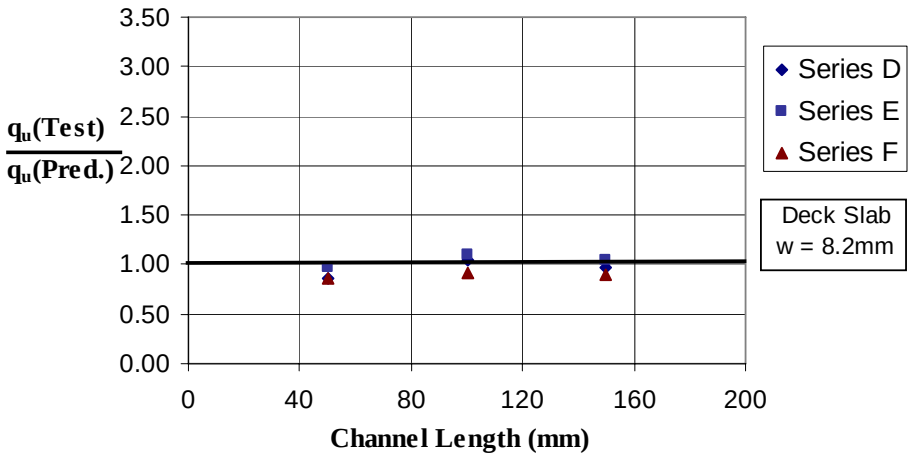

Figure 5.6 Comparison between tested values of shear resistance and those predicted by Equation 5.16 for specimens with an 8.2 mm web thickness.

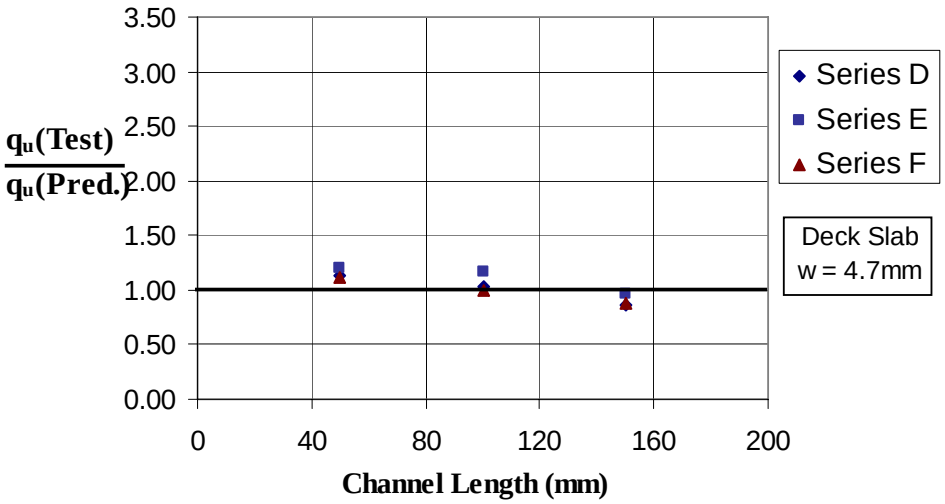

Figure 5.7 Comparison between tested values of shear resistance and those predicted by Equation 5.16 for specimens with a 4.7 mm web thickness.

Appendix G includes a discussion on the possibility of using the proposed equations to predict the capacity of composite beams with 127 mm high channel shear connectors.

CHAPTER SIX

SUMMARY AND CONCLUSIONS

6.1 Summary

The experimental investigation involved the testing of push-out specimens with channel shear connectors. The test program was divided into 2 phases involving the testing of 78 push-out specimens with solid concrete slabs and slabs with wide ribbed metal deck oriented parallel to the beam. The main objectives of this investigation were to evaluate the reliability of the existing CSA provisions for channel shear connectors in composite beams with solid concrete slabs and, if necessary, to develop a new equation which will provide better correlation to experimental results. The investigation also aimed at the development of a new equation for channel shear connectors embedded in slabs with wide ribbed metal deck oriented parallel to the beam.

The test specimens were designed to study the effect of a number of parameters on the shear capacity of channel shear connectors. Six series of push-out specimens were tested in two phases. The primary difference between the two phases was the height of channel connector. Other test parameters included the compressive strength of concrete, length of channel shear connector and the web thickness of the channel.

Three different types of failure mechanisms were observed. In specimens with higher strength concrete, failure occurred by the fracture of the channel near the fillet with the channel web acting like a cantilever beam. Crushing

of concrete adjacent to the channel web was the observed mode of failure in specimens with solid slabs when lower strength concrete was used. In most of the specimens with metal deck slabs, a concrete shear plane type of failure was observed. In the specimens involving this type of failure, the channel connector remained intact and the concrete contained within the flute in front of channel web sheared off along the interface.

The load carrying capacity of a channel connector increased almost linearly with the increase in channel length. On average, the increase was about 39% when the channel length was increased from 50 mm to 100 mm. There was a further increase of 24% when the channel length was increased from 100 mm to 150 mm. The influence of web thickness of the channel connector was significant when the failure occurred due to channel web fracture, but was minimal for concrete crushing type failure. In general, the specimens with a thicker channel web carried only 6.44% higher load when the failure was concrete related. The increase in load was as high as 41% in some cases involving failure due to channel web fracture.

The specimens with solid concrete slabs carried higher loads compared to those with metal deck slabs. The increase was 33% for specimens with 150 mm long channels, but only 12% for those with 50 mm long channel connectors. The influence of web thickness of the channel connector was significant when failure occurred due to channel web fracture, but was minimal for concrete related failures.

Test results indicated that, for the push-out specimens with solid concrete slabs, the current CSA provisions give very conservative values. The

average predicted strength was 46.27% lower than the average observed value. The average of the test/predicted values was 1.94 and the coefficient of variation was found to be 20.57%.

This investigation resulted in the development of a new equation for predicting the shear strength of channel connectors embedded in solid concrete slabs. The proposed equation provides much better correlation to test results than does the current CSA equation. The average absolute difference between the observed values and those predicted by the proposed equation was found to be 5.11%, compared to 46.27% for the CSA equation. The better results may be attributed to the fact that the proposed equation is based on test results of specimens with three different channel lengths (150 mm, 100 mm and 50 mm) whereas most of specimens tested to develop the CSA equation were 6 inches (152 mm) long.

A simplified version of the proposed equation was also found to be more accurate than the CSA equation. The average absolute difference between the observed values and those predicted by the simplified equation was found to be 10.1%. Because of the simplicity of the approximate equation and only slightly lower accuracy, this equation is recommended for use in design.

The results of specimens with metal deck slabs were used to develop a new equation for predicting the shear capacity of channel connectors embedded in slabs with metal deck oriented parallel to the beam. The proposed equation is in good agreement with the observed test values. The average absolute difference between the observed values and the predicted values

was found to be 9.03%. The average arithmetic mean of the test/predicted ratio (μ) of this equation was 1.002. The standard deviation (σ) and the coefficient of variation (C.V.) for the proposed equation were 0.106 and 1.17%, respectively. A simplified version of the proposed equation gives an average absolute difference of approximately 11.8% between the observed values and those predicted by the simplified equation. Hence, the simplified equation is recommended for the design of channel shear connectors in metal deck slabs.

6.2 Conclusions

The following conclusions can be drawn from this investigation:

1. The current CSA provision for the design of shear capacity of channel shear connectors in solid concrete slabs (CAN/CSA-S16-01) under-estimates the shear capacity of the connector. The ratio of the test values of shear strength to the values predicted by the CSA equation varied from nearly 2.5 (for 50 mm channels) to 1.6 (for 150 mm channel connectors). Since no equation for evaluating the shear capacity of a channel in ribbed metal deck is currently available, a similar comparison could not be made.

2. New equations have been developed for the design of shear capacity of channel connectors in solid concrete slabs as well as those with slabs featuring wide ribbed metal deck. These equations include all important parameters, i.e., length of channel, web thickness and height

of channel, compressive strength of concrete and the profile of the metal deck. The average absolute difference between the observed values and predicted values by the proposed equations for solid slabs and metal deck slabs were 5.11% and 9.03%, respectively.

3. The test results showed that the load carrying capacity of the channel connector increased almost linearly with the increase in the channel length. On average, the load carrying capacity increased by about 39% when the channel length was increased from 50 mm to 100 mm. There was a further increase of 24% when the channel length was increased from 100 mm to 150 mm. The rate of increase appears to be approximately the same, regardless of the compressive strength of concrete.

4. For a given length of channel, the concrete strength dictated the failure mode. Channel web fracture type of failure was observed in the specimens with the highest strength concrete, while the specimens with lower and moderate strength concrete were more susceptible to concrete related failures.

5. It was observed that the channels in solid concrete slabs carried over 33% higher loads (for 150 mm long channels) than those in metal deck slabs. This increase was only 12% in the case of 50 mm long channels.

6. The web thickness of the channel had a significant role in dictating the shear strength of the channel when the failure was due to channel web fracture. A minimal influence of channel web thickness was observed for the concrete crushing types of failure.

7. The load-slip curves indicated that the specimens with 127 mm high channel shear connectors were more ductile compared to those with 102 mm high channels. A slight increase in the load carrying capacity was observed for 127 mm height channels, but only when the failure was concrete related. In the case of web fracture type of failures, specimens with channels of shorter height (102 mm) carried slightly higher loads than those with 127 mm high channel connectors.

6.3 Recommendations

Based on research presented in this thesis, the following recommendations can be made:

1. The Illinois technique of fabrication of specimens involves the pouring of concrete in two slabs of the same specimen at different times. In spite of due care taken in controlling the mix design and the curing times of the two slabs, this method resulted in different concrete strengths in the two slabs of a specimen. The German method of fabrication of specimens, although complicated, gives much better results because the casting of two slabs of a specimen takes place at the same time with same batch of concrete. Therefore,

the German method of fabrication is recommended for all future push-out test specimens.

2. It is recommended that further research on channel connectors of different heights should be carried out in order to develop a general equation which would be able to predict the shear capacity of the channel shear connectors of different heights.

REFERENCES

AISC. 1993. Load and resistance factor design specifications for structural steel buildings. American Institute of Steel Construction, Chicago, Illinois.

AISC (1986). "Load and Resistance Factor Design Specification for Structural Steel Buildings." American Institute of Steel Construction, Chicago, IL.

Androutsos, C., and Hosain, M.U. 1994. Design equation for headed studs in narrow ribbed metal deck. Proceeding of the CSCE Annual Conference, Winnipeg, June 1-4, Volume II, pp. 249-258.

Androutsos, C., and Hosain, M.U. 1993. Composite beams with headed studs in narrow ribbed metal deck. Composite Construction in Steel and Concrete II. Special Publication of the ASCE Structural Division, New York, N.Y., pp. 771-782.

Androutsos, C. 1994. Composite beams with headed studs in narrow ribbed metal deck. M.Sc. thesis, Department of Civil Engineering, University of Saskatchewan, Saskatoon.

Brattland, A., and Kennedy, D.J.L. (1986). "Tests of a Full-Scale Composite Truss." Proceedings of the Canadian Structural Engineering Conference, Canadian Institute of Steel Construction, Willowdale, Ontario, 8.1-8.50.

Buckner, D., and Shahrooz, B. M. 1996. Composite construction in steel and concrete III. Proceedings of Engineering Foundation Conference, ASCE, New York, N. Y.

Chien, E.Y.L. and Ritchie, J.K. 1984. Design and construction of composite floor systems. Canadian Institute of Steel Construction, Toronto, Ontario.

CEN (1994). prEN 1994: Eurocode 4, Design of composite steel and concrete structures Part 1.1: General rules and rules for buildings, Comite Europeen de Normalisation (CEN), Brussels, Belgium.

CEN (2001). prEN 1994-1-1:2001: Draft No. 2 of Eurocode 4, Design of composite steel and concrete structures Part 1.1: General rules and rules for buildings, Comite Europeen de Normalisation (CEN), Brussels, Belgium.

Crisinel, M. 1987. New system of connection with non-welded shear connectors. Proceedings of the ASCE/IABSE Engineering Foundation Conference on Composite Construction in Steel and Concrete, Henniker, New Hampshire, 636-645.

CSA (1984a). CAN3-S16.1-M84, Steel Structures for Buildings-Limit State Design, Canadian Standard Association, Rexdale, Ontario.

CSA (1989). CAN/CSA-S16.1-M89, Limit States Design of Steel Structures, Canadian Standard Association, Rexdale, Ontario.

CSA (1994). CAN/CSA-S16.1-M94, Limit States Design of Steel Structures, Canadian Standard Association, Rexdale, Ontario.

CSA (2001) CAN/CSA-S16-01, Limit States Design of Steel Structures, Canadian Standard Association, Rexdale, Ontario.

Culver, C., and Coston, R. 1961. Tests of composite beams with stud shear connectors. Journal of the Structural Division, ASCE, (ST2), paper 2742, 1-17.

Davies, C. 1967. Small-scale push-out tests on welded stud shear connectors. Journal titled “Concrete”, London, 1, 311-316.

Driscoll, G.C., and Slutter, R.G. (1961). “Research on Composite Design at Lehigh University.” Proceedings of the AISC National Engineering Conference, American Institute of Steel Construction, Chicago, IL.

Ernst, S., and Patrick, M. 2004. Novel device for enhancing performance of studs in composite slabs incorporating profiled steel sheeting. Pre-Conference Proceedings, Composite Construction in Steel and Concrete V, The Kruger National Park Conference Centre, South Africa, July 18-23, 2004.

Fisher, J.W., Kim, S.W., and Slutter, R.G. (1967). “Tests of Lightweight Concrete Composite Beams and Push-out Specimens with Cellular Steel Deck.” Fritz Engineering Laboratory Report # 200.67.438.1, Lehigh University, Bethlehem, PA.

Gnanasambandam, C., and Hosain, M.U. 1995. Reevaluation of the Lehigh formula for composite floor systems. Proceedings of the CSCE Annual Conference, Ottawa, June 1-3, Volume IV, pp. 655-664.

Gnanasambandam, C. and Hosain, M.U. (1996). Headed Stud Connectors in Solid Slabs and in Slabs with Wide Ribbed Metal Deck. Structural Engineering Research Report No. 43, August. Department of Civil Engineering, University of Saskatchewan, Saskatoon, Canada, S7N 5A9.

Grant, J.A., Fisher, J.W., and Slutter, R.G. 1977. Composite beams with formed steel deck. AISC Engineering Journal, Vol. 14, No. 1, 24-43.

Hawkins, N.M., and Mitchell, D. (1984). “Seismic Response of Composite Shear Connections.” J. Struct. Engrg., ASCE, 110(9), 2120-2136.

Hegger, J., and Goralski, C. 2004. Structural behaviour of high strength concrete encased composite sections. Pre-Conference Proceedings, Composite Construction in Steel and Concrete V, The Kruger National Park Conference Centre, South Africa, July 18-23, 2004.

Hidehiko ABE and Hosaka, T.2002. Flexible Shear Connectors for Railway Composite Girder Bridges. Composite Construction in Steel and Concrete IV, ASCE, February, 71-80.

Hosain, M. U., Chien, E.Y.L., and Kennedy, D.J.L. 1993. New Canadian provisions for the design of composite beams. Composite Construction in Steel and Concrete II. Special Publication of the ASCE Structural Division, New York, N.Y., pp. 39-48.

Jayas, B.S., and Hosain, M.U. 1989. Behaviour of headed studs in composite beams: full-size tests, Canadian Journal of Civil Engineering, 16(5), 712-723.

Jayas, B.S., and Hosain, M.U. 1988. Behaviour of headed studs in composite beams: push-out tests. Canadian Journal of Civil Engineering, 15, 240-253.

Johnson, R.P. 1970. Research on steel-concrete composite beams. Journal of Structural Division. ASCE, 96(ST3), paper 7122, 445-459.

Kuhlmann, I. U., and Breuninger, I. U. 2000. Behaviour of horizontally lying studs with longitudinal shear force. Composite Construction in Steel and Concrete IV, ASCE, May, 438-449.

Kulak, G.L., Adams, P.F., and Gilmor, M.I. 1990. Limit states design in structural steel. Canadian Institute of Steel Construction, Willowdale, Ontario.

Lawson, R. M. 1993. Shear connection in composite beams. Composite Construction in Steel and Concrete II. Special Publication of the ASCE Structural Division, New York, N.Y., 81-97.

McCormac, J. 1992. Structural steel design: ASD method. Fourth edition. Harper Collins Publishers, New York, N. Y.

Microsoft Excel. 2002. Microsoft Excel Users Guide, Version 2002.

Moore, W.P. 1987. An overview of composite construction in the United States. Proceedings of the ASCE/IABSE Engineering Foundation Conference on Composite Construction in Steel and Concrete, Henniker, New Hampshire, 1-17.

Mottram, J.T., and Johnson, R.P. 1990. Push tests on studs welded through profiled steel sheeting. Structural Engineer, Vol. 68, No. 10, 187-193.

Nishido, T., Fuji, K. and Ariyoshi, T. 2002. Slip Behaviour of Perforated Rib Shear Connector and its Treatment in FEM. Composite Construction in Steel and Concrete, IV, ASCE, February, 415-425.

Oguejiofor, E.C., and Hosain, M.U. 1992. Behaviour of Perfobond Rib Shear Connectors in Composite Beams: Full Size Tests. Canadian Journal of Civil Engineering, Vol. 19, No. 2, pp. 224-235.

Oguejiofor, E.C., and Hosain, M.U. 1993. Shear capacity of perfobond rib connectors. Composite Construction in Steel and Concrete II. Special Publication of the ASCE Structural Division. New York, N.Y., pp. 883-898.

Oguejiofor, E.C., and Hosain, M.U. 1994. A parametric study of perfobond rib shear connectors. Canadian Journal of Civil Engineering, Volume 21, No. 4, pp. 614-625.

Oguejiofor, E.C., and Hosain, M.U. 1995. Tests of Full Size Composite Beams with Perfobond Rib Shear Connectors. Canadian Journal of Civil Engineering, Volume 22, No. 1, pp. 80-92.

Ollgaard, J.G., Slutter, R.G., and Fisher, J.W. 1971. Shear strength of stud connectors in lightweight and normal-weight concrete. AISC Engineering Journal, Vol. 8, 55-64.

Patrick, M., and Bridge, R.Q. 2000. Reinforcing against rib shear failure in composite edge beams. Composite Construction in Steel and Concrete IV, ASCE, May, 298-309.

Quddusi F., and Hosain, M.U. 1993. Behaviour of Slotted and Flexible Perfobond Rib Shear Connectors. Proceedings of the CSCE Annual Conference, Fredericton, June 8-11, Volume II, pp. 629-638.

Rao, S. N. 1970. Composite Construction-Tests on Small Scale Shear Connectors. The Institute of Engineers, Australia, Civil Engineering Transactions, April.

Roberts, W., and Heywood, R. 1992. Shear Connectors for Composite Structures. Physical Infrastructure Centre Digest, **1**(4), Queensland University of Technology, Brisbane, Australia, 4-5.

Robinson, H., and Wallace, I.W. (1973). “Composite Beams with 11/2 inch Metal Deck and Partial and Full Shear Connection.” Transactions of the Canadian Society for Civil Engineering, 6(A-8), I-VIII.

Slutter, R.G., and Driscoll, G. C. 1965. Flexural Strength of Steel-Concrete Composite Beams. ASCE Journal of Structures Division, Volume 91, No. ST1, February, 71-99.

Slutter, R.G., and Driscoll, G. C. 1962. Test results and design recommendations for composite beams. Lehigh University Fritz Engineering Laboratory, Report No. 279.10.

Studnicka, J., Machacek, J., Krpata, A., and Svitakova, M. 2002. Perforated Shear Connector for Composite Steel Concrete Beams. Composite Construction in Steel and Concrete, IV, ASCE, February, 415-425.

Trumpf, H., and Sedlacek, G. 2004. Advanced composite bridge design. Pre-Conference Proceedings, Composite Construction in Steel and Concrete V, The Kruger National Park Conference Centre, South Africa, July 18-23, 2004.

Veldanda, M.R., and Hosain, M.U. 1992. Behavior of perfobond rib shear connectors in composite beams: push-out tests. Canadian Journal of Civil Engineering, Volume 19, Number 1, pp. 1-10.

VicWest (2002). Hi-Bond composite floor deck brochure. Vicwest Products, 1296, South Service Road West, Oakville, ON, L6L 5T7.

Viest, I.M., Siess, C.P., Appleton, J.H. and Newmark, N.M. 1952. Full scale tests on channel shear connectors in composite T-Beams. University of Illinois Bulletin No. 405, Urbana, IL.

Viest, I.M. 1956. Investigation of stud shear connectors for composite concrete and steel T-beams. Journal of the American Concrete Institute, 27(8), 875-891.

Viest, I.M. 1960. Review of research on composite steel-concrete beams. Journal of the Structural Division, ASCE, 86(ST6), Paper 2496, 1-21.

Wu, Hang. 1998. Headed stud shear connectors in full-size composite beams with wide ribbed metal deck. M.Sc. thesis, Department of Civil Engineering, University of Saskatchewan, Saskatoon.

Wu, H. and Hosain, M.U. (1997). Tests on Full Size Composite Beams with Wide Ribbed Metal Deck**.** CSCE Annual Conference, Sherbrooke, Canada, May 28-June 1, Vol. 6, pp. 249 - 256.

Wu, Hang and Hosain, M. U. (1999). Headed stud connectors in full-size composite beams with wide ribbed metal deck. Structural Engineering Research Report No. 45, University of Saskatchewan, Saskatoon, Canada, S7N 5A9, June.

Yam, L.C.P. 1981. Design of composite steel-concrete structures. Surrey University Press, London, U.K.

Zellner, W. 1987. Recent designs of composite bridges and a new type of shear connectors. Proceedings of the ASCE/IABSE Engineering Foundation Conference on Composite Construction, Henniker, New Hampshire, June 7-12, 240-252.

APPENDIX A

Metal Deck Details

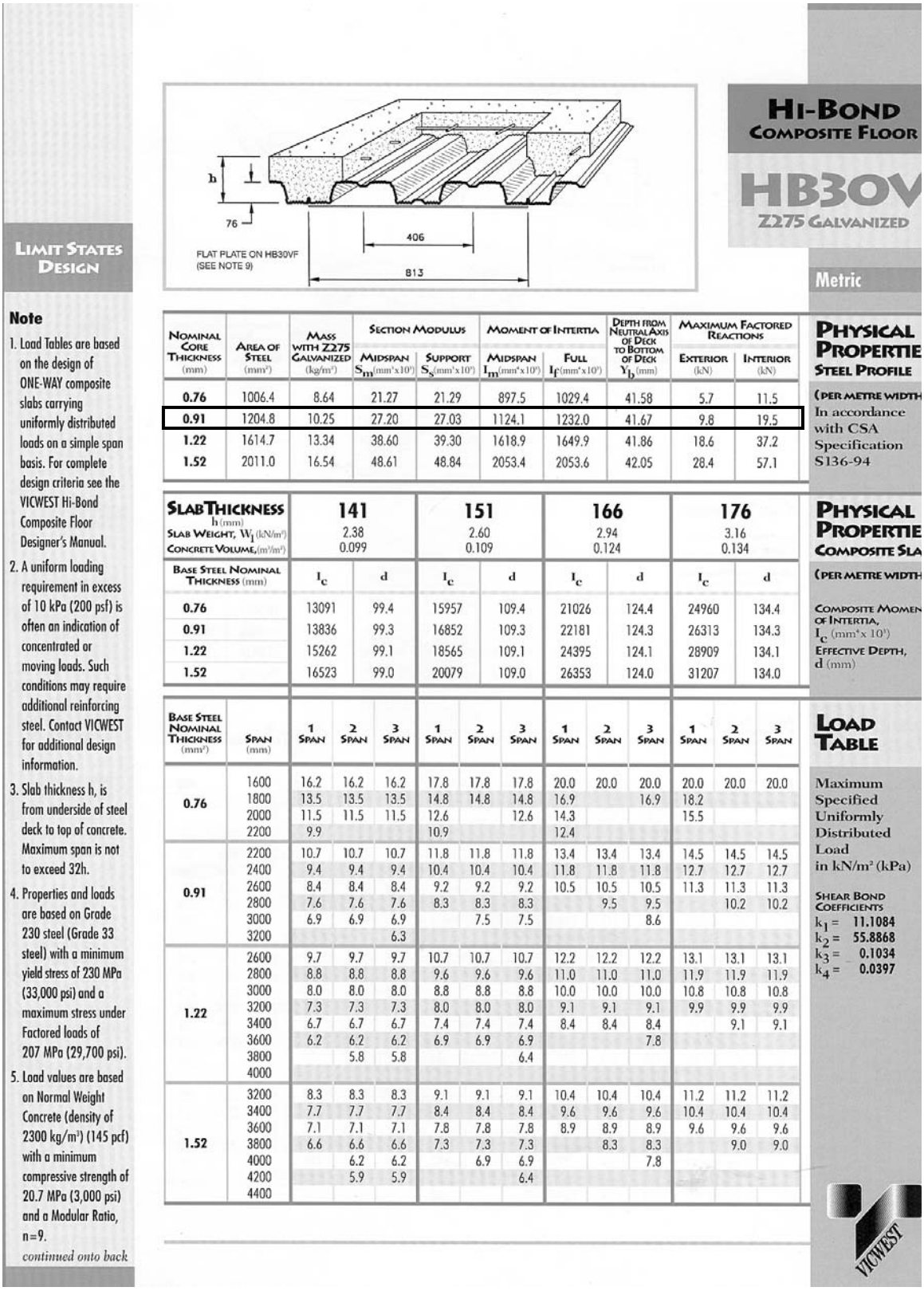

HI-BOND COMPOSITE FLOOR

HB30V

Z275 GALVANIZED

Metric

PHYSICAL PROPERTIES
STEEL PROFILE

(PER METRE WIDTH
In accordance with CSA Specification S136-94

Nominal Core Thickness (mm)	Area of Steel (mm²)	Mass with Z275 Galvanized (kg/m²)	Section Modulus		Moment of Inertia		Depth from Neutral Axis of Deck to Bottom of Deck	Maximum Factored Reactions	
			Midspan S_m (mm³x10³)	Support S_s (mm³x10³)	Midspan I_m (mm⁴x10⁴)	Full I_f (mm⁴x10⁴)	Y_b (mm)	Exterior (kN)	Interior (kN)
0.76	1006.4	8.64	21.27	21.29	897.5	1029.4	41.58	5.7	11.5
0.91	1204.8	10.25	27.20	27.03	1124.1	1232.0	41.67	9.8	19.5
1.22	1614.7	13.34	38.60	39.30	1618.9	1649.9	41.86	18.6	37.2
1.52	2011.0	16.54	48.61	48.84	2053.4	2053.6	42.05	28.4	57.1

PHYSICAL PROPERTIES
COMPOSITE SLA

(PER METRE WIDTH

Composite Moment of Inertia, I_c (mm⁴x 10⁴)
Effective Depth, d (mm)

Slab Thickness h (mm)	141		151		166		176	
Slab Weight, W_f (kN/m²)	2.38		2.60		2.94		3.16	
Concrete Volume, (m³/m²)	0.099		0.109		0.124		0.134	
Base Steel Nominal Thickness (mm)	I_c	d	I_c	d	I_c	d	I_c	d
0.76	13091	99.4	15957	109.4	21026	124.4	24960	134.4
0.91	13836	99.3	16852	109.3	22181	124.3	26313	134.3
1.22	15262	99.1	18565	109.1	24395	124.1	28909	134.1
1.52	16523	99.0	20079	109.0	26353	124.0	31207	134.0

LOAD TABLE

Maximum Specified Uniformly Distributed Load in kN/m² (kPa)

Shear Bond Coefficients
k_1 = 11.1084
k_2 = 55.8868
k_3 = 0.1034
k_4 = 0.0397

Base Steel Nominal Thickness (mm²)	Span (mm)	1 Span	2 Span	3 Span	1 Span	2 Span	3 Span	1 Span	2 Span	3 Span	1 Span	2 Span	3 Span
0.76	1600	16.2	16.2	16.2	17.8	17.8	17.8	20.0	20.0	20.0	20.0	20.0	20.0
	1800	13.5	13.5	13.5	14.8	14.8	14.8	16.9		16.9	18.2		
	2000	11.5	11.5	11.5	12.6		12.6	14.3			15.5		
	2200	9.9			10.9			12.4					
0.91	2200	10.7	10.7	10.7	11.8	11.8	11.8	13.4	13.4	13.4	14.5	14.5	14.5
	2400	9.4	9.4	9.4	10.4	10.4	10.4	11.8	11.8	11.8	12.7	12.7	12.7
	2600	8.4	8.4	8.4	9.2	9.2	9.2	10.5	10.5	10.5	11.3	11.3	11.3
	2800	7.6	7.6	7.6	8.3	8.3	8.3		9.5	9.5		10.2	10.2
	3000	6.9	6.9	6.9		7.5	7.5			8.6			
	3200			6.3									
1.22	2600	9.7	9.7	9.7	10.7	10.7	10.7	12.2	12.2	12.2	13.1	13.1	13.1
	2800	8.8	8.8	8.8	9.6	9.6	9.6	11.0	11.0	11.0	11.9	11.9	11.9
	3000	8.0	8.0	8.0	8.8	8.8	8.8	10.0	10.0	10.0	10.8	10.8	10.8
	3200	7.3	7.3	7.3	8.0	8.0	8.0	9.1	9.1	9.1	9.9	9.9	9.9
	3400	6.7	6.7	6.7	7.4	7.4	7.4	8.4	8.4	8.4		9.1	9.1
	3600	6.2	6.2	6.2	6.9	6.9	6.9			7.8			
	3800		5.8	5.8			6.4						
	4000												
1.52	3200	8.3	8.3	8.3	9.1	9.1	9.1	10.4	10.4	10.4	11.2	11.2	11.2
	3400	7.7	7.7	7.7	8.4	8.4	8.4	9.6	9.6	9.6	10.4	10.4	10.4
	3600	7.1	7.1	7.1	7.8	7.8	7.8	8.9	8.9	8.9	9.6	9.6	9.6
	3800	6.6	6.6	6.6	7.3	7.3	7.3		8.3	8.3		9.0	9.0
	4000		6.2	6.2		6.9	6.9			7.8			
	4200		5.9	5.9			6.4						
	4400												

LIMIT STATES DESIGN

Note

1. Load Tables are based on the design of ONE-WAY composite slabs carrying uniformly distributed loads on a simple span basis. For complete design criteria see the VICWEST Hi-Bond Composite Floor Designer's Manual.
2. A uniform loading requirement in excess of 10 kPa (200 psf) is often an indication of concentrated or moving loads. Such conditions may require additional reinforcing steel. Contact VICWEST for additional design information.
3. Slab thickness h, is from underside of steel deck to top of concrete. Maximum span is not to exceed 32h.
4. Properties and loads are based on Grade 230 steel (Grade 33 steel) with a minimum yield stress of 230 MPa (33,000 psi) and a maximum stress under Factored loads of 207 MPa (29,700 psi).
5. Load values are based on Normal Weight Concrete (density of 2300 kg/m³) (145 pcf) with a minimum compressive strength of 20.7 MPa (3,000 psi) and a Modular Ratio, n=9.

continued onto back

VICWEST

Figure A.1 Physical Properties of HB 30V Metal Deck.

* Properties of the Deck Used – 20 Gauge (Nominal Thickness of Steel = 0.91 mm)

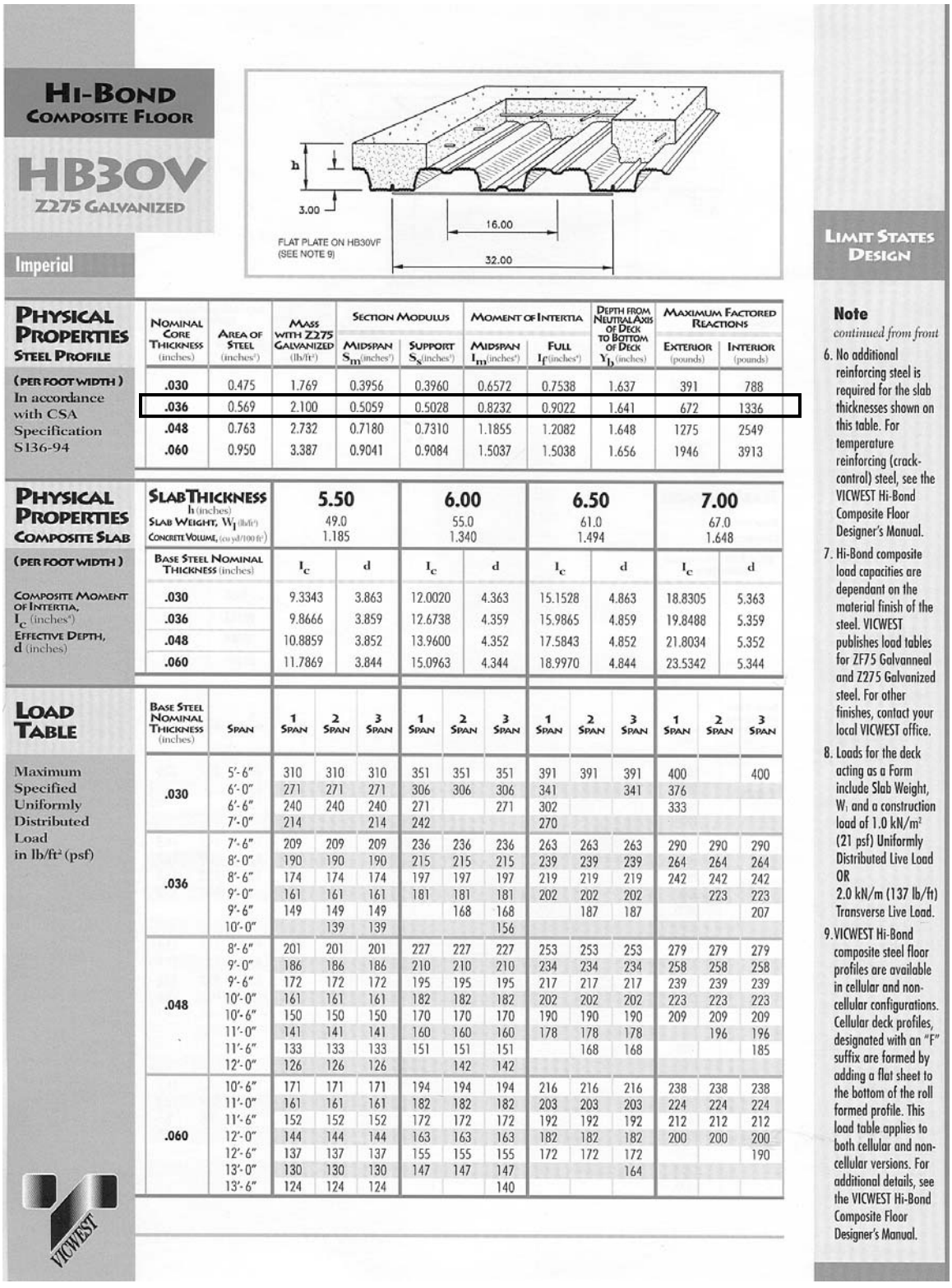

HI-BOND COMPOSITE FLOOR

HB30V

Z275 GALVANIZED

Imperial

h

3.00

16.00

32.00

FLAT PLATE ON HB30VF (SEE NOTE 9)

LIMIT STATES DESIGN

PHYSICAL PROPERTIES STEEL PROFILE

(PER FOOT WIDTH) In accordance with CSA Specification S136-94

Nominal Core Thickness (inches)	Area of Steel (inches²)	Mass with Z275 Galvanized (lb/ft²)	Section Modulus		Moment of Inertia		Depth from Neutral Axis of Deck to Bottom of Deck	Maximum Factored Reactions	
			Midspan S_m (inches³)	Support S_s (inches³)	Midspan I_m (inches⁴)	Full I_f (inches⁴)	Y_b (inches)	Exterior (pounds)	Interior (pounds)
.030	0.475	1.769	0.3956	0.3960	0.6572	0.7538	1.637	391	788
.036	0.569	2.100	0.5059	0.5028	0.8232	0.9022	1.641	672	1336
.048	0.763	2.732	0.7180	0.7310	1.1855	1.2082	1.648	1275	2549
.060	0.950	3.387	0.9041	0.9084	1.5037	1.5038	1.656	1946	3913

PHYSICAL PROPERTIES COMPOSITE SLAB

(PER FOOT WIDTH)

Composite Moment of Intertia, I_c (inches⁴)
Effective Depth, d (inches)

Slab Thickness h (inches)	5.50		6.00		6.50		7.00	
Slab Weight, W_1 (lb/ft²)	49.0		55.0		61.0		67.0	
Concrete Volume, (cu yd/100 ft²)	1.185		1.340		1.494		1.648	
Base Steel Nominal Thickness (inches)	I_c	d	I_c	d	I_c	d	I_c	d
.030	9.3343	3.863	12.0020	4.363	15.1528	4.863	18.8305	5.363
.036	9.8666	3.859	12.6738	4.359	15.9865	4.859	19.8488	5.359
.048	10.8859	3.852	13.9600	4.352	17.5843	4.852	21.8034	5.352
.060	11.7869	3.844	15.0963	4.344	18.9970	4.844	23.5342	5.344

LOAD TABLE

Maximum Specified Uniformly Distributed Load in lb/ft² (psf)

Base Steel Nominal Thickness (inches)	Span	1 Span	2 Span	3 Span	1 Span	2 Span	3 Span	1 Span	2 Span	3 Span	1 Span	2 Span	3 Span
.030	5'-6"	310	310	310	351	351	351	391	391	391	400		400
	6'-0"	271	271	271	306	306	306	341		341	376		
	6'-6"	240	240	240	271		271	302			333		
	7'-0"	214		214	242			270					
.036	7'-6"	209	209	209	236	236	236	263	263	263	290	290	290
	8'-0"	190	190	190	215	215	215	239	239	239	264	264	264
	8'-6"	174	174	174	197	197	197	219	219	219	242	242	242
	9'-0"	161	161	161	181	181	181	202	202	202		223	223
	9'-6"	149	149	149		168	168		187	187			207
	10'-0"		139	139			156						
.048	8'-6"	201	201	201	227	227	227	253	253	253	279	279	279
	9'-0"	186	186	186	210	210	210	234	234	234	258	258	258
	9'-6"	172	172	172	195	195	195	217	217	217	239	239	239
	10'-0"	161	161	161	182	182	182	202	202	202	223	223	223
	10'-6"	150	150	150	170	170	170	190	190	190	209	209	209
	11'-0"	141	141	141	160	160	160	178	178	178		196	196
	11'-6"	133	133	133	151	151	151		168	168			185
	12'-0"	126	126	126		142	142						
.060	10'-6"	171	171	171	194	194	194	216	216	216	238	238	238
	11'-0"	161	161	161	182	182	182	203	203	203	224	224	224
	11'-6"	152	152	152	172	172	172	192	192	192	212	212	212
	12'-0"	144	144	144	163	163	163	182	182	182	200	200	200
	12'-6"	137	137	137	155	155	155	172	172	172			190
	13'-0"	130	130	130	147	147	147			164			
	13'-6"	124	124	124			140						

VICWEST

Note

continued from front

6. No additional reinforcing steel is required for the slab thicknesses shown on this table. For temperature reinforcing (crack-control) steel, see the VICWEST Hi-Bond Composite Floor Designer's Manual.
7. Hi-Bond composite load capacities are dependant on the material finish of the steel. VICWEST publishes load tables for ZF75 Galvanneal and Z275 Galvanized steel. For other finishes, contact your local VICWEST office.
8. Loads for the deck acting as a Form include Slab Weight, W_1 and a construction load of 1.0 kN/m² (21 psf) Uniformly Distributed Live Load OR 2.0 kN/m (137 lb/ft) Transverse Live Load.
9. VICWEST Hi-Bond composite steel floor profiles are available in cellular and non-cellular configurations. Cellular deck profiles, designated with an "F" suffix are formed by adding a flat sheet to the bottom of the roll formed profile. This load table applies to both cellular and non-cellular versions. For additional details, see the VICWEST Hi-Bond Composite Floor Designer's Manual.

Figure A.2 Dimensions of the HB 30V Metal Deck.

* Properties of the Deck Used – 20 Gauge (Nominal Thickness of Steel = 0.036 inch)

APPENDIX B

Construction Details of Test Specimens

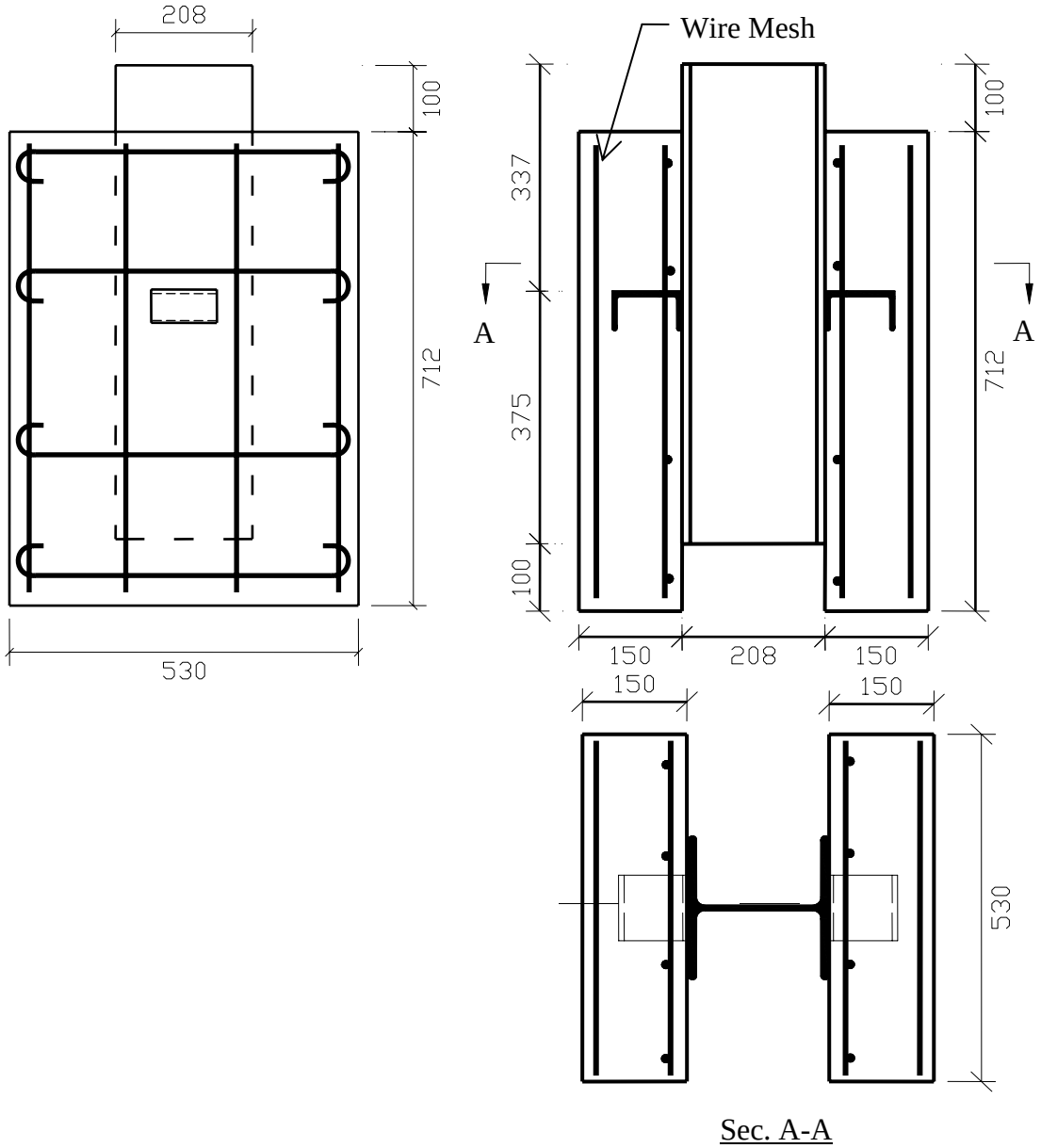

Sec. A-A

NOTES:

1. All dimensions are in mm
2. All reinforcement consists of No. 10 deformed bars
3. Spacing of transverse reinforcement = 220 mm
4. Spacing of longitudinal reinforcement = 160 mm
5. Cover to transverse reinforcement = 25 mm
6. Channel Sizes used = 50 mm, 100 mm and 150 mm
7. All specimens had one layer of 152 x 152 x MW 25.8 wire mesh

Figure B.1 Typical Details for the Push-out Specimens With Solid Slabs.

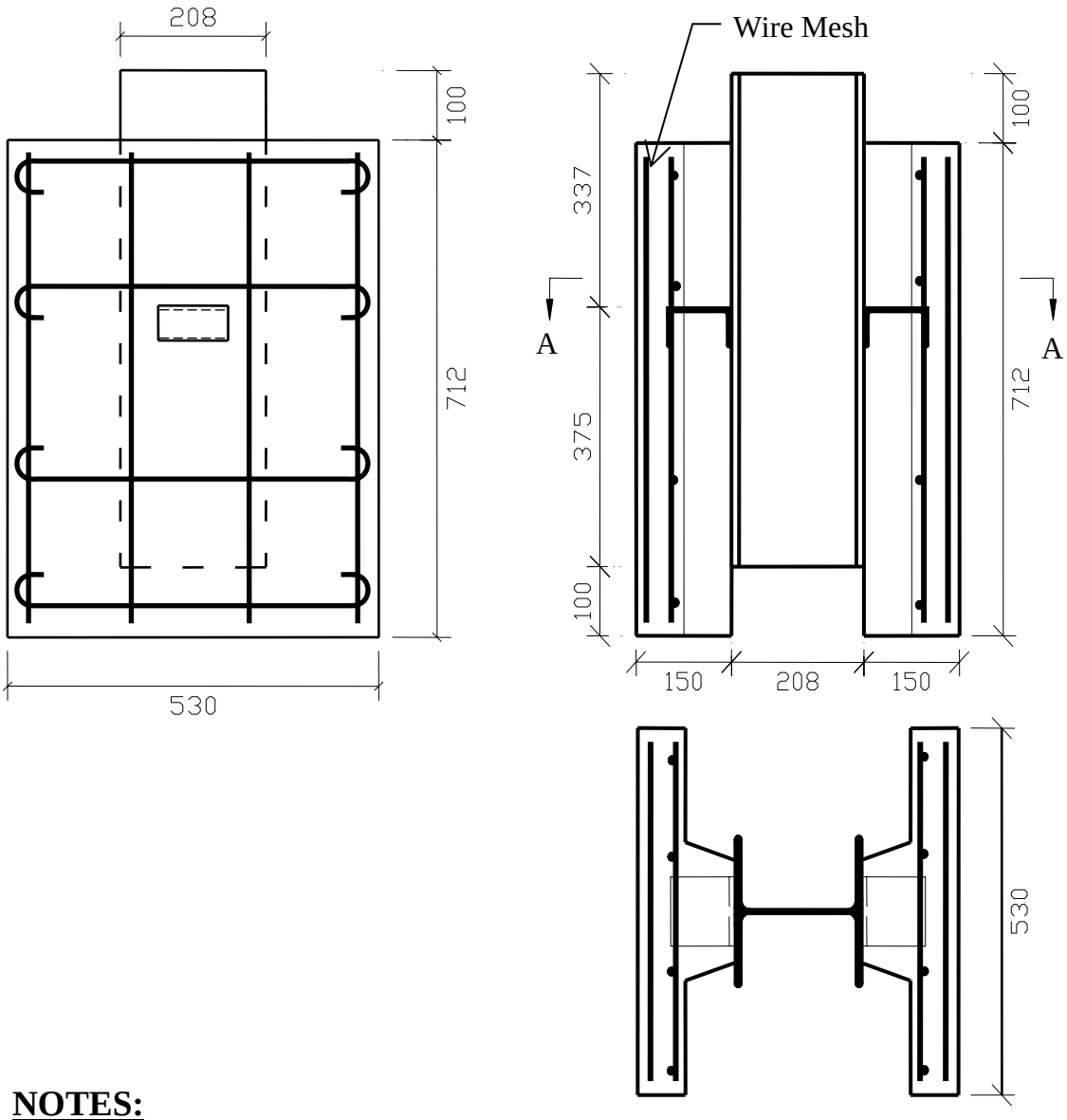

Sec. A-A

NOTES:

1. All dimensions are in mm
2. All reinforcement consists of No. 10 deformed bars
3. Spacing of transverse reinforcement = 220 mm
4. Spacing of longitudinal reinforcement = 160 mm
5. Cover to transverse reinforcement = 25 mm
6. Channel Sizes used = 50 mm, 100 mm and 150 mm
7. All specimens had one layer of 152 x 152 x MW 25.8 wire mesh

Figure B.2 Typical Details for the Push-out Specimens With Metal Deck Slabs.

APPENDIX C

Properties of Steel

Table C-1. Properties of Channels.

Specimens Tested in Series	Average Yield Stress, fy (MPa)	Average Ultimate Stress, fu (MPa)	Average Young's Modulus, Es (MPa)	Average Elongation* %
For Series A & B				
Flange	332.64	473	197561	11.52%
Web	365.4	495.5	209368	9.91%
For Series C & D				
Flange	370.2	508	201504	9.53%
Web	340.48	463.5	193262	15.36%
For Series E & F				
Flange	352	500.12	206400	9.43%
Web	347.28	495.23	198273	7.52%

Table C-2. Properties of Beam Sections.

Specimens Tested in Series	Average Yield Stress, fy (MPa)	Average Ultimate Stress, fu (MPa)	Average Young's Modulus, Es (MPa)	Average Elongation* %
For Series A & B				
Flange	334.4	489.7	188285	21.03%
Web	377.4	512.6	192786	22.4%
For Series C & D				
Flange	325.6	478.2	196008	24.6%
Web	316.6	459.6	191345	20.06%
For Series E & F				
Flange	382.4	505.3	193265	18.64%
Web	355.4	495.23	184874	28.13%

*** Gauge length = 2 inches (50.8 mm)**

Table C-3. Properties of Reinforcing Bars.

Test Series	Average Yield Stress, fy (MPa)	Average Ultimate Stress, fu (MPa)	Average Young's Modulus, Es (MPa)	Average Elongation %
Series A	549.2	786.3	226500	16.5%
Series B	549.2	786.3	226500	16.5%
Series C	549.2	786.3	226500	16.5%
Series D	515.2	680.6	210302	14.3%
Series E	515.2	680.6	210302	14.3%
Series F	515.2	680.6	210302	14.3%

Table C-4. Properties of Wire Mesh Bars.

Test Series	Average Yield Stress, fy (MPa)	Average Ultimate Stress, fu (MPa)	Average Young's Modulus, Es (MPa)	Average Elongation %
Series A	454.2	627.9	203920	6.01%
Series B	454.2	627.9	203920	6.01%
Series C	454.2	627.9	203920	6.01%
Series D	494.8	650.4	213465	5.95%
Series E	494.8	650.4	213465	5.95%
Series F	494.8	650.4	213465	5.95%

APPENDIX D

Experimental Data

Experimental Readings for Push-out specimens

Specimen	A1a
Load Per Channel (kN)	Slip (mm)
4.98	0
9.96	0.085
14.94	0.22
19.92	0.065
24.9	0.15
29.88	0.175
34.86	0.11
39.84	0.13
49.8	0.265
59.76	0.285
69.72	0.285
79.68	0.335
89.64	0.64
99.6	0.445
109.56	0.53
119.52	0.445
129.48	0.535
139.44	0.62
149.4	0.62
169.32	0.69
189.24	0.755
209.16	0.69
229.08	0.995
249	0.82
268.92	0.975
288.84	0.975
308.76	1.02
328.68	1.02
348.6	1.13
368.52	1.195
388.44	1.375
408.36	1.46
428.28	1.62
448.2	1.73
468.12	2.015
488.04	2.48
498	2.61
507.96	2.675
517.92	2.805
527.88	3.16
537.84	3.605
547.8	4.04
557.76	4.395
562.74	4.745
567.72	4.905
572.7	5.32
577.68	5.605
582.66	6.11
587.64	6.33
592.62	6.84
587.64	7.1
587.64	7.455
588.636	7.805
589.632	8.16
590.628	8.38
591.624	8.595
592.62	8.62
593.616	8.795
594.612	8.975
595.608	9.15
596.604	9.365
597.6	9.39
598.596	9.5
599.592	9.65
600.588	9.675
601.584	9.83
601.584	10.05
602.58	10.05
597.6	10.345
587.64	10.95
582.66	10.975
577.68	11.195
572.7	11.42
567.72	11.525
562.74	11.77
557.76	12.1
552.78	12.255
537.84	13.205
522.9	13.89
517.92	14.04
502.98	14.875
488.04	15.08
468.12	15.455
224.1	18.88
219.12	19.26
199.2	21.57
184.26	21.84
179.28	22.35
199.2	22.975
209.16	23.13
219.12	23.62
219.12	23.77
199.2	24.145
179.28	24.47
174.3	25.445

Specimen	A1b
Load Per Channel (kN)	Slip (mm)
4.98	0
9.96	0.09
14.94	0.065
19.92	0.025
24.9	0.13
29.88	0.09
34.86	0.085
39.84	0.045
44.82	0.22
49.8	0.09
59.76	0.175
79.68	0.065
89.64	0.29
99.6	0.22
109.56	0.265
119.52	0.13
129.48	0.22
139.44	0.175
149.4	0.22
169.32	0.155
189.24	0.285
209.16	0.33
229.08	0.51
249	0.38
268.92	0.415
288.84	0.485
308.76	0.46
328.68	0.55
348.6	0.68
368.52	0.835
388.44	0.925
408.36	0.86
428.28	1.035
448.2	1.21
468.12	1.255
488.04	1.57
507.96	1.83
517.92	2.005
527.88	2.075
532.86	2.34
537.84	2.355
547.8	2.53
557.76	2.795
567.72	3.065
577.68	3.26
582.66	3.46
587.64	3.74
592.62	3.92
597.6	4.25
602.58	4.645
602.58	4.885
602.58	5.3
603.576	5.59
597.6	6.16
592.62	6.34
582.66	6.845
532.86	6.795
527.88	7.005
524.892	7.05
522.9	7.225
518.916	7.635
516.924	7.465
513.936	7.47
510.948	7.56
507.96	7.58
503.976	7.82
500.988	7.93
499.992	7.98
498	8.175
496.008	8.24
493.02	8.265
352.584	9.955
351.588	10.045
349.596	10.135
349.596	10.665
333.66	11.025
328.68	11.405
280.872	14.23
273.9	14.78
268.92	15.075
263.94	15.23
258.96	15.45
253.98	15.765
268.92	16.515
273.9	16.45
296.808	17.14
298.8	17.095
302.784	17.385
303.78	17.54
278.88	18.26
224.1	19.25
219.12	19.185
214.14	19.6
204.18	19.64
154.38	22.96

Specimen	A2a
Load Per Channel (kN)	Slip (mm)
4.98	0
9.96	0.06
14.94	0.17
19.92	0.04
24.9	0.045
29.88	0.085
34.86	0.02
39.84	0.195
44.82	0.11
49.8	0.065
59.76	0.04
69.72	0.02
79.68	0.02
89.64	0.125
99.6	0.105
109.56	0.175
119.52	0.15
129.48	0.195
139.44	0.175
149.4	0.195
159.36	0.22
169.32	0.26
179.28	0.415
189.24	0.375
199.2	0.375
209.16	0.415
219.12	0.395
229.08	0.46
239.04	0.525
249	0.5
258.96	0.68
268.92	0.615
278.88	0.725
288.84	0.77
298.8	0.79
308.76	0.815
318.72	1.015
328.68	1.12
338.64	1.275
348.6	1.495
358.56	2.625
368.52	1.825
373.5	1.89
378.48	2.005
383.46	2.155
388.44	2.315
393.42	2.4
398.4	2.53
403.38	2.665
408.36	2.84
413.34	2.95
418.32	3.04
423.3	3.325
428.28	3.41
433.26	3.63
438.24	3.855
443.22	4.12
448.2	4.45
453.18	4.695
457.164	4.995
458.16	5.305
454.176	5.57
452.184	5.86
451.188	6.015
452.184	5.995
453.18	6.06
454.176	6.15
454.176	6.41
456.168	6.455
457.164	6.61
458.16	6.72
459.156	6.9
459.156	7.25
461.148	7.38
463.14	7.425
464.136	7.49
465.132	7.67
466.128	7.78
467.124	7.84
468.12	8.13
468.12	8.305
467.124	8.33
466.128	8.37
464.136	8.57
463.14	8.59
463.14	8.85
463.14	9.095
463.14	9.56
463.14	9.865
463.14	10.15
464.136	10.26
465.132	10.875
466.128	11.38
463.14	9.095
463.14	9.56
463.14	9.865
463.14	10.15
464.136	10.26
465.132	10.875
466.128	11.38

Specimen	A2b
Load Per Channel (kN)	Slip (mm)
4.98	0
9.96	0.11
14.94	0.04
19.92	0.11
24.9	0.11
29.88	0.175
34.86	0.065
39.84	0.13
44.82	0.175
49.8	0.065
59.76	0.175
69.72	0.005
79.68	0.065
89.64	0.195
104.58	0.155
109.56	0.24
119.52	0.395
129.48	0.35
139.44	0.35
149.4	0.305
159.36	0.26
169.32	0.505
179.28	0.415
189.24	0.44
199.2	0.615
209.16	0.685
219.12	0.64
224.1	0.68
229.08	0.64
239.04	0.725
249	0.875
258.96	0.77
268.92	0.83
278.88	1.01
288.84	0.855
298.8	0.945
308.76	1.01
318.72	1.185
328.68	1.45
338.64	1.405
348.6	1.52
358.56	1.625
368.52	1.8
378.48	2.09
388.44	2.35
398.4	2.66
408.36	3.01
418.32	3.495
428.28	3.8
433.26	4
438.24	4.215
443.22	4.46
448.2	4.86
453.18	5.17
456.168	5.455
456.168	5.7
457.164	6.075
457.164	6.29
458.16	6.445
459.156	6.53
460.152	6.71
461.148	6.865
462.144	6.91
462.144	7.28
461.148	7.525
461.148	7.9
461.148	8.145
461.148	8.41
460.152	8.515
459.156	8.58
459.156	8.71
459.156	8.69
460.152	8.89
460.152	9.15
461.148	9.325
462.144	9.395
463.14	9.675
465.132	10.21
467.124	10.495
468.12	10.645
469.116	10.93
470.112	11.085
471.108	11.265
473.1	11.72
474.096	12.005
474.096	12.45
474.096	12.98
474.096	13.48
474.096	13.525
473.1	13.615
473.1	13.835
472.104	13.97
472.104	14.23
471.108	14.255
470.112	14.41

Specimen	A3a
Load Per Channel (kN)	Slip (mm)
4.98	0
9.96	0.11
14.94	0.18
19.92	0.08
24.9	0.045
29.88	0.09
34.86	-0.04
39.84	0.045
54.78	0.245
59.76	0.395
69.72	0.35
79.68	0.595
89.64	0.7
99.6	0.81
104.58	0.81
109.56	0.83
119.52	0.985
129.48	1.095
139.44	1.14
149.4	1.03
159.36	1.185
169.32	1.36
179.28	1.45
189.24	1.78
199.2	1.905
204.18	2.24
209.16	2.545
214.14	2.505
219.12	2.72
224.1	3.07
226.092	3.135
228.084	3.2
229.08	3.31
230.076	3.42
231.072	3.29
232.068	3.555
234.06	3.355
236.052	3.535
237.048	3.575
238.044	3.665
239.04	3.705
240.036	3.645
242.028	3.84
243.024	3.905
244.02	4.015
245.016	3.95
246.012	4.015
247.008	4.04
249	4.15
249.996	4.26
252.984	4.43
253.98	4.455
254.976	4.545
256.968	4.74
258.96	4.765
258.96	5.045
258.96	5.245
259.956	5.16
260.952	5.295
261.948	5.36
262.944	5.425
263.94	5.51
265.932	5.645
266.928	5.865
267.924	5.975
268.92	6.04
269.916	6.085
270.912	6.255
271.908	6.41
272.904	6.55
273.9	6.635
274.896	6.675
276.888	6.855
278.88	7.21
279.876	7.275
280.872	7.515
281.868	7.715
282.864	7.845
283.86	8.22
284.856	8.415
285.852	9.065
286.848	8.9
287.844	9.19
288.84	9.76
286.848	10.09
285.852	10
284.856	10.2
283.86	10.115
282.864	10.2

Specimen	A3b
Load Per Channel (kN)	Slip (mm)
4.98	0
9.96	0.225
14.94	0.2
19.92	0.245
24.9	0.13
29.88	0.2
34.86	0.05
49.8	0.045
59.76	0.245
69.72	0.2
79.68	0.2
89.64	0.245
99.6	0.245
109.56	0.33
119.52	0.355
129.48	0.395
139.44	0.64
149.4	0.62
159.36	0.83
169.32	0.815
179.28	0.995
189.24	1.17
199.2	1.39
209.16	1.56
219.12	1.98
229.08	2.435
234.06	2.505
239.04	2.66
244.02	2.9
249	3.235
253.98	3.3
258.96	3.56
263.94	3.91
268.92	4.505
273.9	4.965
274.896	5.015
275.892	5.185
276.888	5.275
277.884	5.36
278.88	5.495
279.876	5.65
280.872	5.825
281.868	5.915
282.864	5.87
283.86	6
266.928	6.135
268.92	6.155
273.9	6.05
278.88	6.2
279.876	6.22
280.872	6.31
281.868	6.375
282.864	6.505
283.86	6.66
284.856	6.75
285.852	6.925
286.848	6.995
287.844	6.9
288.84	7.12
289.836	7.475
290.832	7.605
291.828	7.755
292.824	8.025
293.82	8.285
295.812	9.035
292.824	9.255
285.852	9.69
282.864	9.585

Specimen	D1S
Load Per Channel (kN)	Slip (mm)
0	0.02
9.96	0.025
14.94	0
19.92	0.025
24.9	0.025
34.86	0.045
44.82	0.055
49.8	0.045
59.76	0.06
69.72	0.065
79.68	0.09
89.64	0.085
99.6	0.105
109.56	0.13
129.48	0.17
139.44	0.195
149.4	0.205
159.36	0.24
179.28	0.27
189.24	0.305
199.2	0.33
209.16	0.36
219.12	0.385
229.08	0.42
239.04	0.45
249	0.48
253.98	0.525
268.92	0.575
278.88	0.605
288.84	0.655
298.8	0.69
308.76	0.765
318.72	0.8
328.68	0.865
338.64	0.925
348.6	1.02
358.56	1.14
368.52	1.275
378.48	1.44
383.46	1.59
388.44	1.735
393.42	1.93
398.4	2.21
403.38	2.625
398.4	3.415
398.4	3.835
398.4	4.795
398.4	5.385
393.42	6.815
388.44	7.695
383.46	8.435
378.48	9.47
358.56	9.29
348.6	9.79
338.64	10.415
328.68	11.02
318.72	11.54
308.76	11.945
298.8	12.48
288.84	13.055
278.88	13.945
268.92	14.615
258.96	15.055
229.08	16.235
219.12	16.82
209.16	17.44
199.2	18.045
189.24	18.545
179.28	19.15
169.32	19.935
159.36	20.855
149.4	21.855
139.44	22.9
129.48	23.845
119.52	25.605
109.56	27.135
99.6	28.835

Specimen	D2S
Load Per Channel (kN)	Slip (mm)
0	0
9.96	0.01
14.94	0.01
19.92	0.025
29.88	0.035
39.84	0.035
49.8	0.07
59.76	0.065
69.72	0.075
79.68	0.085
89.64	0.105
99.6	0.12
109.56	0.145
119.52	0.175
129.48	0.22
139.44	0.23
149.4	0.29
159.36	0.325
119.52	0.35
189.24	0.435
209.16	0.54
219.12	0.595
229.08	0.675
239.04	0.745
258.96	0.905
268.92	1.015
278.88	1.15
293.82	1.34
298.8	1.515
304.278	1.815
313.74	2.145
318.72	2.485
323.7	3.125
325.692	4.25
326.688	4.605
326.688	5.175
323.7	5.95
318.72	6.62
313.74	7.33
293.82	8.025
286.848	8.39
285.852	8.755
278.88	9.195
273.9	9.545
268.92	9.93
258.96	10.495
253.98	11.085
244.02	12.01
224.1	12.725
209.16	13.395
194.22	14.29
174.3	15.67
159.36	16.885
149.4	17.94
139.44	18.925
129.48	20.395
114.54	21.725
104.58	22.715
99.6	23.825
89.64	25.235
74.7	28.575

Specimen	D3S
Load Per Channel (kN)	Slip (mm)
0	0
9.96	0.02
14.94	0.025
24.9	0.045
34.86	0.05
49.8	0.05
59.76	0.085
74.7	0.155
89.64	0.26
99.6	0.31
119.52	0.47
144.42	0.77
159.36	1.005
179.28	1.43
189.24	1.73
199.2	2.12
207.168	2.67
214.14	3.28
216.132	3.715
217.128	4.325
219.12	4.69
220.116	5.1
223.104	5.685
224.1	6.21
228.084	6.845
231.072	7.59
234.06	8.16
239.04	9.19
239.04	9.89
239.04	10.57
239.04	11.365

236.052	12.405
234.06	13.075
233.064	13.76

Specimen	D4S
Load Per Channel (kN)	Slip (mm)
0	0
15.936	0.01
19.92	0
24.9	0.02
29.88	0.02
39.84	0.04
49.8	0.05
59.76	0.055
69.72	0.065
79.68	0.06
99.6	0.105
129.48	0.135
149.4	0.2
169.32	0.25
189.24	0.335
214.14	0.4
229.08	0.465
249	0.545
268.92	0.655
293.82	0.825
308.76	0.94
328.68	1.155
338.64	1.33
348.6	1.5
358.56	1.795
368.52	2.075
378.48	2.39
388.44	3.105
381.468	3.555
379.476	3.825
379.476	4.085
379.476	4.54
379.476	5.025
380.472	5.485
373.5	5.815
366.528	6.27
366.528	6.645
368.52	6.94
370.512	7.335
370.512	7.84
369.516	8.305
378.48	9.64
383.46	10.445
393.42	11.195
396.408	12.575
249	15.755
229.08	16.265
219.12	16.955
184.26	17.98
149.4	18.58
139.44	18.68
134.46	18.71
134.46	18.74
139.44	18.91
129.48	19.365
119.52	19.875
114.54	20.56
109.56	21.01
104.58	21.815
99.6	23.21
94.62	24.34

Specimen	D5S
Load Per Channel (kN)	Slip (mm)
0	0
9.96	0.895
14.94	0.89
19.92	0.91
29.88	0.9
39.84	0.93
49.8	0.935
59.76	0.95
69.72	0.955
89.64	1
109.56	1.065
129.48	1.185
149.4	1.245
169.32	1.385
189.24	1.54
209.16	1.725
229.08	2.005
249	2.415
258.96	2.705
263.94	3.195
268.92	3.805
265.932	4.3
268.92	4.585
273.9	5.01
278.88	5.42
283.86	5.865
288.84	6.4
295.812	7.545
298.8	8.14
301.788	10.13
298.8	10.885
283.86	12.18
278.88	12.93
268.92	13.57
253.98	14.435
229.08	15.365
219.12	16.12
204.18	16.905
194.22	17.72
179.28	18.295
154.38	19.65
144.42	20.17
124.5	21.87
109.56	22.855
99.6	23.965
79.68	25.155

Specimen	D6S
Load Per Channel (kN)	Slip (mm)
0	0
9.96	0
14.94	0.01
24.9	0.03
39.84	0.055
49.8	0.075
59.76	0.08
69.72	0.13
79.68	0.175
89.64	0.265
99.6	0.42
109.56	0.49
119.52	0.66
129.48	0.915
139.44	1.225
149.4	1.68
159.36	2.225
164.34	2.55
169.32	2.835
174.3	3.22
179.28	3.825
184.26	4.365
189.24	4.895
193.224	5.61
194.22	5.945
196.212	6.52
194.22	7.065
195.216	7.53
196.212	8.1
197.208	8.615
198.204	8.935
199.2	9.355
200.196	9.98
201.192	10.535

Specimen	D1D
Load Per Channel (kN)	Slip (mm)
0	0
4.98	0.01
9.96	0
14.94	0.03
19.92	0.02
24.9	0.045
29.88	0.045
39.84	0.05
49.8	0.085
69.72	0.125
79.68	0.14
99.6	0.2
119.52	0.24
144.42	0.33
159.36	0.36
179.28	0.43
204.18	0.53
219.12	0.58
239.04	0.69
258.96	0.785
278.88	0.925
298.8	1.095
308.76	1.245
318.72	1.48
313.74	1.955
303.78	2.445
298.8	2.745
273.9	3.44
224.1	4.87
214.14	5.215
204.18	5.91
199.2	6.52
189.24	7.725
179.28	8.735
174.3	9.22
169.32	9.705
164.34	10.31
159.36	10.935
154.38	11.665
144.42	12.795
124.5	13.615
124.5	14.2
124.5	14.715
124.5	15.36
124.5	16.065
124.5	16.56
121.512	17.34
118.524	18.38
114.54	19.045
112.548	20.155
108.564	21.14
104.58	22.145
103.584	23.255
101.592	23.905
99.6	24.855
98.604	26.3
94.62	27.06
84.66	28.645

Specimen	D2D
Load Per Channel (kN)	Slip (mm)
0	0
4.98	0
9.96	0.01
14.94	0
19.92	0.015
29.88	0.035
39.84	0.03
49.8	0.055
74.7	0.1
89.64	0.12
99.6	0.145
109.56	0.18
119.52	0.215
129.48	0.25
139.44	0.28
159.36	0.35
179.28	0.445
204.18	0.575
219.12	0.68
239.04	0.85
249	0.965
258.96	1.13
268.92	1.355
273.9	1.495
278.88	2.41
224.1	3.57
194.22	4.65
179.28	5.67
159.36	6.73
149.4	7.455
139.44	8.595
132.468	9.525
124.5	10.405
119.52	11.23
114.54	12.06
109.56	12.86
104.58	13.37
109.56	13.955
111.552	15.075
97.608	16.72
99.6	17.175
99.6	17.88

Specimen	D3D
Load Per Channel (kN)	Slip (mm)
0	0.01
9.96	0
14.94	0.02
19.92	0.035
24.9	0.045
29.88	0.075
39.84	0.1
49.8	0.125
69.72	0.19
79.68	0.26
89.64	0.315
99.6	0.38
119.52	0.58
139.44	0.82
149.4	1.015
159.36	1.25
169.32	1.655
174.3	2.045
179.28	2.7
179.28	3.125
177.288	3.87
169.32	4.97
159.36	6.17
154.38	6.63
137.448	7.54
134.46	8.47
119.52	9.84
109.56	10.75
89.64	12.365
74.7	13.505
64.74	14.79
59.76	16.01
59.76	16.895
54.78	17.97
49.8	19.335
45.816	20.835
45.816	21.23

Specimen	D4D
Load Per Channel (kN)	Slip (mm)
0	0
4.98	0.02
9.96	0
14.94	0.025
19.92	0.03
24.9	0.04
29.88	0.05
39.84	0.07
59.76	0.12
79.68	0.155
99.6	0.21
119.52	0.28
139.44	0.36
159.36	0.44
179.28	0.535
199.2	0.645
219.12	0.81
239.04	0.985
258.96	1.21
278.88	1.615
283.86	1.855
281.868	2.195
199.2	5.165
189.24	6.545
159.36	8.55
144.42	9.81
134.46	11
119.52	12.41
114.54	14.32
114.54	15.33
109.56	16.515
109.56	17.56
104.58	18.48
99.6	19.225

Specimen	D5D
Load Per Channel (kN)	Slip (mm)
0	0.005
4.98	0
9.96	0
14.94	0
19.92	0.025
34.86	0.05
49.8	0.095
59.76	0.11
69.72	0.15
79.68	0.175
99.6	0.23
119.52	0.305
139.44	0.415
159.36	0.535
179.28	0.69
199.2	0.925
214.14	1.225
224.1	1.45
234.06	1.785
239.04	2.175
244.02	2.575
234.06	3.095
234.06	3.46
239.04	3.775
242.028	4.39
199.2	6.13
197.208	6.915
189.24	7.545
169.32	8.39
159.36	9.67
159.36	10.14
114.54	12.515
109.56	13.555
104.58	14.69
84.66	16.21
79.68	17.27
74.7	17.985
74.7	19.085
74.7	20.14
74.7	21.22
74.7	22.23
74.7	22.805

Specimen	D6D
Load Per Channel (kN)	Slip (mm)
0	0
9.96	0
14.94	0
19.92	0.02
24.9	0.04
29.88	0.07
39.84	0.08
49.8	0.125
59.76	0.17
69.72	0.225
79.68	0.295
89.64	0.405
104.58	0.615
109.56	0.725
119.52	0.93
129.48	1.25
139.44	1.8
144.42	2.37
149.4	2.68
154.38	3.365
159.36	4.215
159.36	4.715
154.38	5.535
154.38	6.27
151.392	7.04
139.44	8.2
124.5	9.36
119.52	10.625
114.54	12.21
97.608	14.38
91.632	16.165
91.632	17.735
84.66	19.035
73.704	21.755
67.728	23.22
66.732	24.355
59.76	25.4
58.764	26.345
57.768	27.21
55.776	27.595

Specimen	E1S
Load Per Channel (kN)	Slip (mm)
0	0
24.9	0.03
49.8	0.095
74.7	0.125
99.6	0.175
124.5	0.205
149.4	0.275
174.3	0.315
199.2	0.355
249	0.455
273.9	0.505
298.8	0.54
323.7	0.595
348.6	0.635
373.5	0.68
398.4	0.725
423.3	0.8
448.2	0.84
473.1	0.89
498	0.97
522.9	1.04
547.8	1.175
567.72	1.395
572.7	1.485
577.68	1.62
577.68	1.78
574.692	1.86
567.72	2.065
562.74	2.165
561.744	2.35
561.744	2.51
561.744	2.665
562.74	2.81
562.74	3.015
562.74	3.21
561.744	3.45
557.76	3.55
552.78	3.8
547.8	3.955
543.816	4.2
537.84	4.64
532.86	4.94
527.88	5.08
527.88	5.49
527.88	6.01
527.88	6.925
512.94	7.99
516.924	8.91
507.96	9.63
189.24	17.29
169.32	21.04
154.38	21.01

Specimen	E2S
Load Per Channel (kN)	Slip (mm)
0	0.005
4.98	0.005
9.96	0
19.92	0.015
29.88	0.035
49.8	0.035
74.7	0.065
89.64	0.085
109.56	0.125
129.48	0.145
149.4	0.185
169.32	0.245
199.2	0.3
219.12	0.35
239.04	0.405
258.96	0.45
278.88	0.515
298.8	0.605
318.72	0.7
338.64	0.825
358.56	0.925
378.48	1.065
398.4	1.285
408.36	1.405
418.32	1.52
428.28	1.67
438.24	1.815
445.212	1.945
453.18	2.255
461.148	2.485
468.12	2.855
473.1	3.085
479.076	3.495
483.06	3.95
483.06	4.27
479.076	4.805
479.076	5.305
482.064	5.745
484.056	6.35
486.048	7.08
485.052	7.655
487.044	8.24
488.04	9.03
487.044	9.66
483.06	10.37
473.1	11.025
463.14	11.45
433.26	12.19
418.32	12.805
408.36	13.52
394.416	14.195
388.44	14.94
378.48	15.805
298.8	18.055
204.18	18.795
114.54	20.51
89.64	20.36

Specimen	E3S
Load Per Channel (kN)	Slip (mm)
0	0.005
4.98	0.005
9.96	0
19.92	0.005
29.88	0.05
39.84	0.045
49.8	0.06
59.76	0.08
69.72	0.12
89.64	0.145
109.56	0.205
129.48	0.31
149.4	0.385
169.32	0.5
189.24	0.705
209.16	0.92
229.08	1.215
239.04	1.415
249	1.635
258.96	1.915
273.9	2.43
278.88	2.67
283.86	2.88
288.84	3.19
293.82	3.56
303.78	3.935
308.76	4.345
315.732	4.75
318.72	5
323.7	5.445
330.672	5.905
338.64	6.61
345.612	7.48

Specimen	E4S
Load Per Channel (kN)	Slip (mm)
0	0.015
9.96	0
19.92	0.025
29.88	0.035
39.84	0.045
49.8	0.065
59.76	0.065
79.68	0.075
104.58	0.09
124.5	0.12
139.44	0.135
159.36	0.2
179.28	0.245
199.2	0.27
219.12	0.31
239.04	0.355
258.96	0.415
278.88	0.47
298.8	0.525
318.72	0.585
338.64	0.65
358.56	0.735
378.48	0.835
398.4	0.93
418.32	1.065
438.24	1.2
458.16	1.375
478.08	1.59
498	1.805
507.96	1.95
517.92	2.155
527.88	2.45
537.84	2.8
542.82	3.2
532.86	3.39
517.92	3.885
515.928	4.175
502.98	4.525
502.98	4.875
507.96	5.365
512.94	5.765
516.924	6.36
518.916	6.8
524.892	7.42
527.88	7.97
528.876	8.54
530.868	9.32
534.852	9.92
512.94	10.745
502.98	11.42
493.02	11.84

Specimen	E5S
Load Per Channel (kN)	Slip (mm)
0	0.005
9.96	0.005
19.92	0.01
29.88	0.015
39.84	0.05
49.8	0.05
69.72	0.08
89.64	0.1
109.56	0.15
129.48	0.165
149.4	0.235
169.32	0.275
189.24	0.35
209.16	0.405
229.08	0.495
249	0.595
268.92	0.715
288.84	0.87
308.76	1.035
328.68	1.255
348.6	1.57
368.52	1.875
388.44	2.21
408.36	2.77
418.32	3.395
424.296	3.905
432.264	4.57
428.28	5.14
424.296	5.52
427.284	6.04
432.264	6.765
433.26	7.17
418.32	7.975
398.4	8.76
378.48	9.445

Specimen	E6S
Load Per Channel (kN)	Slip (mm)
0	0.025
4.98	0.015
9.96	0
19.92	0.025
29.88	0.025
39.84	0.04
49.8	0.065
59.76	0.09
69.72	0.105
79.68	0.14
99.6	0.235
119.52	0.33
139.44	0.515
159.36	0.73
179.28	1.09
199.2	1.515
219.12	2.28
234.06	3.065
239.04	3.57
244.02	4.235
239.04	4.755

Specimen	E1D
Load Per Channel (kN)	Slip (mm)
0	0.02
4.98	0
9.96	0.02
19.92	0.03
29.88	0.05
39.84	0.08
49.8	0.085
69.72	0.125
89.64	0.175
109.56	0.225
129.48	0.27
159.36	0.325
179.28	0.38
199.2	0.425
219.12	0.47
239.04	0.515
258.96	0.59
278.88	0.685
308.76	0.745
328.68	0.795
348.6	0.875
368.52	0.985
388.44	1.07
408.36	1.185
428.28	1.38
438.24	1.505
443.22	2.125
199.2	8.475
189.24	9.595
179.28	10.5
174.3	11.14
169.32	11.75
159.36	12.855
154.38	13.54
144.42	14.275
140.436	15.165
139.44	15.735
139.44	16.275

Specimen	E2D
Load Per Channel (kN)	Slip (mm)
0	0.01
4.98	0
9.96	0
19.92	0.015
29.88	0.03
39.84	0.04
49.8	0.065
69.72	0.1
79.68	0.125
99.6	0.165
119.52	0.215
139.44	0.265
159.36	0.31
179.28	0.39
199.2	0.46
209.16	0.49
219.12	0.54
229.08	0.575
244.02	0.665
258.96	0.715
268.92	0.785
278.88	0.835
293.82	0.92
298.8	0.965
303.78	1.01
308.76	1.06
313.74	1.08
318.72	1.13
323.7	1.185
328.68	1.23
333.66	1.28
338.64	1.33
343.62	1.375
349.596	1.465
355.572	1.55
361.548	1.64
366.528	1.76
368.52	1.805
373.5	1.905
378.48	2.03
379.476	2.125
380.472	2.285
381.468	2.4
380.472	2.57
378.48	2.655
373.5	2.62
144.42	8.58
139.44	9.585
134.46	10.58
129.48	11.935
126.492	12.585
124.5	13.545
119.52	14.86
114.54	16.385
109.56	16.99
104.58	17.51

Specimen	E3D
Load Per Channel (kN)	Slip (mm)
0	0.025
4.98	0
9.96	0
19.92	0.04
29.88	0.04
39.84	0.05
49.8	0.085
69.72	0.15
89.64	0.225
109.56	0.315
129.48	0.385
149.4	0.58
169.32	0.75
189.24	0.97
209.16	1.255
219.12	1.505
229.08	1.77
239.04	2.075
246.012	2.395
249.996	2.635
254.976	2.99
258.96	3.365
260.952	3.72
258.96	3.825
260.952	4.335
258.96	4.77
253.98	4.945
231.072	5.9
234.06	6.13
234.06	7.145
224.1	7.78
214.14	8.635
214.14	9.8
204.18	11.135
189.24	13.325
164.34	15.525
119.52	18.205
104.58	20.735
89.64	22.415

Specimen	E4D
Load Per Channel (kN)	Slip (mm)
0	0.01
4.98	0
9.96	0.01
14.94	0.015
19.92	0.02
29.88	0.045
39.84	0.065
49.8	0.09
59.76	0.11
69.72	0.125
79.68	0.15
89.64	0.17
109.56	0.215
129.48	0.275
149.4	0.32
169.32	0.365
189.24	0.43
209.16	0.505
229.08	0.55
249	0.64
268.92	0.725
288.84	0.825
298.8	0.885
323.7	1.045
338.64	1.125
348.6	1.23
368.52	1.41
378.48	1.505
388.44	1.64
398.4	1.785
407.364	2.015
407.364	3.365
328.68	3.915
328.68	4.22
323.7	4.74
159.36	10.045
159.36	10.61
161.352	11.13
162.348	11.89
164.34	12.345
164.34	13.025
169.32	13.735
164.34	15.765
149.4	17.57

Specimen	E5D
Load Per Channel (kN)	Slip (mm)
0	0
9.96	0.01
19.92	0.015
39.84	0.06
49.8	0.06
69.72	0.105
89.64	0.15
109.56	0.2
129.48	0.255
149.4	0.31
169.32	0.39
189.24	0.485
209.16	0.59
229.08	0.7
249	0.88
258.96	0.93
268.92	1.03
278.88	1.105
288.84	1.215
298.8	1.305
303.78	1.385
308.76	1.44
313.74	1.515
318.72	1.57
323.7	1.69
328.68	1.755
333.66	1.895
338.64	2.105
340.632	2.27
343.62	2.355
338.64	2.435
339.636	2.695
343.62	2.785
346.608	2.905
348.6	3.065
350.592	3.22
353.58	3.44
353.58	3.78
352.584	4.82
268.92	5.625
253.98	6.175
179.28	8.41
159.36	9.655
144.42	10.605
134.46	11.76
114.54	12.9
109.56	13.825
99.6	15.025
96.612	16.16
94.62	16.78

Specimen	E6D
Load Per Channel (kN)	Slip (mm)
0	0.015
4.98	0
9.96	0.005
19.92	0.015
29.88	0.035
39.84	0.07
49.8	0.105
69.72	0.21
79.68	0.245
89.64	0.3
99.6	0.37
109.56	0.435
119.52	0.56
139.44	0.87
149.4	1.07
159.36	1.265
169.32	1.555
179.28	1.905
189.24	2.245
199.2	2.66
204.18	3.015
208.164	3.49
211.152	3.78
212.148	4.225
212.148	4.51
214.14	4.93
216.132	5.37
218.124	5.795
218.124	6.34
218.124	6.83
217.128	7.355
209.16	7.785

Specimen	F1S
Load Per Channel (kN)	Slip (mm)
0	0.03
4.98	0.015
9.96	0
19.92	0.005
29.88	0.015
39.84	0.035
49.8	0.025
74.7	0.065
99.6	0.08
124.5	0.125
149.4	0.16
174.3	0.22
199.2	0.27
224.1	0.33
249	0.38
273.9	0.435
298.8	0.515
323.7	0.6
348.6	0.7
373.5	0.82
398.4	0.95
408.36	0.51
418.32	1.07
428.28	1.18
438.24	1.265
448.2	1.375
458.16	1.505
468.12	1.785
473.1	2.1
478.08	2.535
483.06	3.13
485.052	3.81
483.06	3.945
478.08	4.375
473.1	4.7
468.12	5.02
463.14	5.295
458.16	5.505
443.22	5.975
438.24	6.115
433.26	6.275
428.28	6.405
418.32	6.75
398.4	7.145
388.44	7.52
380.97	8.245
373.5	8.475
368.52	8.835
353.58	9.255
348.6	9.455
338.64	9.74
328.68	10.21
313.74	10.815
298.8	11.485
288.84	11.985
278.88	12.29
268.92	12.83
258.96	13.315
249	13.87
239.04	14.485
229.08	15.135
219.12	15.73
209.16	16.445
199.2	16.84
189.24	17.49
159.36	17.96
149.4	18.955
144.42	19.36
139.44	19.855
134.46	20.51
129.48	21.175
124.5	21.555
119.52	22.095

Specimen	F2S
Load Per Channel (kN)	Slip (mm)
0	0.005
4.98	0.02
9.96	0
19.92	0.02
29.88	0.03
39.84	0.045
49.8	0.065
74.7	0.105
99.6	0.15
124.5	0.2
149.4	0.27
174.3	0.36
199.2	0.47
224.1	0.575
249	0.745
273.9	0.92
298.8	1.125
308.76	1.28
318.72	1.4
328.68	1.58
338.64	1.855
348.6	2.205
353.58	2.535
358.56	2.735
363.54	2.925
368.52	3.42
373.5	4.13
375.492	5.035
373.5	5.395
369.516	5.89
369.516	6.46
369.516	7.025
366.528	7.56
364.536	7.935
358.56	8.365
353.58	8.835
343.62	9.425
333.66	10.12
323.7	10.735
308.76	11.5
303.78	12.27
302.784	13.415
299.796	14.385
224.1	14.8
214.14	15.45
199.2	16.615
184.26	17.635
174.3	18.6
154.38	19.69
144.42	20.565
129.48	22.155
114.54	24.155
109.56	25.12
99.6	26.72

Specimen	F3S
Load Per Channel (kN)	Slip (mm)
0	0
4.98	0
9.96	0.005
19.92	0.02
29.88	0.03
39.84	0.04
49.8	0.07
74.7	0.155
99.6	0.28
124.5	0.465
149.4	0.66
174.3	0.975
199.2	1.465
209.16	1.71
219.12	2.075
229.08	2.54
239.04	2.945
244.02	3.225
249	3.595
253.98	3.855
258.96	4.29
263.94	4.885
265.932	5.485
258.96	6.225
260.952	6.81
264.936	7.65
267.924	8.415
268.92	9.685

Specimen	F4S
Load Per Channel (kN)	Slip (mm)
0	0.025
4.98	0
9.96	0.025
19.92	0.04
29.88	0.045
49.8	0.08
74.7	0.1
99.6	0.145
134.46	0.18
149.4	0.225
174.3	0.275
199.2	0.35
224.1	0.41
249	0.485
273.9	0.59
298.8	0.71
323.7	0.85
348.6	1.015
373.5	1.265
388.44	1.445
398.4	1.6
408.36	1.775
418.32	2.07
428.28	2.7
442.224	3.45
444.216	4.03
438.24	4.71
440.232	5.77
446.208	6.965
448.2	7.55
450.192	8.435
443.22	9.865
438.24	10.58
437.244	11.58
443.22	12.83
428.28	14.135
423.3	14.745
398.4	15.41
348.6	16.39
308.76	17.215
278.88	17.92
258.96	18.43
239.04	19.31
219.12	20.08
199.2	20.895
179.28	22.105
169.32	22.68
159.36	23.8
149.4	24.55
139.44	25.605
134.46	26.09
129.48	26.62
124.5	27.03
119.52	27.705
114.54	28.3

356.568	9.91

Specimen	F5S
Load Per Channel (kN)	Slip (mm)
0	0.005
4.98	0.01
9.96	0
19.92	0.01
29.88	0.02
39.84	0.035
59.76	0.08
74.7	0.115
99.6	0.165
124.5	0.255
149.4	0.335
174.3	0.46
199.2	0.625
224.1	0.795
249	1.075
273.9	1.415
298.8	1.945
308.76	2.26
318.72	2.57
328.68	3.03
338.64	3.56
343.62	3.88
348.6	4.335
354.576	4.955
358.56	5.685
354.576	6.64
352.584	7.125
353.58	7.65
355.572	8.1
354.576	8.765

Specimen	F6S
Load Per Channel (kN)	Slip (mm)
0	0.02
4.98	0
9.96	0.015
19.92	0.035
29.88	0.07
39.84	0.08
49.8	0.095
74.7	0.215
99.6	0.375
124.5	0.71
149.4	1.305
174.3	2.075
199.2	3.44
209.16	4.545
219.12	5.5
222.108	6.645

Specimen	F1D
Load Per Channel (kN)	Slip (mm)
0	0.005
4.98	0
9.96	0.015
14.94	0.015
19.92	0.02
29.88	0.05
39.84	0.05
49.8	0.085
74.7	0.14
99.6	0.2
124.5	0.26
149.4	0.325
174.3	0.4
199.2	0.485
224.1	0.55
249	0.665
273.9	0.8
298.8	0.925
308.76	1.005
318.72	1.11
328.68	1.195
338.64	1.33
347.604	1.75
343.62	1.905
338.64	2.145
333.66	2.36
308.76	3.16
303.78	3.32
298.8	3.8
273.9	4.725
268.92	5.21
258.96	6.03
253.98	6.32
249	6.475
154.38	8.81
154.38	9.995
149.4	10.51
144.42	10.98
139.44	11.75
134.46	12.5
129.48	13.18
124.5	13.985

Specimen	F2D
Load Per Channel (kN)	Slip (mm)
0	0.025
4.98	0
9.96	0.025
19.92	0.035
29.88	0.035
39.84	0.075
49.8	0.085
74.7	0.155
99.6	0.25
124.5	0.33
149.4	0.41
169.32	0.545
179.28	0.61
189.24	0.675
199.2	0.75
209.16	0.82
219.12	0.895
229.08	0.97
239.04	1.07
249	1.165
258.96	1.265
268.92	1.435
278.88	1.625
285.852	1.915
288.84	2.4
278.88	2.725
279.876	3.065
274.896	3.58
204.18	5.53
161.352	6.97
163.344	7.685
163.344	8.25
163.344	8.88
144.42	10.03
139.44	11.175
130.476	12.1
124.5	12.965
123.504	13.695
121.512	14.04
120.516	14.525

Specimen	F3D
Load Per Channel (kN)	Slip (mm)
0	0.01
4.98	0.005
9.96	0.01
19.92	0.03
29.88	0.06
39.84	0.08
49.8	0.115
59.76	0.145
79.68	0.25
99.6	0.365
119.52	0.515
139.44	0.705
149.4	0.845
159.36	1.07
169.32	1.2
179.28	1.48
184.26	1.755
189.24	1.945
194.22	2.175
199.2	2.445
204.18	2.77
208.164	3.325
206.172	4.005
207.168	4.675
208.164	5.17
204.18	5.74
201.192	6.375
194.22	6.975
189.24	7.63
179.28	8.625
169.32	9.185
169.32	9.925
164.34	10.7
159.36	11.675
154.38	12.445
114.54	14.09
114.54	14.92
109.56	16.035
99.6	17.325
89.64	18.395
84.66	19.575
79.68	21.095
74.7	21.96
69.72	22.995
64.74	24.5
54.78	26.925

Specimen	F4D
Load Per Channel (kN)	Slip (mm)
0	0.015
4.98	0.015
9.96	0
14.94	0.015
19.92	0.03
29.88	0.06
39.84	0.08
49.8	0.1
74.7	0.175
99.6	0.23
124.5	0.32
149.4	0.38
174.3	0.505
199.2	0.61
224.1	0.735
249	0.89
273.9	1.07
298.8	1.365
323.7	1.74
333.66	1.98
336.648	2.395
336.648	2.58
328.68	3.155
298.8	3.255
249	3.99
154.38	10.185
134.46	10.765
134.46	11.92
134.46	12.445
132.468	13.4
129.48	13.88
124.5	14.95
119.52	15.44
114.54	16.6
109.56	17.67
104.58	18.765
99.6	19.805

Specimen	F5D
Load Per Channel (kN)	Slip (mm)
0	0
4.98	0.01
9.96	0
19.92	0.03
29.88	0.055
39.84	0.08
49.8	0.08
59.76	0.125
74.7	0.16
99.6	0.22
124.5	0.335
149.4	0.455
174.3	0.575
199.2	0.77
219.12	0.955
229.08	1.07
239.04	1.23
249	1.365
258.96	1.585
266.928	2.03
268.92	2.395
270.912	2.855
268.92	3.15
272.904	3.805
273.9	4.68
204.18	6.445
213.144	7.13
205.176	8.33
194.22	9.675
126.492	12.935
115.536	14.14
109.56	14.785
99.6	16.52
89.64	17.695

Specimen	F6D
Load Per Channel (kN)	Slip (mm)
0	0
4.98	0.005
9.96	0.01
19.92	0.045
29.88	0.05
39.84	0.09
49.8	0.14
59.76	0.17
69.72	0.215
79.68	0.275
99.6	0.455
119.52	0.675
139.44	1.05
149.4	1.35
159.36	1.79
169.32	2.43
174.3	2.89
179.28	3.425
182.268	4.07
181.272	4.965
181.272	5.56
177.288	6.38
176.292	7.19
174.3	7.78
173.304	8.59
165.336	9.945

APPENDIX E

More Pictures of Failed Specimens

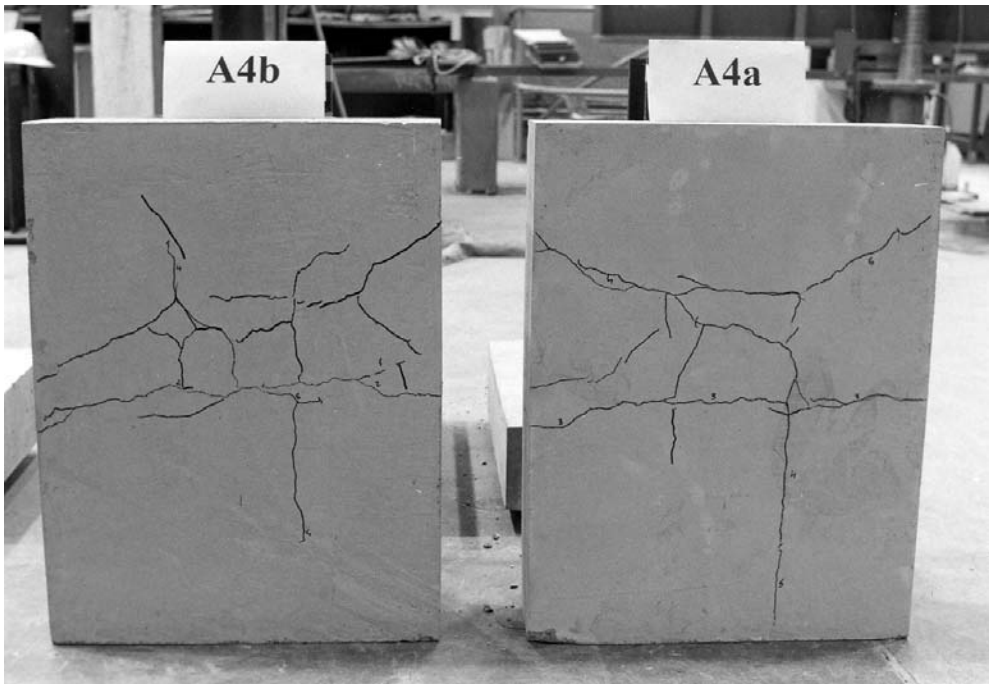

Figure E.1 Crack Pattern on Slabs of Failed Push-out Specimens.

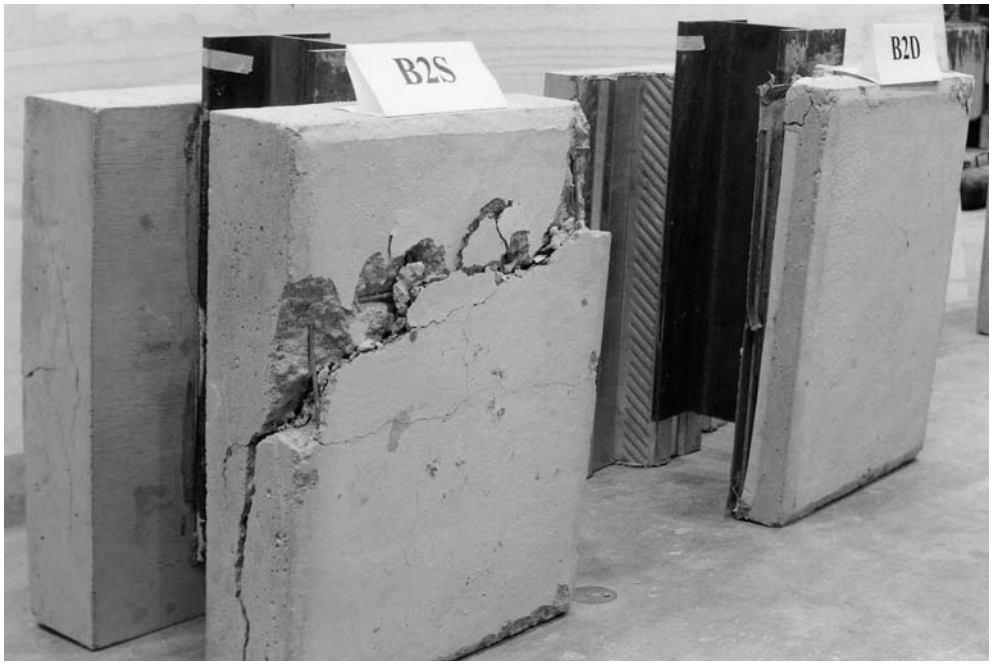

Figure E.2 Concrete Crushing Failure of Specimens with Solid Slabs.

Figure E.3 Typical Shear Plane Failure of Specimens with Deck Slabs.

Figure E.4 View of Failed Specimen with Deck Slabs.

Figure E.5 Detached Slab of Failed Specimen with Deck Slabs.

Figure E.6 Cracking Pattern of Specimen with Solid and Deck Slabs.

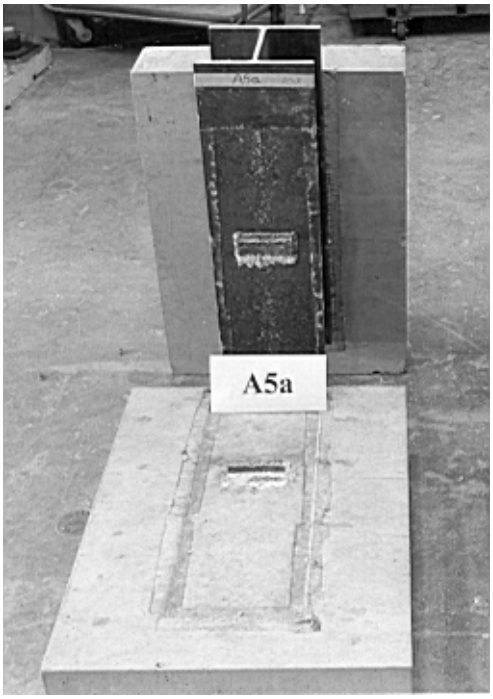

Figure E.7 Typical Channel Fracture Failure in Solid Slab Specimen.

Figure E.8 Typical Shear Plane Failure in Deck Slab Specimen.

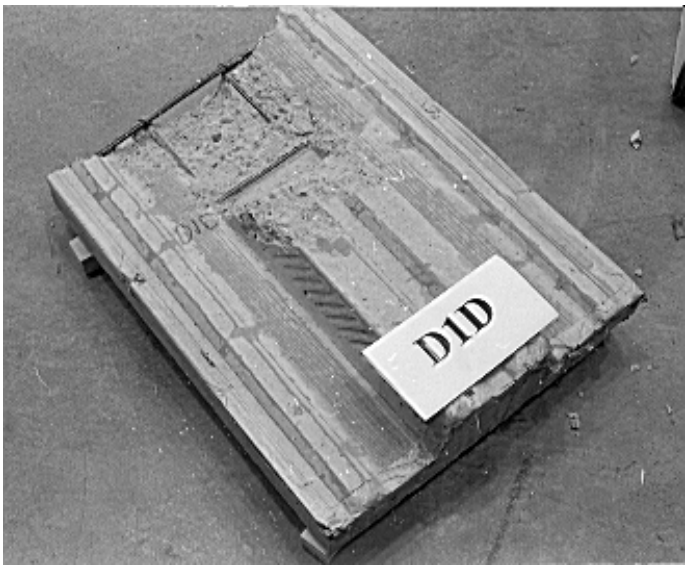

Figure E.9 Typical Deck Slab after Shear Plane Failure.

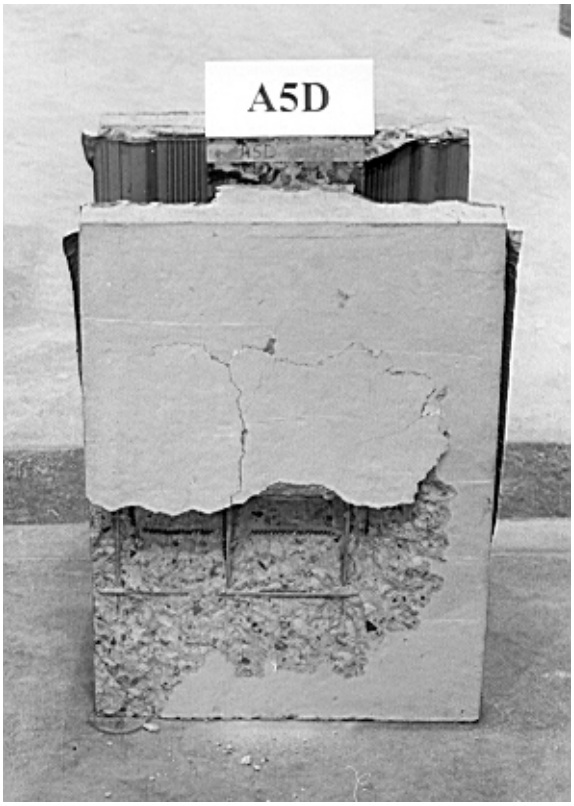

Figure E.10 Typical Deck Slab Failure.

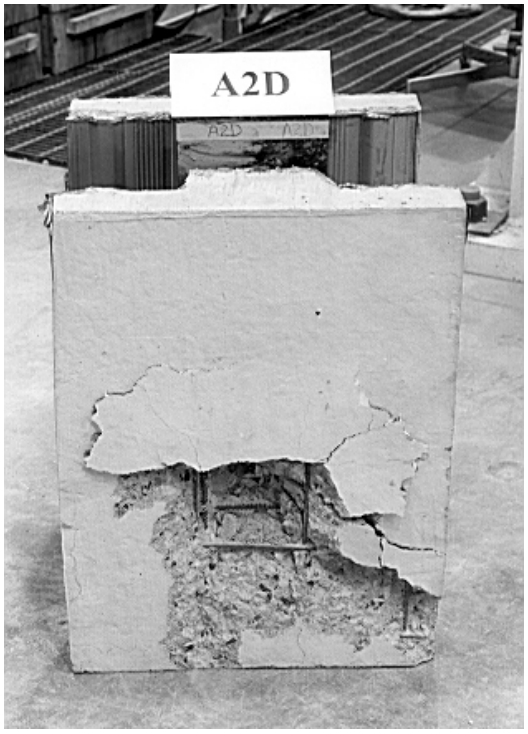

Figure E.11 Typical Deck Slab Failure.

Figure E.12 Top View of Detached Deck Slab after Failure.

Figure E.13 Typical Crushing-Splitting Failure of Solid Slab Specimens.

Figure E.14 Typical Crushing-Splitting Failure of Solid Slab Specimens.

APPENDIX F

Regression Analysis

Table F.1 Observed and Predicted Results for Push-out Specimens by Equation 5.16.

Specimen	f'c	Channel Length	Web Thickness	Ultimate Shear Strength per Channel (kN)		Ratio of Test/ Predicted
	(MPa)	(mm)	(mm)	Test	Eq.5.16	
D1D	21.18	150	8.2	318.7	330.41	0.96
D2D	21.18	100	8.2	278.9	269.17	1.04
D3D	21.18	50	8.2	179.3	207.92	0.86
D4D	21.18	150	4.7	283.85	328.56	0.86
D5D	21.18	100	4.7	244	235.11	1.04
D6D	21.18	50	4.7	159.35	141.65	1.12
E1D	34.8	150	8.2	443.2	423.53	1.05
E2D	34.8	100	8.2	381.45	345.02	1.11
E3D	34.8	50	8.2	260.95	266.52	0.98
E4D	34.8	150	4.7	407.35	421.16	0.97
E5D	34.8	100	4.7	353.6	301.36	1.17
E6D	34.8	50	4.7	218.1	181.57	1.20
F1D	28.57	150	8.2	347.6	383.75	0.91
F2D	28.57	100	8.2	288.85	312.62	0.92
F3D	28.57	50	8.2	208.15	241.49	0.86
F4D	28.57	150	4.7	336.65	381.60	0.88
F5D	28.57	100	4.7	273.9	273.06	1.00
F6D	28.57	50	4.7	182.25	164.51	1.11

Table F.2 Regression Analysis for Proposed Equation (Eq. G.11) for Solid Slabs.

Specimen	Concrete Strength (f'c) (MPa)	Channel Length L (mm)	Web Thickness w (mm)	Flange Width b (mm)	Channel Height H (mm)	Flange Thickness t (mm)	Tested Ultimate Load per Channel (N)	Predicted Ultimate Load per Channel (N)	Test over Predicted Ratio
D1S	21.18	150	8.2	43	102	7.5	403400	472965.449	0.85291643
D2S	21.18	100	8.2	43	102	7.5	326700	349976.967	0.93349
D3S	21.18	50	8.2	43	102	7.5	239050	226988.485	1.05313712
D4S	21.18	150	4.7	40	102	7.5	396400	403132.014	0.98330072
D5S	21.18	100	4.7	40	102	7.5	301800	280143.532	1.0773049
D6S	21.18	50	4.7	40	102	7.5	201200	157155.05	1.2802643
E1S	34.8	150	8.2	43	102	7.5	583650	606256.014	0.9627121
E2S	34.8	100	8.2	43	102	7.5	488050	448607.063	1.08792313
E3S	34.8	50	8.2	43	102	7.5	345600	290958.112	1.18779984
E4S	34.8	150	4.7	40	102	7.5	542800	516742.203	1.05042707
E5S	34.8	100	4.7	40	102	7.5	433250	359093.252	1.20651111
E6S	34.8	50	4.7	40	102	7.5	244000	201444.301	1.21125293
F1S	28.57	150	8.2	43	102	7.5	485050	549315.126	0.88300864
F2S	28.57	100	8.2	43	102	7.5	375500	406472.908	0.9238008
F3S	28.57	50	8.2	43	102	7.5	268900	263630.691	1.01998746
F4S	28.57	150	4.7	40	102	7.5	450200	468208.648	0.96153713
F5S	28.57	100	4.7	40	102	7.5	358550	325366.43	1.1019883
F6S	28.57	50	4.7	40	102	7.5	222100	182524.213	1.21682486
						SUM	6666200	6508980.46	1.02415425
									Average

Table F.3 Regression Analysis for Proposed Equation (Eq. G.11) for Solid Slabs.

	A	336	sigma	0.123
	B	5.24	C.V.	0.0122
			R^2	0.865

Table F.4 Regression Analysis for Proposed Equation (Eq. G.16) for Deck Slabs.

Specimen	Concrete Strength (f'c) (MPa)	Ratio of Deck Profile Wd/Hd	Width of Deck Rib Wd	Channel Length L (mm)	Web Thickness w (mm)	Flange Width b (mm)	Channel Height H (mm)	Flange Thickness t (mm)	Tested Ultimate Load per Channel (N)	Predicted Ultimate Load per Channel (N)	Test over Predicted Ratio
D1D	21.18	2.33	177.8	150	8.2	43	102	7.5	318700	364201.993	0.87506385
D2D	21.18	2.33	177.8	100	8.2	43	102	7.5	278900	271216.567	1.02832951
D3D	21.18	2.33	177.8	50	8.2	43	102	7.5	179300	178231.141	1.00599704
D4D	21.18	2.33	177.8	150	4.7	40	102	7.5	283850	306961.6	0.9247085
D5D	21.18	2.33	177.8	100	4.7	40	102	7.5	244000	213976.174	1.14031387
D6D	21.18	2.33	177.8	50	4.7	40	102	7.5	159350	120990.748	1.31704285
E1D	34.8	2.33	177.8	150	8.2	43	102	7.5	443200	466840.97	0.94935969
E2D	34.8	2.33	177.8	100	8.2	43	102	7.5	381450	347650.501	1.09722264
E3D	34.8	2.33	177.8	50	8.2	43	102	7.5	260950	228460.031	1.14221292
E4D	34.8	2.33	177.8	150	4.7	40	102	7.5	407350	393469.156	1.0352781
E5D	34.8	2.33	177.8	100	4.7	40	102	7.5	353600	274278.687	1.2891997
E6D	34.8	2.33	177.8	50	4.7	40	102	7.5	218100	155088.218	1.40629638
F1D	28.57	2.33	177.8	150	8.2	43	102	7.5	347600	422994.247	0.82176059
F2D	28.57	2.33	177.8	100	8.2	43	102	7.5	288850	314998.407	0.91698876
F3D	28.57	2.33	177.8	50	8.2	43	102	7.5	208150	207002.567	1.00554309
F4D	28.57	2.33	177.8	150	4.7	40	102	7.5	336650	356513.674	0.94428356
F5D	28.57	2.33	177.8	100	4.7	40	102	7.5	273900	248517.834	1.10213418
766	28.57	2.33	177.8	50	4.7	40	102	7.5	182250	140521.994	1.29695
								SUM	5166150	5011914.51	1.03077377
											Average

Table F.5 Regression Analysis for Proposed Equation (Eq. g.16) for Deck Slabs.

	A	1.7	sigma	0.162
	B	275.4	C.V.	0.0137
			R^2	0.766

APPENDIX G

Simplification of Proposed Design Equations

G.1 Simplification of the Proposed Equation (Solid Slab)

Eq. [5.8] from Chapter 5, which is reproduced below, provides very good prediction of test results. However, the form of the equation may be considered too complicated for inclusion in the design standard. A series of regression analyses were carried out to obtain a simplified version of Eq. [5.8] at the expense of some accuracy.

$$q_u = [597(w)(t) + 5.4(L)(H) - 19(w)(L) - 23.7(w^2)]\sqrt{f'_c} \qquad [5.8]$$

where:

q_u = Predicted ultimate load per channel connector [N]
t = Flange thickness of channel connector [mm]
w = Web thickness of channel connector [mm]
L = Length of channel connector [mm]
H = Height of channel connector [mm]
f'_c = Specified compressive strength of concrete [MPa]

It was considered that the product of two variables of a channel connector (web thickness and flange thickness) in the first part of the equation is not a significant factor in the shear capacity of the connector. Without the introduction of the product of these two variables, Eq. [5.8] can be represented in the following forms:

$$q_u = A(L)(w)\sqrt{f'_c} + B(w^2)(L)/(H)\sqrt{f'_c} + C(L)(t)\sqrt{f'_c} \qquad [G.1]$$

$$q_u = A(L)(w)\sqrt{f'_c} + B(w^2)(L)/(t)\sqrt{f'_c} + C(L)(t)\sqrt{f'_c} \qquad [G.2]$$

$$q_u = A(L)(w)\sqrt{f'_c} + B(w^2)\sqrt{f'_c} + C(L)(H)\sqrt{f'_c} \quad [G.3]$$

$$q_u = A(L)(w)\sqrt{f'_c} + B(w^2)\sqrt{f'_c} + C(L)(t)\sqrt{f'_c} \quad [G.4]$$

$$q_u = A(L)(w)\sqrt{f'_c} + B(w^2)(L)/(H)\sqrt{f'_c} + C(L)(H)\sqrt{f'_c} \quad [G.5]$$

$$q_u = A(L)(w)\sqrt{f'_c} + B(w^2)(L)/(t)\sqrt{f'_c} + C(L)(H)\sqrt{f'_c} \quad [G.6]$$

To further simplify the equation, only the terms involving the nonlinear relationship of web thickness along with a linear variation of channel length were involved in the following equations:

$$q_u = A(L)(w)\sqrt{f'_c} + B(w^2)(L)/(H)\sqrt{f'_c} \quad [G.7]$$

$$q_u = A(L)(w)\sqrt{f'_c} + B(w^2)(L)/(t)\sqrt{f'_c} \quad [G.8]$$

A regression analysis indicated that Eqs. [G.3] and [G.4] provide the best correlation to the test data. Equation G.3 includes the surface area (L x H) of the channel transferring the shear load onto the concrete which is an important parameter. It has a direct impact on the intensity of pressure over the surface of concrete which plays an important role in the load capacity of a connector, especially in the concrete crushing type of failure. Since most

of the specimens (9 out of 18) involved in this analysis failed due to a concrete crushing type of failure, it is more logical to use this term in the equation.

The least squares regression analysis carried out for Eq. [G.3] yielded:

A = -45.4 B = 562 C = 7.3

By substituting these values into Eq. [G.3], the simplified form of proposed equation is as follows:

$$q_u = [-45.4(L)(w) + 562(w^2) + 7.3(L)(H)]\sqrt{f'_c} \qquad [G.9]$$

The results of the statistical analysis of the predicted values by Eq. [G.9] revealed that the average absolute difference between the observed values and those predicted by Eq. [G.9] is 6.3% as compared to 5.2% for Eq. [5.8]. The average arithmetic mean of the test/predicted ratio (μ), the standard deviation (σ) and the coefficient of variation (C.V.) for the proposed Eq. [G.9] is shown in Table 5.5. This table also includes these statistical parameters for Eq. [5.8] and CSA provision, for comparison.

Table G.1 Statistical Analysis of Predicted Values: Proposed Equations.

Statistics	CSA	Eq. 5.8	Eq. G.9
μ	1.94	0.988	1.006
σ	0.398	0.057	0.072
C.V.	20.57%	1.11%	1.15%

Eq. [G.9] gives a good correlation with the test results. However, the first part of the equation involves a negative constant. Also, this equation can be simplified further, as shown below:

$$q_u = A(w^2)\sqrt{f'_c} + B(L)(H)\sqrt{f'_c} \qquad [G.10]$$

The least squares regression analysis for this form of equation resulted in following constants:

A = 336 B = 5.24

By substituting these constants into Eq. [G.10], the final form of a simplified equation is as follows:

$$q_u = [336(w^2) + 5.24(L)(H)]\sqrt{f'_c} \qquad [G.11]$$

The results obtained from the statistical analysis of the predicted values by Eq. [G.11] showed that the average absolute difference between the observed values and those predicted by Eq. [G.11] is 10.1% as compared to 6.3% for Eq. [G.9]. The average arithmetic mean of the test/predicted ratio

(μ), the standard deviation (σ) and the coefficient of variation (C.V.) for the proposed Eq. [G.11] are 1.055, 0.123 and 1.22%, respectively. Because of the simplicity of Eq. [G.11], along with its only slightly lower accuracy, the equation is recommended for design purposes. In any case, Eq. [G.11] provides much better predictions than those obtained using the current CSA equation.

Since the height of the channel connector (H) was the same in all the specimens, it is recommended that Eq. [G.11] with the following limit:
H = 102 mm.

G.2 Simplification of the Proposed Equation (Metal Deck Slab)

One of the ways to simplify Eq. [5.16], at the expense of some accuracy, would be to reduce the number of terms to two. As indicated in Section G.1, the first term of Eq. [5.16] which contains the surface area of the channel in contact with the concrete slab (LxH) is an important component and should not be excluded. That will lead to two trial combinations, i.e., Equations [5.28] and [5.29]. Two additional trial equations may be obtained by switching the area parameters, (L)(H) with (w)(L) in Eq. [G.12] and (L)(H) with (w^2) in Eq. [G.13]. Thus, Equations [G.14] and [G.15] will be obtained.

$$q_u = A(L)(H)\frac{w_d}{h_d}\sqrt{f'_c} + B(w)(L)\sqrt{f'_c} \qquad [G.12]$$

$$q_u = A(L)(H)\frac{w_d}{h_d}\sqrt{f'_c} + B(w^2)\sqrt{f'_c} \qquad [G.13]$$

$$q_u = A(w)(L)\frac{w_d}{h_d}\sqrt{f'_c} + B(L)(H)\sqrt{f'_c} \qquad [G.14]$$

$$q_u = A(w^2)\frac{w_d}{h_d}\sqrt{f'_c} + B(L)(H)\sqrt{f'_c} \qquad [G.15]$$

A regression analysis indicated that Eq. [G.13] provided the best correlation to the test data. The least squares regression analysis carried out for Eq. [G.13] yielded:

A = 1.7

B = 275.4

By substituting these values into Eq. [G.13], the final simplified form of the proposed equation is as follows:

$$q_u = [1.7(L)(H)\frac{w_d}{h_d} + 275.4(w^2)]\sqrt{f'_c} \qquad [G.16]$$

Figures G.1 and G.2 reflect the accuracy performance of Eq. [G.16]. A statistical analysis revealed that the average absolute difference between the observed values and those predicted by Eq. [G.16] is 11.8%, as compared to 9.03% for Eq. [5.16]. The average arithmetic mean of the test/predicted ratio (μ), the standard deviation (σ) and the coefficient of variation (C.V.) for the proposed Eq. [G.16] are shown in Table G.2. This table also includes these statistical parameters for Eq. [5.16], for comparison. Because of the simplicity of Eq. [G.16], this equation is recommended for design purposes.

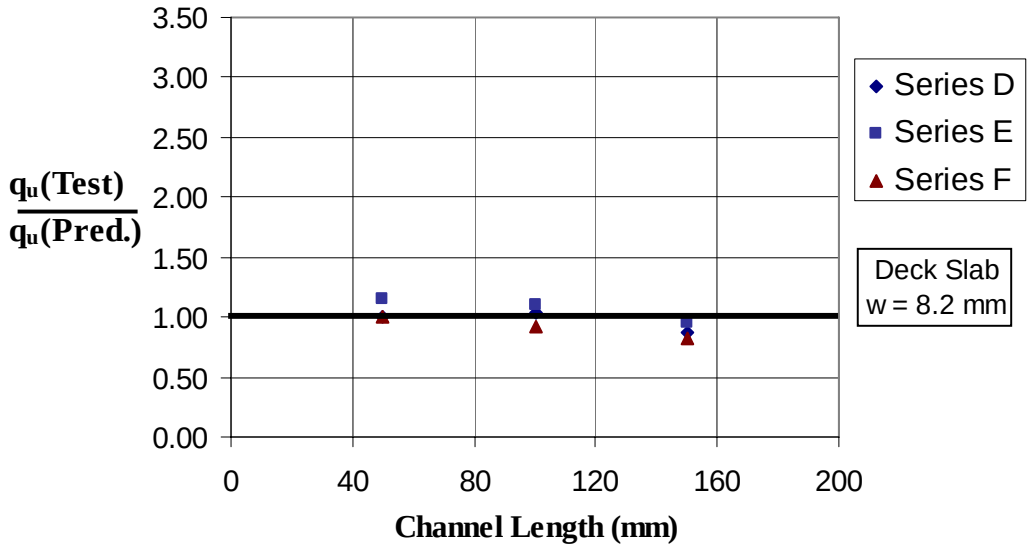

Figure G.1 Comparison between tested values of shear resistance and those predicted by Equation G.16 for specimens with an 8.2 mm web thickness.

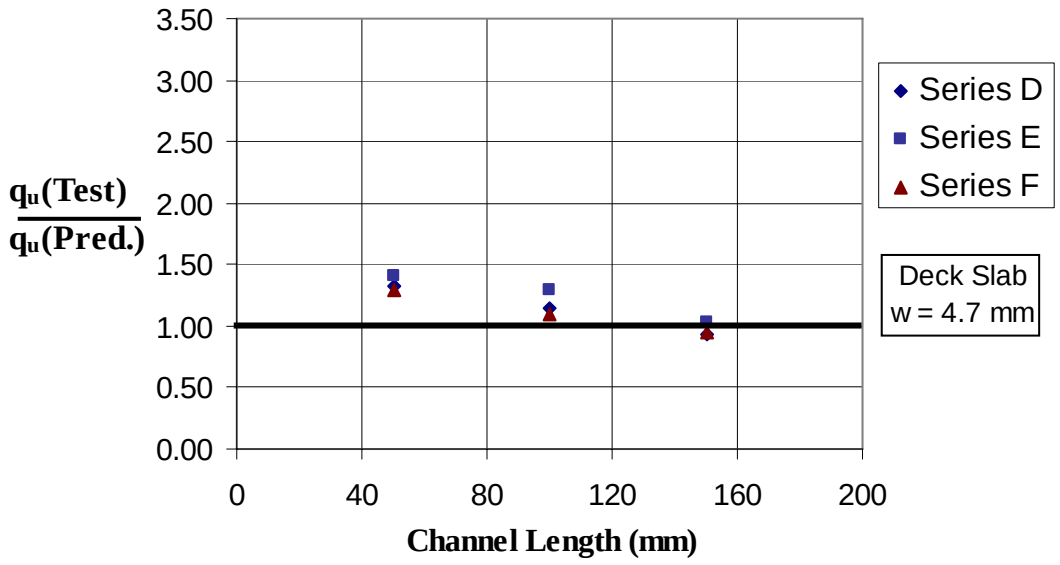

Figure G.2 Comparison between tested values of shear resistance and those predicted by Equation G.16 for specimens with a 4.7 mm web thickness.

Table G.2 Statistical Analysis of Predicted Values for Proposed Equations.

Statistics	Eq. 5.16	Eq. G.16
μ	1.002	1.072
σ	0.106	0.162
C.V.	1.17%	1.37%

Once again, the height of the channel connector (H) of all the specimens used in this analysis was 102 mm. Hence, it is recommended that Eq. [G.16] be used with the following limit:

H = 102 mm

G.3 Application of Proposed Equations to 127 mm High Channels

G.3.1 Solid Slabs

The detailed results of the test values of specimens and those predicted by Eq. [G.11] are listed in Table G.3. Figure G.3 shows the performance of Eq. [G.11] when applied to 127 mm high channels with 8.3 mm web thickness. Similar results for channel with 4.7 mm web thickness are presented in Fig. G.4.

Equation G.11 appears to provide reasonably accurate values for channel with 4.7 mm web thickness. In the case of channels with 8.2 mm web thickness, the discrepancy is quite high and is also on the unsafe side. The average absolute difference between the observed values and those predicted by Eq. [G.11] is 12.36%. The average arithmetic mean of the test/predicted ratio (μ) is 0.915. As indicated in Section G.1, the corresponding values for 102 mm high channels were 10.1% and 1.055, respectively. Considering the two μ values (0.915 vs. 1.055), it appears that Eq. [G.11] underestimates the shear capacity of 127 mm high channels by approximately 9%. In the absence of a more accurate equation, Eq. [G.11] may be used for 127 mm channels with a reduction factor of 0.9.

Table G.3 Statistical Analysis of Predicted Values for Proposed Equations.

Specimen	f'c (MPa)	Channel Length (mm)	Web Thickness (mm)	Ultimate Shear Strength per Channel (kN)		Ratio of Test/ Predicted
				Test	Eq.G.11	
A1a	30.49	152.4	8.3	602.6	687.86	0.88
A1b	30.49	152.4	8.3	603.6	687.86	0.88
A2a	33.87	101.6	8.3	472.1	528.24	0.89
A2b	33.87	101.6	8.3	474.1	528.24	0.90
A3a	33.87	50.8	8.3	288.85	331.49	0.87
A3b	33.87	50.8	8.3	295.8	331.49	0.89
A4a	33.87	152.4	4.8	563.75	635.30	0.89
A4b	33.87	152.4	4.8	576.7	635.30	0.91
A5a	33.87	101.6	4.8	436.25	438.56	0.99
A5b	33.87	101.6	4.8	464.15	438.56	1.06
A6a	33.87	50.8	4.8	250.5	241.81	1.04
A6b	33.87	50.8	4.8	256.95	241.81	1.06
B1S	18.65	150	8.3	368.5	531.07	0.69
B2S	18.65	100	8.3	330.15	387.38	0.85
B3S	24.24	50	8.3	236.55	277.81	0.85
B4S	18.65	150	4.8	408.85	464.53	0.88
B5S	24.24	100	4.8	336.65	365.77	0.92
B6S	24.24	50	4.8	224.85	201.95	1.11
C1S	44.9	150	8.3	694.7	824.02	0.84
C2S	44.9	100	8.3	516.45	601.06	0.86
C3S	44.9	50	8.3	313.75	378.10	0.83
C4S	44.9	150	4.8	677.3	720.77	0.94
C5S	44.9	100	4.8	486.05	497.81	0.98
C6S	44.9	50	4.8	262.95	274.85	0.96

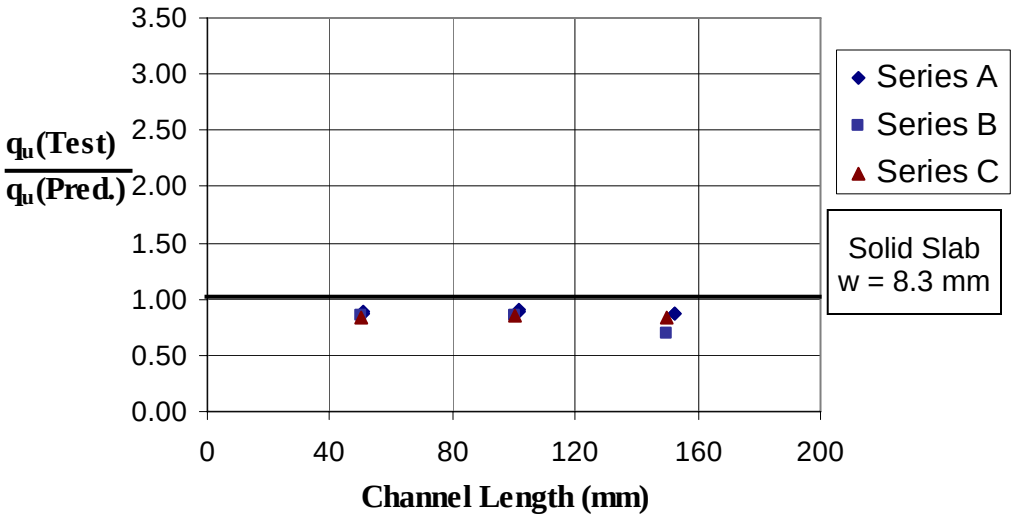

Figure G.3 Comparison between tested values of shear resistance and those predicted by Equation G.11 for specimens with an 8.3 mm web thickness.

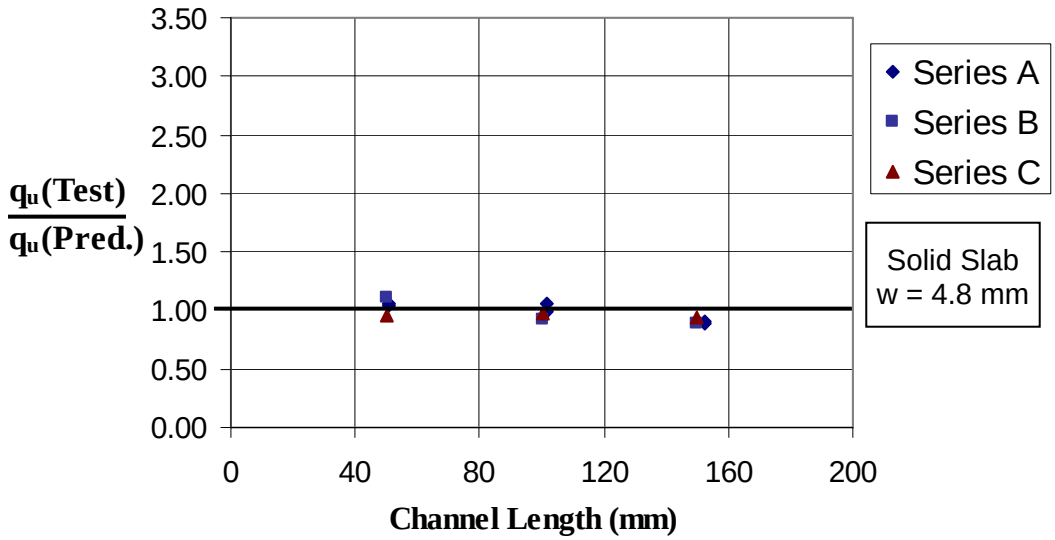

Figure G.4 Comparison between tested values of shear resistance and those predicted by Equation G.11 for specimens with a 4.8 mm web thickness.

G.3.2 Deck Slabs

The detailed results of the test values of specimens and those predicted by Eq. [G.16] are listed in Table G.4. Figure G.5 shows the performance of Eq. [G.16] when applied to 127 mm high channels with 8.3 mm web thickness. Similar results for channel with 4.7 mm web thickness are presented in Fig. G.6.

Equation G.16 appears to provide reasonably accurate values for 127 mm high channel embedded in deck slabs. The average absolute difference between the observed values and those predicted by Eq. [G.16] is 11.85%. The average arithmetic mean of the test/predicted ratio (μ) is 0.973. As listed earlier in Section G.2, the corresponding values for 102 mm high channels were 11.8% and 1.072, respectively. Considering the two μ values (0.973 vs. 1.072), it appears that Eq. [G.16] can also be used to predict the shear capacity of 127 mm high channels.

Table G.4 Statistical Analysis of Predicted Values for Proposed Equations.

Specimen	f'c	Channel Length	Web Thickness	Ultimate Shear Strength per Channel (kN)		Ratio of Test/ Predicted
	(MPa)	(mm)	(mm)	Test	Eq.G.16	
A1D	27.14	152.4	8.3	388.45	498.33	0.78
A2D	27.14	101.6	8.3	344.6	365.17	0.94
A3D	33.42	50.8	8.3	254	257.47	0.99
A4D	27.14	152.4	4.8	390.45	432.53	0.90
A5D	27.14	101.6	4.8	339.65	299.37	1.13
A6D	33.42	50.8	4.8	212.15	184.45	1.15
B1D	18.65	150	8.3	278.4	407.88	0.68
B2D	18.65	100	8.3	292.8	299.24	0.98
B3D	18.65	50	8.3	190.75	190.60	1.00
B4D	18.65	150	4.8	277.9	353.33	0.79
B5D	18.65	100	4.8	234.05	244.69	0.96
B6D	24.24	50	4.8	180.3	155.11	1.16
C1D	37	150	8.3	498	574.50	0.87
C2D	37	100	8.3	463.15	421.48	1.10
C3D	44.9	50	8.3	285.85	295.73	0.97
C4D	37	150	4.8	476.1	497.68	0.96
C5D	44.9	100	4.8	406.35	379.67	1.07
C6D	44.9	50	4.8	231.05	211.10	1.09

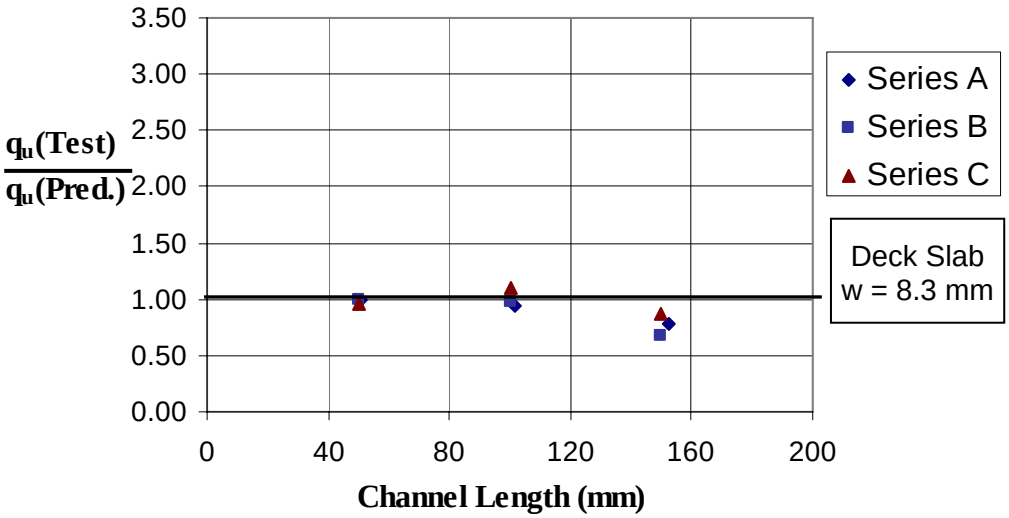

Figure G.5 Comparison between tested values of shear resistance and those predicted by Equation G.16 for specimens with an 8.3 mm web thickness.

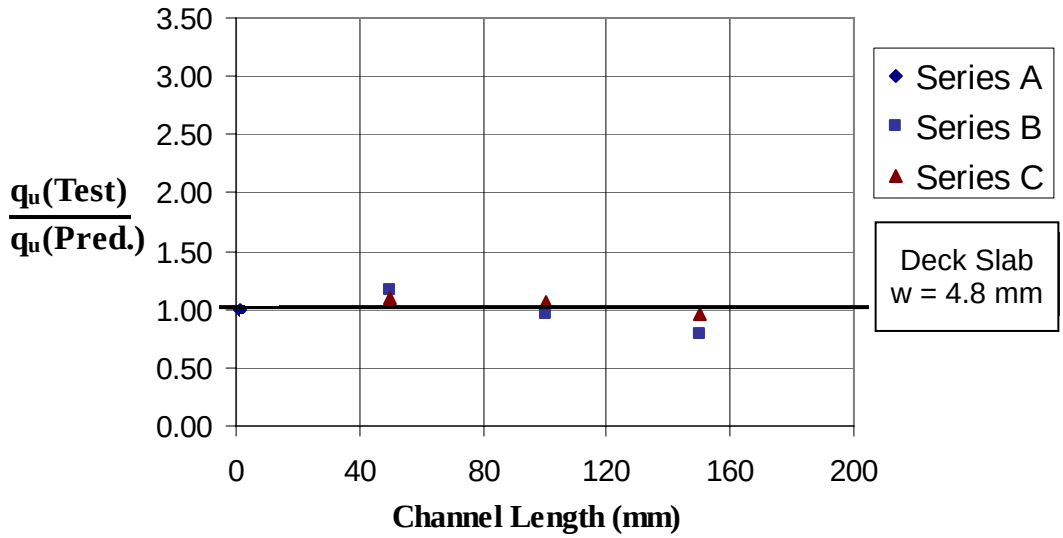

Figure G.6 Comparison between tested values of shear resistance and those predicted by Equation G.16 for specimens with a 4.8 mm web thickness.